Novel motion capture methods for sports analysis: case studies of cycling and rugby goal kicking

by
Stephen John Cockcroft

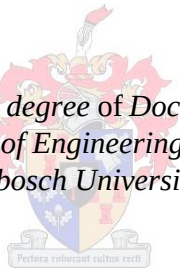

Dissertation presented for the degree of *Doctor of Engineering in the Faculty of Engineering at Stellenbosch University*

Supervisor: Dr Jacobus Hendrik Muller
Co-supervisor: Dr David Jacobus van den Heever

December 2015

DECLARATION

By submitting this dissertation electronically, I declare that the entirety of the work contained therein is my own, original work, that I am the sole author thereof (save to the extent explicitly otherwise stated), that reproduction and publication thereof by Stellenbosch University will not infringe any third party rights and that I have not previously in its entirety or in part submitted it for obtaining any qualification.

This dissertation includes 3 original papers published in peer-reviewed journals and 3 unpublished publications. The development and writing of the papers (published and unpublished) were the principal responsibility of myself and, for each of the cases where this is not the case, a declaration is included in the dissertation indicating the nature and extent of the contributions of co-authors.

December 2015

ABSTRACT

The quest to understand and optimize human movement performance has advanced rapidly in recent years through innovations in movement science and technology. Motion capture technologies have become significantly more mobile, powerful and unobtrusive, enabling new research opportunities. This has resulted in the continuous development of novel quantitative methods for observing and interpreting expert performance in professional sports. A contribution is presented towards this ongoing endeavor via original methodologies for measurements of cycling kinematics using wireless inertial and magnetic measurement systems (IMMSs) and technique analysis of expert rugby union goal kicking using stereophotogrammetry.

Three studies are presented detailing the design and validation of sensor fusion algorithms for IMMS tracking of cycling kinematics. The algorithms utilize a nonlinear complementary filtering structure together with domain constraints related to pendulum and planar motion. Using stereophotogrammetry to validate the tracking performance, it is shown that these filter adaptations eliminate typical measurement errors caused by continuous and time-varying dynamic accelerations and magnetic field disturbances. The first of the IMMS studies illustrated the use of a functional calibration technique to estimate the radius of rotation of an IMMS attached to the thigh. This technique was shown to reduce IMMS tracking errors per axis to 1°. A detailed assessment of the effect of soft tissue artifact on hip angle measurements is also given, and estimates of hip kinematics in the sagittal plane were accurate to within 1-2°. The following two studies focus on IMMS tracking of crank angles in the presence of severe magnetic interference, which precludes the use of traditional static pose calibrations. Two magnetometer-free algorithms are presented, one not requiring a sensor-to-segment calibration and another utilizing a functional calibration technique. Both methods were found to perform with accuracies of 2-3°. A novel optical motion capture method for tracking the crank angle was also developed using a two-segment definition.

Three more studies present a novel technique analysis of fifteen professional goal kickers using stereophotogrammetry. The first study investigated the distance and angulation of the individual steps of the run-up as well as foot positioning relative to the tee and found that anthropometry did not play a major role in determining run-up

geometry. The second study assessed phase timing, speed and acceleration during the approach and found that this only had a moderate to small association with foot speed at ball contact. The third study reports on rotational alignment of the thorax, pelvis and feet relative to the tee and target and discusses evidence for a tension arc movement strategy in the spine rotation angle. The most important finding in all three studies was high inter-individual variability and low intra-individual variability, which highlights the nonlinear, athlete-specific dynamics of motor control in sports.

In short, this work contributes towards understanding and overcoming challenges to cycling analysis using IMMSs. The tracking algorithms are resistant to errors caused by magnetic interference, centripetal accelerations and sensor-to-segment calibration. Similarly, the technique analysis of rugby goal kicking contributes towards evidence-based coaching by providing novel methodologies and data for understanding performance.

OPSOMMING

Die strewe om menslike bewegingsprestasie te verstaan en te optimeer het in die onlangse tyd snelle vooruitgang beleef met vernuwende bewegingswetenskap en -tegnologie. Bewegingvasleggingstegnologie is deesdae beduidend sterker, meer mobiel en onopvallend, wat nuwe navorsingsgeleenthede skep. Dít lei tot die voortgesette ontwikkeling van nuwe kwantitatiewe metodes om die prestasie van beroepsportlui waar te neem en te vertolk. Hierdie navorsing lewer ’n bydrae tot dié deurlopende pogings in die vorm van oorspronklike metodologieë vir die meting van fietsrykinematika met behulp van draadlose traagheids- en magnetiese metingstelsels (TMMS’e), sowel as tegniekontleding van doelskoppe deur beroepsrugbyspelers met behulp van stereofotogrammetrie.

Die drie studies wat hier aangebied word, toon die besonderhede van die ontwerp en bekragtiging van sensorfusie-algoritmes vir die TMMS-nasporing van fietsrykinematika. Die algoritmes maak gebruik van ’n nielinîere aanvullende filterstruktuur, tesame met domeinbeperkings vir slinger- en vlakbewegings. Met behulp van stereofotogrammetrie om die nasporingsprestasie te bekragtig, word daar aangetoon dat hierdie filteraanpassings tipiese metingsfoute uitskakel wat gewoonlik uit deurlopende en tydwisselende dinamiese versnellings en versteurings in die magnetiese veld spruit. Die eerste van die TMMS-studies illustreer die gebruik van ’n funksionele kalibreertegniek om die draai-omtrek te skat van ’n TMMS wat aan die bobeen vasgemaak is. Daar word bewys dat hierdie tegniek TMMS-nasporingsfoute per as tot 1° verminder. Hierdie studie bied ook ’n voerige beoordeling van die sagteweefselartefak by heuphoekmetings, en kon heupkinematika op die sagittale vlak akkuraat tot op 1-2° na skat. Die volgende twee studies konsentreer op TMMS-nasporing van draaihoeke in die teenwoordigheid van erge magnetiese inmenging, wat die gebruik van tradisionele statiese houdingskalibrering onmoontlik maak. Twee magnetometer-vrye algoritmes is ontwikkel – een sonder ’n sensor-tot-segment-kalibrering en een wat van ’n funksionele kalibreertegniek gebruik maak. Albei metodes het akkurate resultate tot op 2-3° na opgelewer. Daarbenewens is ’n vernuwende optiese bewegingvasleggingsmetode ontwikkel vir die nasporing van die draaihoek met behulp van ’n tweesegment-definisie.

Drie verdere studies bied ’n voerige tegniekontleding van 15 beroepsdoelskoppers met behulp van stereofotogrammetrie. In die eerste studie word die afstand en hoek van die individuele treë in die aanloop sowel as die voetplasing in verhouding tot die skopring ondersoek, en word daar bevind dat antropometrie geen beduidende rol in die bepaling van aanloopgeometrie gespeel het nie. Die tweede studie beoordeel fasetydsberekening, snelheid en versnelling in die aanloop, en dui op slegs ’n matige tot swak verband met voetsnelheid by balkontak. Die derde studie doen verslag oor die draairigting van die toraks, pelvis en voete in verhouding tot die skopring en teiken, en bespreek die bewyse vir ’n spanningsboog-bewegingstrategie in die draaihoek van die ruggraat. Die belangrikste bevinding in ál drie studies is hoë inter-individuele veranderlikheid en lae intra-individuele veranderlikheid, wat die nieliniêre, atleetspesifieke dinamika van motoriese beheer in sport beklemtoon.

Die metodes wat vir hierdie studie ontwikkel is, dra by tot die verstaan en oorkomming van die uitdagings van fietsryanalise deur middel van TMMS’e. Die nasporingsalgoritmes wat ontwikkel is tydens die studie is immuun teen foute veroorsaak deur magnetiesesteuring, sentripitaleversnelling en sensor-tot-segment kalibrasie. Die tegniekontleding van rugbydoelskoppe in hierdie studie bied ook ’n magdom nuwe kennis oor bewegingspatrone by beroepspelers en lê die grondslag vir bewysgegronde afrigting en oefening..

DEDICATION

To my parents, Steve and Ingrid, thank you for everything.

ACKNOWLEDGEMENTS

First and foremost, I would like to acknowledge the help of my colleagues in the Biomedical Engineering Research Group. This project would not have been possible without my original supervisor, Prof. Cornie Scheffer. He was there from the beginning, eight years ago in my Honours year, always providing opportunities and a nourishing environment. I am also grateful to Dr. Cobus Muller and Dr. Dawie van der Heever for their generous support throughout the project. I am proud to be part of this group.

Secondly, I have a deep appreciation for the staff at the motion analysis laboratory where the tests for this project were conducted. In particular, I am very grateful for the long-term guidance and mentorship of Prof. Quinette Louw, as well as to Dominic Fisher for helping with the marker placements and providing countless hours of conversation regarding the results. Louis Koen was also a helpful resource when a coaching perspective was needed for the goal kicking studies.

Lastly, I am grateful to many friends and family who were very supportive during the time I was busy with my studies. Most of all, I would like to thank my wife Rosanne for walking this long road with me. I could not have done it without you.

CONTENTS

LIST OF FIGURES

LIST OF TABLES

NOMENCLATURE

Abbreviations

ACF	Anatomical coordinate frame
CM	Centre of mass
CMAE	Combined mean absolute error
CoR	Centre of rotation
CRANK	Constrained rotational acceleration and kinematics
DAC	Dynamic acceleration compensation
EKF	Extended Kalman filter
FQA	Factored quaternion algorithm
HC	Heading Constraint
IMMS	Inertial and Magnetic Measurement Unit
KCR	Kinematic Constraint Rotation
KF	Kalman Filter
KL	Kicking leg
MAE	Mean absolute error
PCF	Passive complementary filter
PCF_HC	Passive complementary filter with heading constraint
SL	Support leg
STA	Soft tissue artifact
VAU	Vertical acceleration update

1. Introduction

1.1. Quantitative Analysis of Human Movement

Human movement results from muscular forces acting on the skeletal system in order for the body to overcome gravity and navigate the environment. Through cognitive processes, these muscular forces are controlled by the nervous system and fueled by the cardiopulmonary system (Figure 1). The phenomenon of human movement is so ubiquitous that its complexity is not often appreciated. Besides the numerous intricate interactions between (amongst others) the musculoskeletal, neurological and cardiopulmonary systems, mobility is also influenced by a wide array of environmental, sociological and psychological factors [1, 2]. Therefore, understanding the underlying mechanisms characterizing both healthy and impaired movement for different physical tasks, contexts and populations is a massive undertaking requiring on-going trans-disciplinary research.

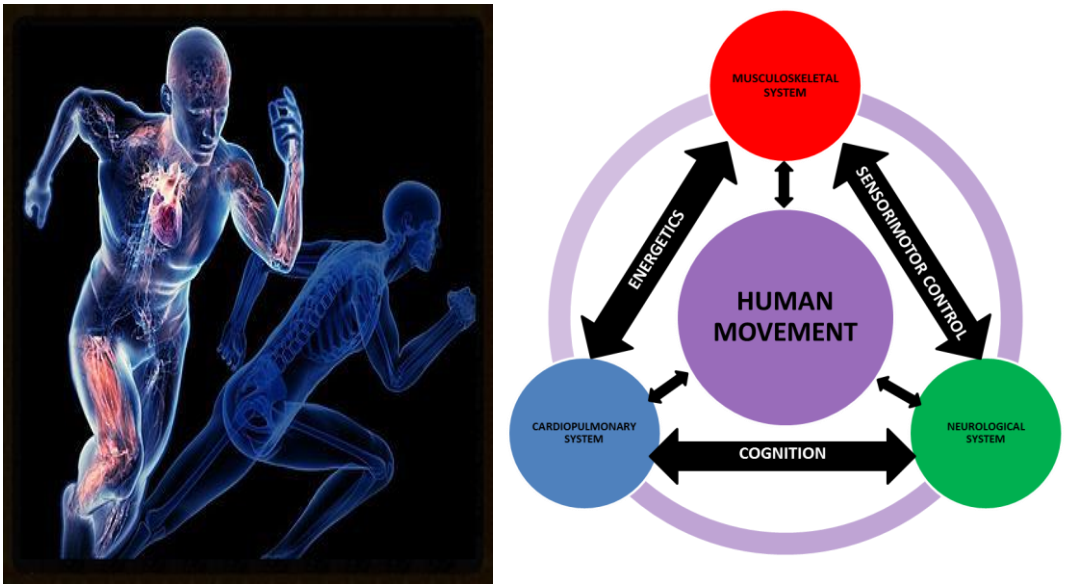

(Image: http://eliteathletedaily.com)

Figure 1: Sensorimotor control, energetics and cognition all play an important role in human movement function

This study falls within this broad framework, but its scope is restricted to the analysis of musculoskeletal biomechanics at the functional system level (as opposed to molecular, cellular or tissue biomechanics). More specifically, the work focuses on

short-term kinematic analyses of specific skeletal segments and joints during sports, which involve measurements with a high temporal-spatial resolution on the scale of single degrees of rotation, millimeters of displacement and milliseconds. The work is thus differentiated from longer-term macro-level studies involving daily activity monitoring using GPS or pedometers, and also does not include any data on forces (kinetics) or muscle activity (electromyography) during movement. To further contextualize this study, the following section gives an overview of the modern applications, historical development and current challenges within this specific area of quantitative human movement analysis.

1.1.1. Modern applications

Human movement analysis is relevant to a broad range of applications (Figure 2). Firstly, the growing body of knowledge about human movement is being utilized increasingly for evidence-based clinical healthcare interventions in order to improve quality of life. Pre- and post-intervention movement analysis is helpful for guiding surgical decisions and assessing outcomes, for example in arthroplasty patients with osteoarthritis [3] or single-event-multiple-level surgery on children with cerebral palsy [4]. Similarly, in the allied health professions it is used to track rehabilitation progress for patients with impaired physical mobility due to chronic disease, aging and trauma [5]. Measurements of human movement have also been used to determine risk factors and biomarkers for preventative and diagnostic screening, as well as for the development of biomedical devices [2]. Overall, since physical mobility is necessary for people to maintain employability and independence in their daily lives, quantitative human movement analysis is playing an important role in improving livelihoods and reducing the global burden of immobility on healthcare systems.

Quantifying human movement is also valuable in applications where it is important to simulate or identify it (Figure 2). For instance, real-world simulations of human movement are desirable in the field of robotics where humanoid robots are designed to ambulate as naturally as possible [6]. Realistic digital reconstructions of humanoid models have also become crucial in the creation of visual entertainment products such as movies and games. Animated characters can be made to mimic the idiosyncratic movements of famous celebrities (e.g. specific athletes) or of the user interacting with a product (e.g. visual-perceptual interfaces in gaming consoles) based on motion tracking and analysis [7]. Similarly, computer vision techniques continue to be developed for smart surveillance systems that can detect human movement, recognize

individuals by their characteristic movement patterns and classify their behaviors from video footage [8]. Therefore, quantitative human movement analysis has played an important role in the development of humanoid robotics, virtual reality and biometric security systems.

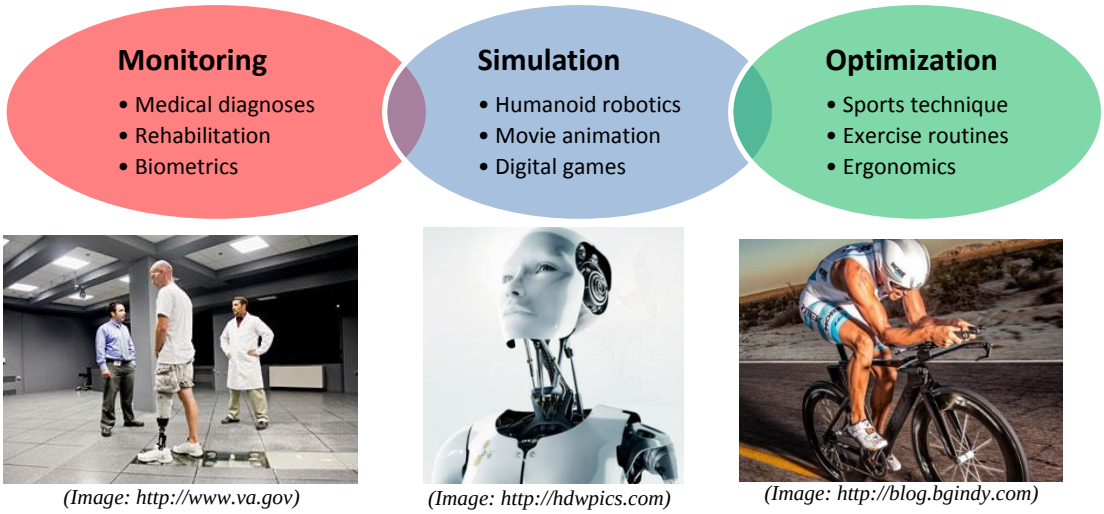

Figure 2: Overlapping application areas for quantitative human movement analysis

Most relevantly for this study, human movement analysis is playing an increasingly important role in optimizing human performance. One application area is in the field of occupational ergonomics, where quantitative movement analysis is used to inform the regulations for enhancing safety and productivity in the workplace [9]. Moreover, worldwide there is a growing awareness in society as well as governments about the importance of promoting health and wellness through exercise and recreational activities [10, 11]. Insights from quantitative movement analysis are being applied to personal training regimes, coaching methodologies, sportswear and sports equipment design in order to improve general health as well as elite performance [12]. This is particularly prevalent in professional sports where high performance athletes seek to gain a competitive edge through movement optimizations [13].

1.1.2. Historical development

Over the centuries, the evolution of quantitative human movement analysis has been driven by accelerating developments in science and technology. The earliest recorded accounts of movement analysis go back as far as the fourth and fifth century BC, where Aristotle and his Greek contemporaries postulated methods of describing human and animal movements that were difficult to discern with the naked eye [14].

However, another two millennia would pass before the fields of anatomy and mathematics developed sufficiently to describe human movement quantitatively.

During the renaissance and enlightenment periods in Europe (14^{th}-18^{th} centuries), the likes of Da Vinci, Vesalius (the "Father of Anatomy") and Borelli (the "Father of Biomechanics") produced pioneering works on the anatomy [15] and locomotion [16] of the human body respectively (Figure 3). Meanwhile, mathematicians such as Cardan, Descartes, Newton and Euler were developing the analytical tools required to quantitatively describe human motion [17]. It was at this stage that the combined knowledge of Newton's laws of motion (mechanics) and functional anatomy gave rise to the field of quantitative biomechanics. However, it would be another 100 years before technologies became available for actually taking any biomechanical measurements.

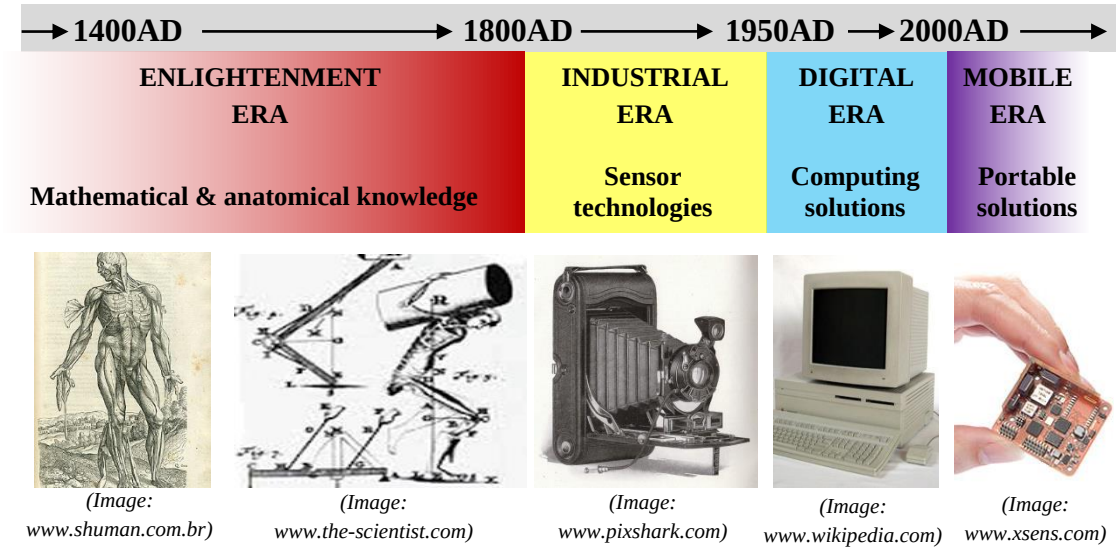

Figure 3: A broad historical overview of the eras in which the tools required for movement analysis developed

The development of sensor technologies such as photography and chronography during the Industrial Revolution (19th century) enabled French and German researchers to begin experimental studies of movement sequences during walking [18]. Progressive advancements in chronophotography and the theoretical analysis of walking mechanics culminated in the first three-dimensional gait analysis conducted in Leipzig in 1895 [17]. At the end of the Second World War 50 years later, the need to rehabilitate injured war veterans led to the establishment of the world's first gait analysis laboratory in 1945 in Berkeley, USA. However, despite tremendous progress

in the understanding of walking biomechanics during subsequent years, work was hindered by the need to perform manual calculations to derive biomechanical outcomes from the data – a feat which required hundreds of man hours per subject analysis.

The arrival of the digital era in the second half of the 20th century finally provided the computing power and data storage capacity to perform automated quantitative movement analyses quickly, reliably and on a large scale. This lead to a proliferation of human movement laboratories and the emergence of the first commercial motion capture systems by the 1980's [19]. At this stage, camera-based systems were already established as the gold-standard approach, although other systems based on magnetic and acoustic sensors were also developed. Within a few years, the first standardized protocols were made available for performing routine gait analysis for clinical decision-making, and by the turn of the century the general consensus was that quantitative gait analysis was coming of age [20]. However, most other movements remained largely unexplored and test conditions were still somewhat cumbersome due to the size and wired nature of the available equipment.

The new millennium has brought with it the era of mobile technology, which has expanded the scope of human motion analysis exponentially [21]. There have been several key drivers. Firstly, micro-manufacturing has drastically reduced the size and cost of inertial sensors, making them much more portable and unobtrusive to place them on test subjects [1]. Almost all movement analysis sensors are now compact self-contained units with on-board data storage, processing power, battery power and Wi-Fi transmission capabilities. This is enabling previously unfeasible experiments and the seamless integration of hardware and software platforms. Sensor technologies can now measure more aspects of human movement in far more situations and in far greater detail than ever before. As detailed earlier in Chapter 1.1.1, this technological revolution in the 21st century is finally helping human movement analysis to migrate outside of the laboratory and outside of the classical bounds of gait analysis into other movement contexts such as sports [22].

1.1.3. Challenges related to sports analysis

In comparison to gait analysis, which has been researched and developed for over half a century, three-dimensional quantitative movement analysis in sports has only become widespread in the last two decades. Due the complexity and dynamism of sports movements, several challenges need to be addressed to accomplish valid and

unobtrusive methods for data collection in the natural sporting environment, and effective interpretive frameworks for analysis of movement technique (Figure 4).

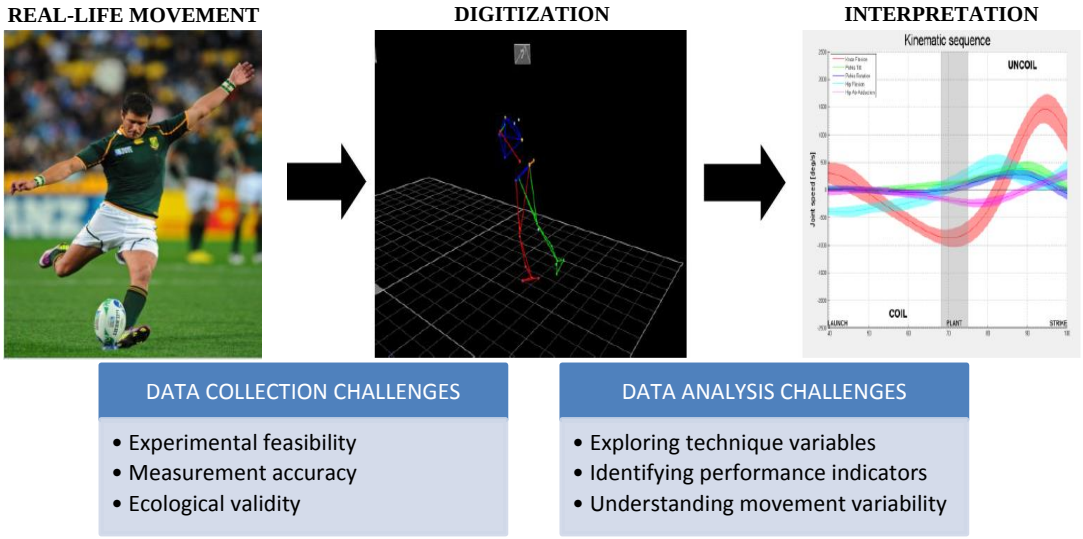

(Image top left: http://www.gilbertrugbyblog.com)

Figure 4: The range of challenges in collecting and analyzing movement data for sports performance optimization

Reaching the goal of non-invasive field testing is dependent upon the development of portable, non-invasive sensing capabilities. In the case of some sports this remains unfeasible due to basic technological barriers. For example, three-dimensional motion analysis for some water sports is not currently feasible [23]. Even for sports where data collection is feasible, mobile body-mounted instruments are often not sufficiently robust to operate accurately and reliably when subjected to vigorous motion, excessive sweat, physical impacts or other undesirable environmental factors [24]. For these reasons, quantitative analysis is still often conducted in controlled laboratory conditions to ensure the accuracy of measurements, although this can significantly reduce the ecological validity of research findings [25]. Therefore, in order to advance the field of quantitative movement analysis for sports, novel technologies and data collection methods are still required for improving the feasibility, accuracy and validity of experiments in harsh sporting environments.

A second challenge in sports analysis is the development of appropriate analytical frameworks for interpreting specific sports movements. Without a way of quantitatively describing and understanding the underlying mechanisms related to performance, it remains unclear how to utilize measurement data. Despite numerous

studies of well-funded sports such as golf and soccer, many smaller sports remain largely under-researched in terms of comprehensive technique analysis using gold-standard three-dimensional motion capture systems. Technique analysis is the process of determining the correlation between technique variables and performance variables [26]. Performance variables are directly related to the achievement of the desired outcome (e.g. more club head speed increases golf shot distance), whereas technique variables are descriptors of how the performance variable was achieved (e.g. larger range of pelvic rotation increased club head speed). The first step in technique analysis is to develop a temporal framework for breaking down the movement into appropriate time phases using well-defined, reliable movement events. Technique variables (e.g. joint angles) are then typically assessed using amplitude analysis at a specific event or during a specific phase, and correlated to performance variables using statistical methods. This provides an initial basic understanding of which technique variables are important.

One example of such a framework is kinematic sequencing, which relates to the proximal-to-distal summation of segmental speed during kicking, throwing and hitting movements [27]. Kinematic sequences can be optimized for maximum distal speed at the point of contact or release, thus ensuring maximal projectile distance (which usually affects performance). The kinematic sequence framework has been successfully applied to golf, where it has been shown that elite golf swings are all characterized by a specific kinematic sequence despite notable differences in movement technique [28]. This highlights the high level of motor abundance in the body (multiple kinematic pathways to the same outcome), and necessitates a differentiation between technique and performance when analyzing sports movements [29]. As stated above, this kind of foundational analysis is still required in many sports in order to provide a platform for more advanced analysis.

Advanced analyses focus on understanding the motor control strategies developed by the brain in order to optimize sports technique and how these strategies are affected by intrinsic and extrinsic factors. The key phenomenon in this regard is movement variability, the nature of which has sparked considerable academic debate in the wider field of motor control [30]. In the past, inter-subject variability was considered to be indicative of sub-optimal movement patterns that need to be corrected through rigid coaching interventions towards a single optimal technique. This perspective is changing as researchers and coaches embrace the idea that optimal technique is not constrained to a single motor control strategy but rather is dependent on a number of

subject-specific factors [31]. Moreover, intra-subject variability has been traditionally interpreted as undesirable noise in the motor control system, causing athletes to strive for perfect repeatability through large training volumes. However, recent studies have suggested that intra-subject variability may have a functional purpose such as reducing injury risk or helping the motor control system adapt to disturbances [32, 29]. Therefore, beyond achieving accurate measurements, perhaps the most significant challenge in sports analysis using quantitative movement data is attaining a helpful understanding of movement variability and how to address it in coaching.

1.2. Modern Human Motion Capture Systems

Quantitative human movement analysis is performed using motion capture systems. Current technologies for motion capture typically involve a signal source and markers attached to the body (Figure 5). There are also some emerging image processing technologies which detect virtual landmarks on the body from camera footage (markerless systems [33, 18]), as well as proprioceptive sensing technologies such as e-textiles [34, 35] that can quantify movement without a signal source (sourceless). These emerging technologies fall outside the scope of this thesis and the text will henceforth focus only on source-based marker systems.

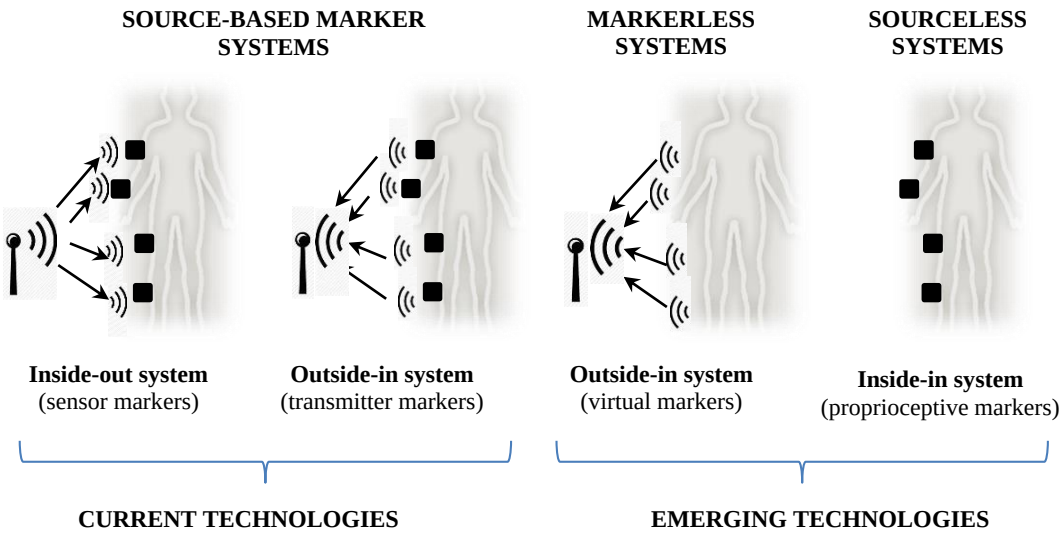

Figure 5: The four broad categories of motion capture systems, two current and two emerging, based on the location of the sensor technology used

Source-based marker systems are transmitter-receiver technologies which utilize a particular type of signal to register body movement relative to an external reference

(usually the ground). The signal is usually generated by the system, for example infrared light, but it may also be a naturally occurring signal such as gravity. There are two basic types of source-based marker systems, depending on the location of the sensors receiving the signal: outside-in tracking systems and inside-out tracking systems (Figure 5). Outside-in systems employ sensors outside of the movement space to track a signal coming from inside the movement space i.e. from the body. In contrast, inside-out systems use sensors fixed to the body to track an external signal source. Note that sourceless systems are thus characterized as inside-in (the 'signal' is thus the movement itself) and markerless systems are outside-in as the signal is natural light reflected off the body.

The major advantage of modern source-based marker systems over 2D video analysis is that they track movement in three dimensions of space. Body segments are typically modeled as rigid inter-connected skeletal bones. Describing the three-dimensional kinematics of a rigid body segment requires knowledge of two Cartesian coordinate systems (frames): a technical frame attached to the segment and a global reference frame attached to the external environment and considered stationary. Therefore, the advantages and disadvantages of different source-based marker systems are determined by the nature of the transmitter signal and how well it propagates between the technical frame and the global frame under different conditions. This is illustrated in the following two subsections which elaborate on the advantages and disadvantages of the dominant motion capture technologies.

1.2.1. Optical motion capture systems

The current gold-standard motion capture technology for kinematic analysis is stereophotogrammetry. Stereophotogrammetry systems have a classical outside-in architecture with markers on the body either reflecting or emitting an artificially generated light signal (often infra-red) back to an array of ground-fixed cameras. Triangulation techniques are then used to estimate the coordinates of individual markers on an object within a virtual motion capture volume; the physical area in which markers are visible to at least two cameras (Figure 6a). This is determined by the number and configuration of the cameras used, the position (origin) and orientation (axis directions) of which are determined by a calibration procedure relative to a ground-fixed reference frame. A minimum of three markers attached to the same rigid body segment is then required for tracking the angulation of that segment's technical frame (Figure 6b).

Optical motion capture measurements have a high resolution in space (sub-millimeter accuracy) and time (sampling rates of over 500 Hz), making them ideal for recording highly dynamic sports movements. However, these systems have two important disadvantages: small measurement volumes and marker occlusions. Firstly, optical systems typically have small volumes because the camera hardware required (and thus the cost) scales linearly with volume size. Typical configurations which are still affordable to academic institutions include 6-10 cameras, although larger configurations with dozens of cameras are available. A typical 8-camera configuration enables a maximum volume of approximately 8m x 4m x 2m (length x breadth x height). This is ideal for earth-stationary movements such as a golf swing, jumping or standing balance tasks but problematic for translational activities such as road cycling - unless done using a stationary trainer, which may compromise test validity.

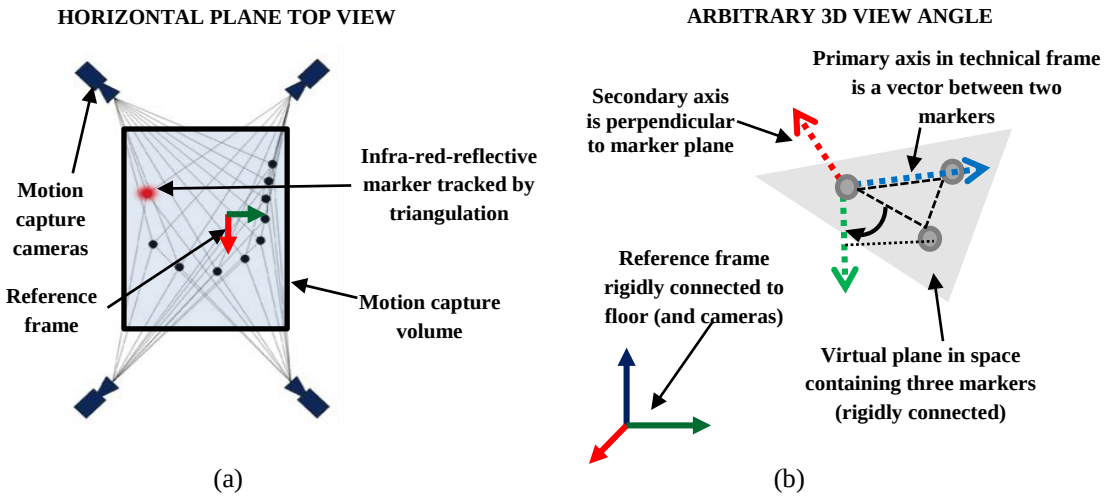

Figure 6: The range of challenges in collecting and analyzing movement data for optimizing sports performance

The second disadvantage of stereophotogrammetry is that the cameras suffer from marker occlusion due to an object obstructing their view. Markers can be occluded by clothing, which means test participants are often required to wear minimal apparel during testing which can be uncomfortable both physically (due to extreme temperatures) and emotionally (due to privacy concerns). Markers can also be occluded by objects that test participants interact with (assistive devices, a chair and table, a set of stairs etc.) which means that the tests are usually limited to uncluttered, highly controlled scenarios. Lastly, occlusions commonly occur due to view

obstructions caused by the test participant's body, which can complicate testing in some movement contexts.

1.2.2. Inertial and magnetic motion capture systems

The main competing motion capture technology used for quantitative human movement analysis is inertial and magnetic measurement systems (IMMSs). In contrast to optical motion capture systems, IMMSs work on the principle of inside-out tracking [36]. The IMMS is a body sensor which tracks two naturally occurring signals external to the body: the gravitational and magnetic fields of the earth. These two field vectors are ubiquitous signal sources that can be used to define an inertial north-east-up reference frame with an essentially unlimited capture volume. Each body segment is mounted with an individual IMMS, the axes of which constitute the segment technical frame, such that a body-network of IMMSs can be used to track a multi-segment body relative to the same inertial reference frame. Therefore, whereas optical systems track the technical frame within the reference frame, each IMMS tracks the reference frame within the technical frame (Figure 7).

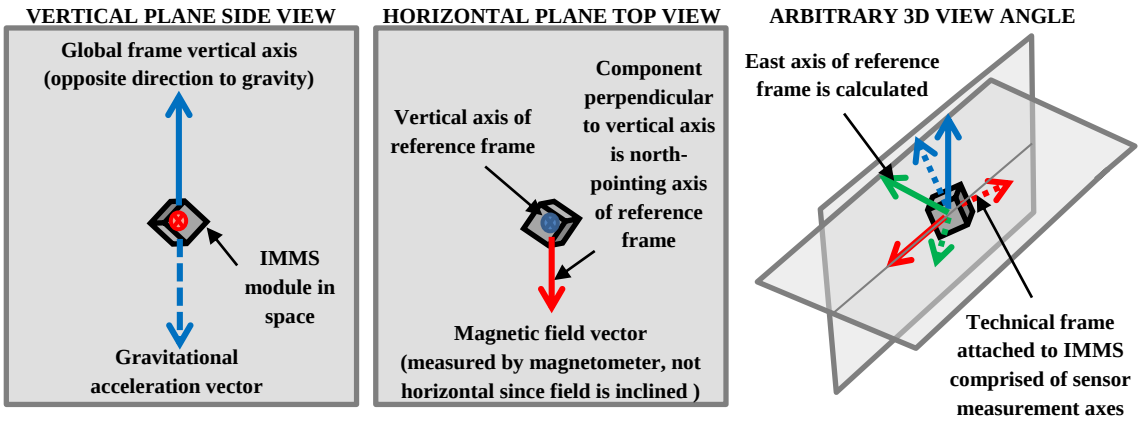

Figure 7: Inertial and magnetic measurement systems in the sensor frame by sensing the global (a) vertical and (b) magnetic north directions, allowing it to reconstruct (c) the reference frame in the sensor technical frame

An IMMS contains triaxial accelerometers and magnetometers which are capable of tracking the vertical axis (Figure 7a) and magnetic north axis (Figure 7b) of the inertial reference frame respectively [37]. The third east-pointing axis is then calculated from the other two (Figure 7c). While usually stable over time,

accelerometer tracking of the gravitational vector is compromised by high-frequency noise during vigorous motion due to the presence of indistinguishable dynamic acceleration artifacts in the measured signal. Similarly, magnetometer tracking of the heading vector is compromised if the local magnetic field is distorted by nearby ferromagnetic materials (e.g. steel objects) or electromagnetic fields (e.g. mobile phones).

To compensate for these errors, IMMSs also contain triaxial gyroscopes which track the angular velocity of the technical frame. This signal can be numerically integrated to track the angular rotation of the technical frame (once detected using vector observation). Gyroscope tracking demonstrates high fidelity during short-term rapid motions but is prone to boundless drift error over time due to the accumulation of non-white noise during integration [38]. Therefore, in essence, an IMMS tracks its own movement in the inertial frame simultaneously using two different tracking methods (vector observations and gyroscope integration). These two methods have complementary error characteristics in the frequency domain which can be exploited using sensor fusion techniques (mathematical optimization algorithms) to produce a single optimal estimate of IMMS [39]. However, IMMS sensor fusion algorithms typically fail after a minute or two in the presence of dynamic accelerations or magnetic interferences which are continuous and time-varying, as they are thus unable to correct gyroscope drift errors. In some cases, additional information from auxiliary sensors or prior knowledge of the system dynamics (domain constraints) can be exploited in the sensor fusion scheme to compensate for prolonged corruption of the IMMS reference vectors [38].

IMMSs also have several notable advantages over optical systems. They are easier to use, less costly, have an essentially unlimited motion capture volume (i.e. truly mobile) and are immune to the occlusion problems suffered by optical systems, allowing them to be used under clothes and in cluttered test environments. However, one of the major disadvantages of IMMSs is that they are inherently three-degrees-of-freedom orientation trackers that do not sense the absolute position of the technical frame in the reference frame [38]. Relative linear displacements of the technical frame can be estimated by double-integration of the (gravity-corrected) accelerometer signal, although this is only reliable for a few seconds at a time due to exponential drift errors. Nevertheless, domain constraints - related to prior knowledge of user anthropometry (segment dimensions) and joint constraints - have been exploited in

proprietary algorithms to enable accurate tracking of translation (e.g. step lengths, total distance travelled) during ambulation with a body network of IMMSs [40].

1.2.3. Biomechanical modeling

Quantitative human movement analysis usually requires that segment motion be expressed relative to intuitive anatomical planes of motion as stipulated by a given convention (e.g. the conventions of the International Society for Biomechanics [41, 42]). These anatomical planes of motion of a given segment are defined by an internal coordinate system (the anatomical frame) attached to the underlying skeletal bones [43]. Therefore, the anatomical frame is not directly observable by optical or IMMS motion capture systems, which instead track the movement of skin-mounted technical frames that do not provide information about segment morphology. Biomechanical modeling involves the estimation of the body's anatomical frames using one of two numerical techniques: direct kinematics and inverse kinematics. Inverse kinematics involves fitting a scaled model of the articulated human body to the measured combined technical frame data using optimization methods such as weighted-least-squares minimization [44]. In contrast, direct kinematics approaches estimate each anatomical frame separately by assuming a direct relationship between the technical frame and anatomical frame attached to the same segments [43]. This thesis does not cover inverse kinematics techniques, and will henceforth focus only on direct kinematics techniques for biomechanical modeling.

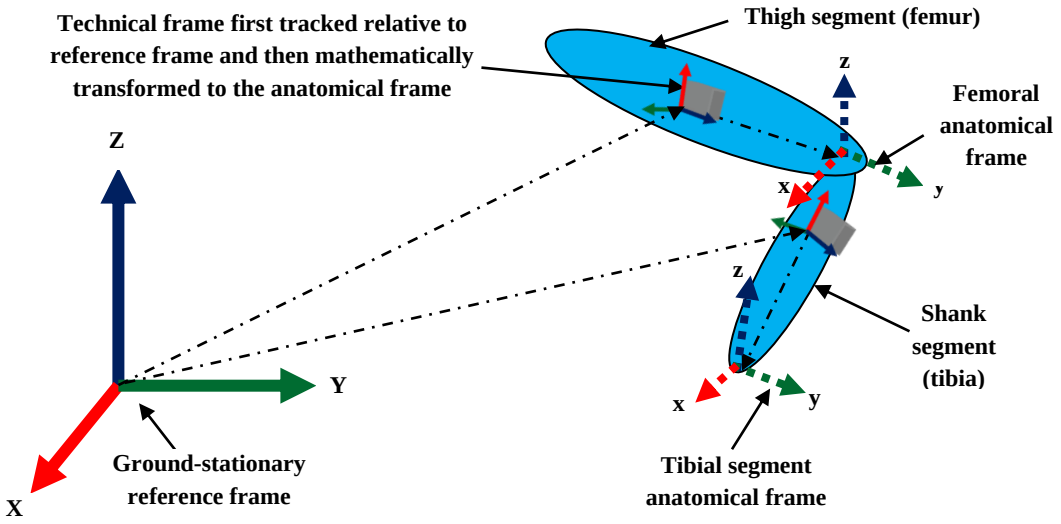

Figure 8: Tracking of internal anatomical coordinate systems requires technical frame measurements as well as knowledge of the relationship between the technical and anatomical frames.

Direct kinematics methods estimate the anatomical frame based on its alignment to the measured technical frame on the same segment (Figure 8). This relationship can be expressed as a coordinate system transformation, usually determined *a priori* using calibration techniques and assumed to be time-invariant (under the rigid body assumption). Therefore, in addition to the uncertainty of motion capture measurements of the technical frame, biomechanical modeling of the body introduces two additional sources of error: anatomical frame calibration errors [45] and soft tissue artifact [46]. Calibration error occurs when the relative alignment between a technical and anatomical frame is estimated incorrectly. Since the axes of anatomical frames are often joint rotation axes, calibration errors can be thought of as misalignment between the estimated anatomical and true anatomical axes. On the other hand, soft tissue artifacts are dynamic changes in the alignment of the technical frame and the anatomical frame due to displacement of the skin-mounted markers relative to the underlying bone.

Anatomical frame calibrations can be performed in different ways. Optical motion capture systems locate anatomical axes using either skeletal landmarks or controlled functional movements. Markers placed on bony landmarks can be used to estimate joint axes (e.g. the line between two markers on the femoral epicondyles approximates the knee axis) as well as joint centers (e.g. the mid-point between two femoral epicondyle markers approximates the knee joint center). Functional techniques are controlled movements which make joint axes and centers observable relative to the technical frame when joint constraints are taken into account. Functional calibration methods are also applicable to IMMS systems, but anatomical landmark position methods are not feasible with IMMSs since IMMSs cannot measure absolute position. Another method which has been traditionally used for IMMS motion capture is static pose calibrations, in which the position and orientation of anatomical frames is simply assumed for a prescribed body pose e.g. a static T-pose.

One of the most common biomechanical modeling outcomes for human movement analysis is joint angles. Joint angles represent the relative alignment of two body segments connected by a shared skeletal joint. This can be expressed mathematically as the orientation of the one segment's anatomical frame within the anatomical frame of the second segment [43]. The relationship between two frames in space can be fully described by a minimum of six scalar values. For example, position p of the

tibial anatomical frame A1 relative to a femoral anatomical frame A2 can be described as using a combination of the relative linear and angular position:

$$p_{A2\rightarrow A1} = [t_x \quad t_y \quad t_z \quad r_x \quad r_y \quad r_z] \tag{1}$$

Here the three-dimensional vector t represents translation of the tibial frame origin within the femoral frame axis and three-dimensional vector r represents angular rotations between the frames in a prescribed Euler rotation sequence. This type of Euler format can be used in this case for quantifying knee joint angles in the three anatomical planes at a specific point in time. This is the common-place parameterization used in clinical settings as Euler angles are geometrically intuitive to interpret. However, to avoid the well-known gimbal-lock phenomenon[1] associated with Euler angle notation, the relative angulation r between frames is often described in software algorithms using one of two alternative mathematical parameterizations: rotation matrices or unit quaternions.

The rotation matrix R is a conceptually intuitive notation in that it describes the orientation of one frame's axes (X-Y-Z) as base vectors within a second x-y-z frame:

$$R_{T\rightarrow G} = \begin{bmatrix} X_x & Y_x & Z_x \\ X_y & Y_y & Z_y \\ X_z & Y_z & Z_z \end{bmatrix} \tag{2}$$

It is also unique in that the transpose merely represents the orientation of the second frame's axes (X-Y-Z) as base vectors within the first frame (x-y-z).

$$R_{T\rightarrow G}{}^T = R_{G\rightarrow T} \tag{3}$$

Besides skeletal joint angles, rotation matrices can be used throughout in motion capture systems to describe movement of the anatomical and technical frames within the global reference frame, the transformation between technical and anatomical frames and even the alignment between two different global frames when comparing data from two different motion capture systems. Rotation matrices and their transposes also allow for easy transformations and rotations of vectors and point coordinates between different frames through simple matrix multiplication. However,

[1] Originally coined to describe rotational alignment of two rings in a mechanical gimbal, the phrase "gimbal lock" also refers to related mathematical singularities which occur when describing rotations near multiples of 90° using Euler angle notation.

rotation matrices are not particularly efficient or numerically stable when subjected to highly iterative calculations because of their relatively large size (9 elements) and associated difficulties in enforcing the internal constraints of orthogonality and unity.

Due to the numerical challenges associated with rotation matrices, the most widely used notation for describing the orientation of frames is the unit quaternion, a four-element vector which is mathematically interchangeable with a rotation matrix by a given function $f_{R\to q}$:

$$q_{T\to R} = f_{R\to q}(R_{T\to R}) = [q_1 \quad q_2 \quad q_3 \quad q_4] \tag{4}$$

As with rotation matrices, quaternions enable transformations and rotations between coordinate systems. However, quaternion mathematics differs somewhat and is typically seen as less intuitive to interpret. Nevertheless, quaternions are immune to gimbal lock, more efficient than rotation matrices and very simple to normalize.

1.3. Overview of Study

1.3.1. Motivation

This study forms part of efforts to develop technical capacity for quantitative human movement analysis within the department's biomedical engineering research group. As discussed in Section 1.1.1, movement analysis is utilized in a wide variety of healthcare, industrial and recreational applications. Innovation in these types of applications requires some level of engineering expertise to be realized. Moreover, advancements in motion capture technologies within the last decade suggest that the field will continue to grow in significance in years to come (Section 1.1.2). The knowledge gained from this thesis will also prove valuable in a number of future research projects within the research group involving computational modeling of musculoskeletal biomechanics, design of biomedical devices for telemedicine and the development of bio-mechatronic devices such as prosthetics. The biomedical research group also aims to use the capabilities gained from this study to collaborate more extensively with other research groups in disciplines such as Robotics, Physiology, Orthopedics, Physiotherapy and Sports Science.

In comparison to gait analysis, sports analysis poses additional technical challenges when collecting and analyzing motion capture data (Section 1.1.3). Therefore, high performance sports analysis was chosen as the topic for this thesis to develop technical expertise in the research group in the two leading motion capture

technologies: optical and IMMS systems (Section 1.2). Two sports movements were chosen as case studies of IMMS and optical motion capture applications: road cycling and rugby union goal kicking respectively (Figure 9). These two sports play an important role in the health and wellness of in South Africa, and are also very well suited as demonstrators for skills in motion capture and human movement analysis.

(Image top left: http://blog.bgindy.com)

(Image top left: http://www.gilbertrugbyblog.com)

Figure 9: Broad work scope and key features of sporting movements chosen as case studies for this project

Road cycling is an ideal case study for mobile IMMS technologies as field-testing for cycling requires outdoor tracking over large distances, which is not possible with optical systems. The ultimate goal in this regard is to be able to measure biomechanical outcomes for the whole body during field-testing on the road. This kind of information would enable real-time feedback applications for dynamic bicycle fitting services or ecologically valid research into ways of enhancing performance or preventing injury. However, to the author's knowledge this feat has not yet been achieved as these measurements are not all feasible. Nonetheless, the cycling motion is a closed loop mechanical system with a number of domain constraints which could be incorporated into novel sensor fusions schemes to improve IMMS tracking accuracy. The development and validation of such mathematical algorithms for wireless IMMSs - attached to the cyclist or bicycle - form the bulk of the design work for this thesis.

In contrast to cycling, rugby union goal kicking is a complex movement that is poorly understood scientifically, providing an opportunity to apply technique analysis to it for the first time using gold-standard optical motion capture methods. Therefore, the major part of the experimental analysis component for this thesis is covered by the work on rugby goal kicking. These studies also form part of a larger research project in collaboration with the national goal kicking coach which aims to develop scientific

coaching methods for youth. The envisaged end result is the development of a country-wide goal kicking program for coaches, which would make a considerable impact on the sport nationally.

1.3.2. Problem statement and objectives

An important goal in road cycling science is comprehensive in-field analysis of cyclist biomechanics. A few recent studies have investigated the use of wireless IMMSs for real-time outdoor analysis of individual cycling parameters [47-51]. Even so, a number of challenges remain to the feasibility of measuring full-body cycling kinematics on the road with IMMSs. The first challenge is that the cycling movement is sustained over long periods of time and exhibits large and continuous centripetal accelerations. This compromises IMMS tracking of the gravity reference vector and ultimately leads to drift errors using standard IMMS sensor fusion algorithms. The author could find only one published IMMS algorithm addressing this problem in which a gyroscope reset method was used to track knee joint angles with no drift [49]. However, the study in [49] was limited in a few important aspects: it was conducted with two-dimensional sensors and not three-dimensional sensors, accelerometers were not used for gravity sensing and the results excluded hip joint angles. Hip angles require tracking of the pelvis segment, which is subject to notable soft tissue artifacts when moving between different postures and hip flexion angles [52]. Since typical anatomical frame definitions involve standing calibrations, hip angle measurements during cycling can be significantly affected. Therefore, the first aim of the study was to

A1. Develop and validate an IMMS sensor fusion algorithm for analyzing hip joint angles during cycling which contains compensation for centripetal accelerations and investigates the effect of soft tissue artifacts in calibration.

The second challenge for IMMS tracking of cycling is continuous and time-varying magnetic interference near the pedals. Previous work has shown that this magnetic interference can be caused by ferromagnetic components present in many bicycles, which induces errors in IMMSs tracking of the heading reference vector during dynamic motion [47-48]. Moreover, magnetic disturbances can corrupt IMMS tracking during static calibration methods that estimate the sensor-to-segment frame alignment required to measure crank arm angles [40]. The crank angle is an important outcome in the analysis of a range of cycling biomechanics outcomes relating to

pedaling efficiency [53], bicycle fitting [54], muscle activation patterns [55] and joint angle kinematics [56] and kinetics [57]. However, one problem with measuring crank angles with IMMSs is that wired IMMSs cannot be used due to cable entanglement. Therefore, this measurement approach has only recently been made feasible with the use of wireless IMMSs. Again, only one study was found in the literature which used wireless IMMSs for measuring crank angles [58]. However, this study only measured the crank angle using gyroscope integration, which is only valid for 30 seconds or less. They also did not present a state-of-the-art sensor-to-segment frame method and instead manually fixed the IMMS to the crank arm, which can be unreliable. Therefore, the second aim of the study was to:

A2. Develop and validate an IMMS sensor fusion algorithm for measuring crank angles during cycling which contains compensation for magnetic interference and performs automatic sensor-to-segment frame alignment

In terms of rugby union goal kicking, a survey of the literature on three-dimensional motion capture studies of elite performance revealed a paucity of available research. Moreover, findings from experiments involving other kicking motions such as in-step soccer kicking and rugby league punting have limited applicability to rugby union goal kicking due to differences in ball geometry, placement and flight trajectory. Therefore, seminal three-dimensional motion capture studies of professional goal kicking biomechanics, and the relationship between technique and performance variables, are required to fill this gap in knowledge. Furthermore, the level of inter- and intra-subject variability is not known or understood for this population and such data would be an important reference for future studies. In particular, coaches may be interested in aspects of kicking technique which are easy to adjust through training interventions, such as movement patterns during the approach to the ball. Therefore, the final aim was to:

A3. Perform a technique and variability analysis of elite rugby union goal kicking using optical motion capture technology

1.3.3. Summary of thesis articles and co-author contributions

This thesis is submitted as a compilation of six articles either already accepted or submitted for publication in academic journals. These are evenly split between the two case study sports (cycling and rugby union) in two sections. The first section in the main body of the thesis contains three articles which cover the design work

conducted for cycling analysis using wireless IMMSs. All three of these articles were submitted to the ***IEEE Sensors Journal (impact factor: 1.85)***.

Paper 1 [59] in Section 2 addresses the first aim of the thesis (A1 in Section 1.3.2). It details the development of the Pendulum Filter, a nonlinear complementary filter for IMMS tracking during cycling. The Pendulum filter contains a novel algorithm for estimating and eradicating centripetal accelerations in order to improve tracking of an IMMS mounted on the thigh during pedaling. A validation of the Pendulum Filter and a proprietary IMMS sensor fusion algorithm using optical motion capture is presented, and give an analysis of the influence of soft tissue artifacts due to different anatomical frame calibration poses.

Nature of contribution	**Extent of contribution (%)**
Conceptualization, data collection, analysis, writing	100%

The following co-authors have contributed to Paper 1:

Name	**email address**	**Nature of contribution**	**Extent of contribution (%)**
Prof C Scheffer	NA (deceased)	Supervision	NA
Dr JH Muller	cobusmul@sun.ac.za	Supervision	NA

Paper 2 [60] in Section 3 addresses the second aim of the thesis (A2 in Section 1.3.2). This article presents a nonlinear complementary filter (the CRANK Filter) that enables the measurement of crank angles during cycling using a wireless IMMS. It also gives details on a novel method of benchmarking IMMS crank angle measurements against an optical motion capture system. This study exploits the kinematic constraints of a crank arm's planar motion to enable magnetometer-free crank arm tracking in conditions of severe magnetic disturbances and without the need for a sensor-to-segment calibration.

Nature of contribution	**Extent of contribution (%)**
Conceptualization, data collection, analysis, writing	100%

The following co-authors have contributed to Paper 2:

Name	email address	Nature of contribution	Extent of contribution (%)
Prof C Scheffer	NA (deceased)	Supervision	NA
Dr JH Muller	cobusmul@sun.ac.za	Supervision	NA

Paper 3 (SUBMITTED) in Section 4 addresses the second aim of the thesis (A2 in Section 1.3.2). This study advances the work from Paper 2 by developing functional calibration methods for obtaining the sensor-to-segment transformation of the crank arm IMMS. This approach also exploits additional kinematic constraints in the pedaling motion within a nonlinear complementary filter framework to track crank angle profiles. This study also presents an improved benchmarking method using stereophotogrammetry compared to the method in Paper 2.

Nature of contribution	Extent of contribution (%)
Conceptualization, data collection, analysis, writing	100%

The following co-authors have contributed to Paper 3:

Name	email address	Nature of contribution	Extent of contribution (%)
Prof C Scheffer	NA (deceased)	Supervision	NA
Dr JH Muller	cobusmul@sun.ac.za	Supervision	NA

The next three articles in the second section cover the experimental work done for the rugby goal kicking analysis using an optical motion capture system. All three studies involve analysis of the same data set of 15 expert rugby union goal kickers and each addresses the third aim of the study using different techniques and variables (A3 in Chapter 1.3.2). Also common to each study is the novel breakdown of the rugby union goal kick which was developed as part of the technique analysis. These studies were submitted to the UK ***Journal of Sports Science (impact factor 2:25)***.

Paper 4 [61] in Section 5 presents a study of the step angulation, step distances and foot positioning relative to the tee amongst professional rugby union goal kickers. The article reports the variability between kickers in the group as well as individual kicker variability between trials, and examines correlations between the technique variables as well between technique variables and anthropometric measures.

Nature of contribution	Extent of contribution (%)
Conceptualization, data collection, analysis, writing	100%

The following co-authors have contributed to Paper 4:

Name	email address	Nature of contribution	Extent of contribution (%)
Dr van den Heever	dawie@sun.ac.za	Supervision	NA

In **Paper 5 (SUBMITTED)** in Section 6, the results of an analysis of phase timing and body speed and acceleration during the approach to the ball are presented. In this study we describe the inter-individual and intra-individual variability of the approach variables and correlate them to a key performance variable: foot speed at ball contact.

Nature of contribution	Extent of contribution (%)
Conceptualization, data collection, analysis, writing	100%

The following co-authors have contributed to Paper 5:

Name	email address	Nature of contribution	Extent of contribution (%)
Dr JH Muller	cobusmul@sun.ac.za	Supervision	NA
Dr van den Heever	dawie@sun.ac.za	Supervision	NA

Paper 6 (SUBMITTED) in Section 7 contains an analysis of the rotational alignment to tee and target of the thorax, pelvis and feet. Along with the usual description of group and individual variability, it investigates the effect of the approach angle on these variables, as well as the relationships between them at different points in the kick. There is also analysis of the relative rotation of the thorax and pelvis (lumbar spine angle) in relation to theories involving the stretch-shortening cycle of muscles.

Nature of contribution	Extent of contribution (%)
Conceptualization, data collection, analysis, writing	100%

The following co-authors have contributed to Paper 6:

Name	email address	Nature of contribution	Extent of contribution (%)
Dr JH Muller	cobusmul@sun.ac.za	Supervision	NA
Dr van den Heever	dawie@sun.ac.za	Supervision	NA

1.4. References

[1] A. Godfrey, R. Conway, D. Meagher and G. ÓLaighin, "Direct measurement of human movement by accelerometry," *Med. Eng. Phys.*, vol. 30, no. 1, pp. 1364–1386, 2008.

[2] T. W. Lu and C. F. Chang, "Biomechanics of human movement and its clinical applications," *The Kaohsiung J. Med. Sci.*, vol. 28, no. 2, pp. S13-S25, 2012.

[3] L. Sosdian, F. Dobson, T. V. Wrigley, K. Paterson, K. Bennell, M. Dowsey and R. S. Hinman, "Longitudinal changes in knee kinematics and moments following knee arthroplasty: A systematic review," *The Knee*, vol. 21, no. 6, pp. 994-1008, 2014.

[4] C. P. Carty, H. P. Walsh, J. G. Gillett, T. Phillips, J. M. Edwards and R. N. Boyd, "The effect of femoral derotation osteotomy on transverse plane hip and pelvic kinematics in children with cerebral palsy: A systematic review and meta-analysis," *Gait Posture*, vol. 40, no. 3, pp. 333-340, 2014.

[5] H. Zhou and H. Hu, "Human motion tracking for rehabilitation - A survey," *Biomed. Signal Process Control*, vol. 3, no. 1, pp. 1-18, 2008.

[6] O. Terlemez, S. Ulbrich, C. Mandery, M. Do, N. Vahrenkamp and T. Asfour, "Master Motor Map (MMM)—Framework and toolkit for capturing, representing, and reproducing human motion on humanoid robots." *in IEEE-RAS Int. Conf. on Humanoid Robots (Humanoids'14)*, Madrid, 2014.

[7] R. Nakatsu and J. Hoshino, Entertainment Computing: Technologies and Application, vol. 112, New York: Springer, 2013.

[8] L. Wang, W. Hu and T. Tan, "Recent developments in human motion analysis," *Pattern Recognit.*, vol. 36, no. 3, pp. 585-601, 2003.

[9] D. Wang, F. Dai and X. Ning, "Risk Assessment of Work-Related Musculoskeletal Disorders in Construction: State-of-the-Art Review," *J. Constr. Eng. Manage.*, vol. 141, no. 6, pp. 04015008, 2015.

[10] D. W. Dunstan, B. Howard, G. N. Healy and N. Owen, "Too much sitting–a health hazard," *Diabetes Res. Clin. Pr.*, vol. 97, no. 3, pp. 368-376, 2012.

[11] H. W. Kohl, C. L. Craig, E. V. Lambert, S. Inoue, J. R. Alkandari, G. Leetongin and L. P. A. S. W. Group., "The pandemic of physical inactivity: global action for public health," *The Lancet*, vol. 380, no. 9838, pp. 294-305, 2012.

[12] F. K. Fuss, A. Subic, M. Strangwood and R. Mehta, Routledge handbook of sports technology and engineering, New York: Routledge, 2013.

[13] A. Huchez, D. Haering, P. Holvoët, F. Barbier and M. Begon, "Local versus global optimal sports techniques in a group of athletes," *Comput. Methods Biomech. Biomed. Engin.*, vol. 18, no. 8, pp. 829-838, 2015.

[14] G. Lorini, "The concept of movement before Giovanni Alfonso Borelli," *Arch Putti Chir Organi Mov.*, vol. 39, no. 1, pp. 147-54, 1991.

[15] A. Vesalius, De humani corporis fabrica (No. 4), San Francisco: Norman Publishing, 1998.

[16] G. Borelli, On the movement of animals. Translated by Maquet P, Berlin: Springer-Verlag, 1989.

[17] R. Baker, "The history of gait analysis before the advent of modern computers," *Gait Posture*, vol. 26, no. 1, pp. 331–342, 2007.

[18] L. Mündermann and S. A. T. Corazza, "The evolution of methods for the capture of human movement leading to markerless motion capture for biomechanical applications," *J. Neuroeng. Rehabil.*, vol. 3, no. 1, pp. 6-18, 2006.

[19] D. H. Sutherland, "The evolution of clinical gait analysis: Part II Kinematics," *Gait Posture*, vol. 16, no. 2, pp. 159-179, 2002.

[20] S. R. Simon, "Quantification of human motion: gait analysis—benefits and limitations to its application to clinical problems," *J. Biomech.*, vol. 37, no. 12, pp. 1869-1880, 2004.

[21] E. Foxlin, "Motion tracking requirements and technologies," in Handbook, 2002, pp. 163–210.

[22] A. Baca, P. Dabnichki, M. Heller and P. Kornfeind, "Ubiquitous computing in sports: A review and analysis," *J. Sports Sci.*, vol. 27, no. 12, pp. 1335-1346, 2009.

[23] T. Monnet, M. Samson, A. Bernard, L. David and P. Lacouture, "Measurement of three-dimensional hand kinematics during swimming with a motion capture system: a feasibility study," *Sports Engineering*, vol. 17, no. 3, pp. 171-181, 2014.

[24] R. K. Harle and A. Hopper, "Sports Sensing: An Olympic Challenge for Computing," *IEEE Computer*, vol. 45, no. 6, pp. 98-101, 2012.

[25] S. Jobson, A. Nevill, S. George, A. Jeukendrup and L. Passfield, "Influence of body position when considering the ecological validity of laboratory time-trial cycling performance," *J. Sports Sci.*, vol. 26, no. 12, pp. 1269–1278, 2008.

[26] A. Lees, "Technique analysis in sports: a critical review," *J. Sports Sci.*, vol. 20, no. 10, pp. 813-828, 2002.

[27] C. A. Putnam, "Sequential motions of body segments in striking and throwing skills: Descriptions and explanations," *J. Biomech.*, vol. 26, no. 1, pp. 125-135, 1993.

[28] F. Tinmark, J. Hellström, K. Halvorsen and A. Thorstensson, "Elite golfers' kinematic sequence in full-swing and partial-swing shots," *Sports Biomech.*, vol. 9, no. 4, pp. 236-244, 2010.

[29] M. L. Latash, "The Bliss of Motor Abundance," *Experimental Brain Research. Experimentelle Hirnforschung. Experimentation Cerebrale*, vol. 217, no. 1, pp. 1-5, 2012.

[30] N. Stergiou and L. M. Decker, "Human movement variability, nonlinear dynamics, and pathology: is there a connection?," *Hum. Movement Sci.*, vol. 30, no. 5, pp. 869-888, 2011.

[31] L. Seifert, C. Button and K. Davids, "Key properties of expert movement systems in sport," *Sports Med.*, vol. 43, no. 3, pp. 167-178, 2013.

[32] R. Bartlett, J. Wheat and M. Robins, "Is movement variability important for sports biomechanists?," *Sports Biomech.*, vol. 6, no. 2, pp. 224-243, 2007.

[33] E. Ceseracciu, Z. Sawacha and C. Cobelli, "Comparison of Markerless and Marker-Based Motion Capture Technologies through Simultaneous Data Collection during Gait: Proof of Concept," *PLoS ONE*, vol. 9, no. 3, pp. e87640, 2014.

[34] Y. Mengüç, Y. L. Park, H. Pei, D. Vogt, P. M. Austin, E. Winchell and C. J. Walsh, "Wearable soft sensing suit for human gait measurement," *Int. J. Robot. Res.*, vol. 33, no. 14, pp. 1748-1764, 2014.

[35] J. Edmison, M. Jones, T. Lockhart and T. Martin, "An e-textile system for motion analysis," *Stud. Health Technol. Inform.*, vol. 108, no. 1, pp. 292–301, 2004.

[36] A. M. Sabatini, "Estimating three-dimensional orientation of human body parts by inertial/magnetic sensing," *Sensors*, vol. 11, no. 2, pp. 1489-1525, 2011.

[37] F. L. Markley and D. Mortari, "How to estimate attitude from vector observations," *in Proceedings of the AAS/AIAA Astrodynamics Specialist Conference*, 1999.

[38] O. J. Woodman, "An introduction to inertial navigation," University of Cambridge Computer Laboratory, Cambridge, 2007.

[39] J. L. Crassidis, F.L. Markley and Y. Cheng, "Survey of nonlinear attitude estimation methods," *J. Guid. Control Dynam.*, vol. 30, no. 1, pp. 12-28, 2007.

[40] D. Roetenberg, H. Luinge and P. Slycke, "Xsens MVN: Full 6DOF Human Motion Tracking Using Miniature Inertial Sensors," Xsens Technologies B.V., 8 April 2009. [Online]. Available: http://www.xsens.com/images/stories/PDF/MVN_white_paper.pdf. [Accessed 10 January 2010].

[41] G. Wu, F. C. Van der Helm, H. D. Veeger, M. Makhsous, P. Van Roy, C. Anglin and B. Buchholz, "ISB recommendation on definitions of joint coordinate systems of various joints for the reporting of human joint motion—

Part II: shoulder, elbow,wrist and hand," *J. Biomech.*, vol. 38, no. 5, pp. 981-992, 2005.

[42] G. Wu, S. Siegler, P. Allard, C. Kirtley, A. Leardini, D. Rosenbaum and I. Stokes, "ISB recommendation on definitions of joint coordinate system of various joints for the reporting of human joint motion—part I: ankle, hip, and spine," *J. Biomech.*, vol. 35, no. 4, pp. 543-548, 2002.

[43] A. Cappozzo, U. Della Croce, A. Leardini and L. Chiari, "Human movement analysis using stereophotogrammetry: Part 1: theoretical background," *Gait Posture*, vol. 21, no. 2, pp. 186-196, 2005.

[44] S. L. Delp, F. C. Anderson, A. S. Arnold, P. Loan, A. Habib, C. T. John and D. G. Thelen, "OpenSim: open-source software to create and analyze dynamic simulations of movement," *IEEE T. Bio-Med. Eng.*, vol. 54, no. 11, pp. 1940-1950, 2007.

[45] U. Della Croce, A. Leardini, L. Chiari and A. Cappozzo, "Human movement analysis using stereophotogrammetry: Part 4: assessment of anatomical landmark misplacement and its effects on joint kinematics," *Gait Posture*, vol. 22, no. 1, pp. 226-237, 2005.

[46] A. Leardini, L. Chiari, U. D. Croce and A. Cappozzo, "Human movement analysis using stereophotogrammetry: Part 3. Soft tissue artifact assessment and compensation," *Gait Posture*, vol. 21, no. 2, pp. 212-225, 2005.

[47] S. Cockcroft and C. Scheffer, "Determining the feasibility of measuring outdoor road cycling kinematics using inertial motion capture technology," *SAIEE Africa Research Journal*, vol. 102, no. 1, pp. 31 – 39, 2011.

[48] J. Cockcroft, "An evaluation of inertial motion capture technology for use in the analysis and optimization of road cycling kinematics," University of Stellenbosch, Stellenbosch, 2011.

[49] R. Marin-Perianu, M. Marin-Perianu, P. Havinga, S. Taylor, R. Begg, M. Palaniswami and D. Rouffet, " A performance analysis of a wireless body-area network monitoring system for professional cycling," *Pers. Ubiquit. Comput.*, vol. 17, no. 1, pp. 197-209, 2013.

[50] Y. Zhang, K. Chen and J. Yi, "Rider trunk and bicycle pose estimation with fusion of force/inertial sensors," *IEEE T. Bio-Med. Eng.*, vol. 60, no. 9, pp. 2541-2551, 2013.

[51] J. Xu, X. Nan, V. Ebken, Y. Wang, G. Pottie and W. Kaiser, "Integrated Inertial Sensors and Mobile Computing for Real-Time Cycling Performance Guidance via Pedaling Profile Classification", *J. Biomed. Inform., IEEE*, vol. 19 no. 2, pp. 440-445, 2014.

[52] R. Hara, M. Sangeux, R. Baker and J. McGinley, "Quantification of pelvic soft tissue artifact in multiple static positions," *Gait Posture*, vol. 39, no. 2, pp. 712-717, 2014.

[53] R. R. Bini, P. A. Hume and A. Cerviri, "A comparison of cycling SRM crank and strain gauge instrumented pedal measures of peak torque, crank angle at peak torque and power output," *Procedia Eng.*, vol. 13, pp. 56-61, 2011.

[54] V. Ferrer-Roca, A. Roig, P. Galilea and J. García-López, "Influence of saddle height on lower limb kinematics in well-trained cyclists: Static vs. dynamic evaluation in bike fitting," *J. Strength Cond.*, vol. 26, no. 11, pp. 3025-3029, 2012.

[55] F. Hug and S. Dorel, "Electromyographic analysis of pedaling: a review," *Journal of Electromyography and Kinesiology*, vol. 19, no. 2, pp. 182-198, 2009.

[56] R. R. Bini, P. A. Hume and J. Croft, "Cyclists and triathletes have different body positions on the bicycle," *Eur. J. Sport Sci.*, vol. 14, no. 1, pp. S109-S115, 2014.

[57] S. J. Elmer, P. R. Barratt, T. Korff and J. C. Martin, "Joint-specific power production during submaximal and maximal cycling," *Med Sci Sports Exerc*, vol. 43, no. 10, pp. 1940-1947, 2011.

[58] T. Kitawaki and H. Oka, "A measurement system for the bicycle crank angle using a wireless motion sensor attached to the crank arm," *J. Sci. Cycling*, vol. 1, no. 2, pp. 13–19, 2013.

[59] J. Cockcroft, J. Muller and C. Scheffer, "A novel complimentary filter for tracking hip angles during cycling using wireless inertial sensors and dynamic acceleration estimation," *IEEE Sensors J.*, vol. 14, no. 8, pp. 2864 - 2871, 2014.

[60] J. Cockcroft, J. H. Muller and C. Scheffer, "A complementary filter for tracking bicycle crank angles using inertial sensors, kinematic constraints and vertical acceleration updates," *IEEE Sensors J.*, vol. 15, no. 8, pp. 4218 - 4225, 2015

[61] J. Cockcroft, D. van den Heever, "A descriptive study of step alignment and foot positioning relative to the tee by professional rugby union goal kickers ," *J. Sports Sci.*, "In-press", 2015

2. Paper 1: A Novel Complementary Filter for Tracking Hip Angles during Cycling using Wireless Inertial Sensors and Dynamic Acceleration Estimation

Abstract: *As wireless motion sensors become more compact and robust, new opportunities emerge to develop wearable measurement technologies for in-field sports analysis. This paper presents a nonlinear complementary filter for tracking 3-D hip joint angles during cycling using inertial and magnetic measurement systems (IMMSs). The filter utilizes a novel method of dynamic acceleration compensation in the sensor frame based on the assumption of pendulum motion of the thigh around the hip joint center. A dynamic calibration is proposed in which the center of rotation of the thigh IMMS can be estimated during a functional hip movement in standing. Validation results from a gold-standard optical system showed that the filter IMMS tracking is drift-free with mean absolute errors of less than 3° for all IMMS axes combined at low, medium, and high pedaling speeds. Hip angles were also validated using the Vicon biomechanical model for standing and sitting calibration poses as well as true and normalized soft tissue artifact (STA). The best mean absolute errors for the sagittal, frontal, and transverse planes were 0.8°, 6.7°, and 2.2°, respectively. Variability due to calibrations and STA ranged from 1.4° to 8.1°. This demonstrates the high accuracies possible for IMMS tracking using algorithms designed for specific sports despite larger errors due to modeling.*

Citation:

J. Cockcroft, J. H. Muller and C. Scheffer, "A novel complementary filter for tracking hip angles during cycling using wireless inertial sensors and dynamic acceleration estimation," *IEEE Sensors J.*, vol. 14, no. 8, pp. 2864 – 2871, Aug. 2014.

2.1. Introduction

In the past, sports science research has been conducted using laboratory-based measurement technologies. Inevitably, the ecological validity of findings in these controlled environments has been debated [1]–[3]. However, the development of compact wearable sensors is now enabling in-field biomechanical analysis for a growing number of sports [4], [5]. An example of this is inertial and magnetic measurement systems (IMMSs), small wireless sensor units containing orthogonal triads of accelerometers, gyroscopes and magnetometers [6]. IMMSs have the key

advantage of tracking their own orientation proprioceptively without the external infrastructure required by other motion capture systems [7], [8]. This enables outdoor tracking of three-dimensional body segment orientation and multi-segment outputs such as joint angles using biomechanical modeling techniques [9]. However, despite utilization in a number of human movement applications such as pedestrian tracking [10], clinical gait analysis [11], activity monitoring [12] and rehabilitation [13], the full-scale adoption of IMMSs in sports science is hindered by a lack of accuracy in joint angle estimation.

IMMS joint angle estimation is a two-step process: tracking the IMMSs attached to the body and then transforming IMMS orientations to an anatomical coordinate frame (ACF) defined for each segment. Therefore, the two primary sources of error in IMMS joint angle estimation are misalignment of IMMSs in relation to their segment ACFs, and error in IMMS tracking. IMMSs are unable to directly measure ACF orientation, necessitating calibrations in which the IMMS-to-segment orientation is estimated from a static pose with known ACF orientations [9]. Although further dynamic calibrations can then be implemented for correcting knee joint axis misalignment, a weakness of IMMS joint angle estimation is that the orientation of the pelvis is unknown during calibration, directly affecting the reliability of hip joint output. Moreover, variable and transient misalignment can occur due to the well-known effects of soft tissue artifact (STA).

A variety of algorithms exist for IMMS tracking, all of which ‘blend’ two measurements of the IMMS orientation. The first type of measurement is gyroscope tracking, using strapdown integration methods, which provides excellent high frequency motion registration. However, it suffers from well-known drift and quantization errors and requires external initialization due to a lack of absolute measurements [14]. In the second method, accelerometers and magnetometers track orientation by sensing Earth’s gravitational and magnetic fields, respectively, using static frame vector-matching techniques. Conversely, this provides absolute measurements with good accuracy at low frequencies but high levels of noise during rapid motion or magnetic interferences [15]. Therefore, all IMMSs utilize some form of mathematical sensor fusion to exploit these complementary measurement features.

Crassidis *et al.* [16] provide a comprehensive survey of research developments in the area of orientation tracking algorithms. The traditional ‘workhorse’ for optimal IMMS sensor fusion is the extended Kalman filter (EKF) which has performed well

in many applications. However, the EKF has known limitations, most significantly its basis upon a linearization of the system. Efforts to overcome this have led to the development of more sophisticated statistical optimization methods such as unscented Kalman and particle filters. Secondly, the large covariance matrices of an EKF make it notoriously difficult to tune [17]. From early years this drove the utilization of simpler deterministic complementary filters that require the tuning of only one or two scalar gains [18]. More recently, more robust non-linear complementary filters have been developed for UAV tracking [19] that have shown comparable performance to the EKF. Non-linear observers have the desirable feature of being asymptotically stable, i.e. converging from any initial condition [20].

Other developments in IMMS tracking have focused on the incorporation of prior knowledge about the system [14]. For example, non-holomic constraints such as zero lateral velocity have also been successfully implemented in ground vehicle tracking [21], [22]. In pedestrian tracking using foot-mounted IMMSs, updates for zero velocity, zero-attitude and zero-integrated heading rate during strategic points in a movement have also yielded improvements to tracking accuracy [10]. In multi-IMMS body-networks, holonomic constraints on the degrees of freedom in an anatomical joint of the body model can reduce orientation errors [23]. Without aiding sensors such as Global Positioning Systems (GPS), a crucial aspect of IMMS tracking is compensation for dynamic accelerations which otherwise corrupt gravity estimates and cause drift errors. While basic methods employ time-averaging in the sensor coordinate frame [24], this is susceptible to bias errors due to centripetal accelerations [25]. To the authors' best knowledge there is only one published method for centripetal acceleration compensation in the sensor frame, which is only relevant to UAV flight with a wind-speed sensor [26]. The majority of published methods are based on the assumption of zero-mean accelerations in the global frame [27], [28], although researchers have commented on the scarcity of details for these methods in scientific literature [29].

One sport which stands to benefit from IMMS technology is road cycling, where outdoor measurements could better inform efforts to improve biomechanical efficiency and minimize injury risk. However, there are also challenges. The movement is sustained over long periods of time and exhibits large and continuous centripetal accelerations, both of which lead to drift errors. The margins for improvement in body position are also small, requiring high accuracy. The feasibility of testing cycling using IMMSs has already been demonstrated with a proprietary

tracking algorithm [30], [31]. The authors could find only one published algorithm designed for cycling in which a gyroscope reset method was used to track joint kinematics with no drift [32]. However, the study in [32] was limited. It was conducted with two-dimensional sensors, accelerometers were not used for inclination sensing and the results excluded hip angles. The aim of this study was to develop a method for measuring hip angles in cycling which combines the measurement capabilities of IMMSs with the power and simplicity of non-linear complementary filtering.

2.2. Methods

2.2.1. Experiments

One subject was tested pedaling on a competition standard road bicycle attached to a stationary trainer in an indoor laboratory. The subject was instructed to cycle for three consecutive 5-minute periods at a self-selected slow (measured cadence ≈ 45 rpm), medium (≈ 65 rpm) and fast (≈ 85 rpm) pedaling speed respectively. Pelvis and thigh segment kinematics were measured using wireless IMMSs developed by Xsens (MTw Development Kit, B.V. Technologies, Enschede, Netherlands). The pelvis IMMS was attached to the sacrum and the left and right thigh IMMSs were fixed on the distal third on the line between the greater trochanter and the lateral epicondyle of the knee. To limit magnetic interference, the testing was conducted in a magnetically clean location according to recommendations proposed by Veeger et al. [33].

To validate the IMMS filter results, the orientation of each IMMS was also tracked using a gold-standard optical motion capture system (Vicon MX, Oxford Metrics Group, Oxford). Three passive-reflective markers were attached to a rigid L-shaped plastic cluster which was tightly taped to the casing of each IMMS. The cluster markers were then used to reconstruct the IMMS orientation in the Vicon laboratory frame according to the method proposed by Veeger et al. [33]. Pelvis and thigh segment markers were also placed on the subject according to the instructions for the standard Vicon Plug-in Gait biomechanical model. The hip joint angle output from the model was used as a ground-truth reference to validate the hip angles calculated using the IMMSs. Model calibrations for both systems were performed using a static T-pose. During the three speed trials the data from the IMMSs and Vicon were collected synchronously at 75 Hz with a trigger signal using the coaxial cables, ports and settings prescribed in the Xsens documentation.

2.2.2. Filter design

This study involved the adaptation of a passive complementary filter (PCF) from the class of deterministic non-linear observers proposed by Mahoney [20]. The output from the PCF is an estimate of the IMMS orientation q with respect to a north-east-up global frame, represented by the quaternion parameterization in Hamilton notation with

$$\hat{q} = [\hat{s}\ \hat{\boldsymbol{v}}] \tag{5}$$

where s is the scalar component, $\boldsymbol{v}$ is a three-element vector and the accent symbol $\hat{q}$ represents an estimate of the true quantity q. The filter receives three-dimensional measurement inputs from a gyroscope, accelerometer and magnetometer designated y_G, y_A and y_M respectively. The sensor models for each were:

$$y_G(t) = \omega^S(t) + b^S(t) \tag{6}$$

$$y_A(t) = a^S(t) - g^S(t) \tag{7}$$

$$y_M(t) = m^S(t) + d^S(t) \tag{8}$$

Here ω^S, a^S, g^S and m^S are three-dimensional vectors angular velocity, dynamic and gravitational accelerations and magnetic field intensity respectively. The gyroscope signal contains a bias b^S and the magnetometer signal contains magnetic field disturbances d^S. All terms are expressed in the sensor frame, designated by superscript S The relationship between q and ω is governed by the following differential equation for rigid body kinematics:

$$\hat{\dot{q}} = \frac{1}{2} q \otimes p(\hat{\omega}) \tag{9}$$

The symbol $\otimes$ in (9) refers to a quaternion multiplication and the pure quaternion form of ω is $p(\omega) = [0 \quad \omega\ ]$. The filter thus needs to estimate ω from (6) and use it to integrate (9) to track q from an initial condition q_0. This is done by compensating for b^S in (6) using (7-8). The basic structure of the PCF is given below. Details can be found in [20].

$$q_e = \hat{q} \otimes q_{SF} = [s_e \quad \boldsymbol{v}_e] \tag{10}$$

$$\omega_e = 2 s_e \boldsymbol{v}_e \tag{11}$$

$$\hat{b} = -K_I \omega_e \tag{12}$$

$$\hat{\omega} = y_G - \hat{b} + K_P\omega_e \quad (13)$$

Figure 10 gives a summary of the adapted PCF, hereafter named the Pendulum Filter since it is based on the assumption of pendulum motion for the thigh IMMS. The PCF estimates $\hat{\omega}$ according to equations (9-13). The filter performs online bias correction in (12) using an integrator and incorporates a feedback ω_e: the error between the last estimate $\hat{q}$ error and the orientation q_{SF} reconstructed with the accelerometer and magnetometer. The Factored Quaternion Algorithm (FQA) was chosen to calculate q_{SF} for this study as, unlike other methods, it decouples the effects of magnetic interference from the inclination angles [34]. The dynamic acceleration compensation method in Figure 10 is described next in Chapter 2.2.3.

The filter gain K_I was set at a value twenty times smaller than the proportional gain K_P, which was optimized for the slow, medium and fast trials individually. The optimization was conducted by running the filter through a 1D grid search of K_P between the extreme values of 0 (gyroscope tracking only) and 5 (effectively FQA only). The optimum gain value was chosen as the value resulting in the lowest combined minimum mean absolute error (CMAE) for all three axes. Thigh IMMS tracking and gain optimization was implemented for both the Pendulum Filter as well as the basic PCF without dynamic acceleration compensation (DAC), to allow for comparison, while only the PCF filter was used for the pelvis IMMS.

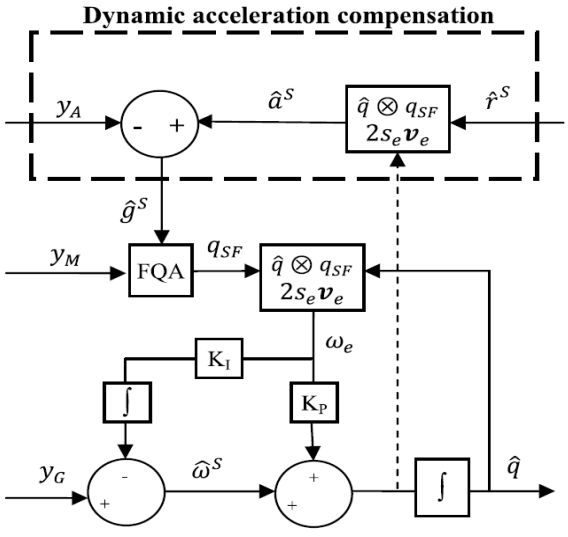

Figure 10: Block diagram of the Pendulum Filter with DAC

2.2.3. Dynamic acceleration compensation

One of the limitations of Mahoney's PCF in [20] is that it assumes that the dynamic acceleration in the sensor frame is both weak ($a^S \ll g^S$) and zero-mean. However, neither assumption holds for cycling where leg segments experience significant centripetal accelerations. In this study, the centripetal accelerations were sinusoidal with peaks of approximately $0.2g$, $0.6g$ and $1g$ for the slow, medium and fast pedaling speeds respectively. Separate tests showed that during sprinting cadences, a^S could exceed $3g$. Without DAC, a^S in (7) acts as noise which severely corrupts the accelerometer's estimate of gravity in (7). Figure 11 illustrates how the Pendulum Filter compensates for dynamic accelerations in the accelerometer signal in order to produce a better gravity estimate $\hat{g}^S$.

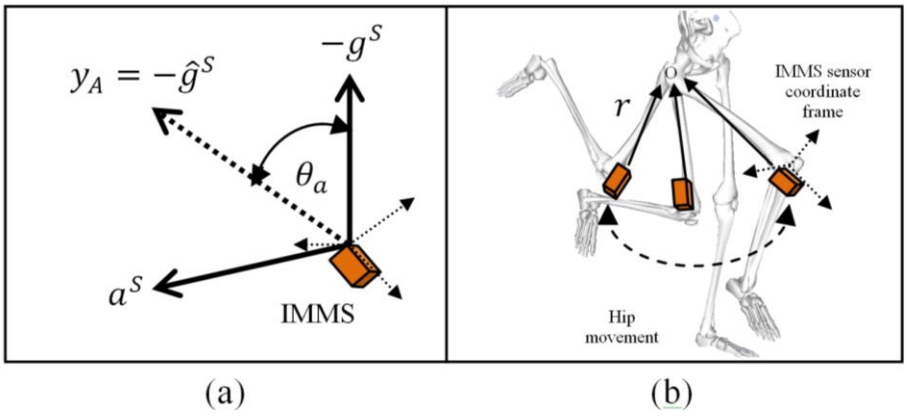

Figure 11: The (a) errors in gravity tracking without DAC and (b) the calibration hip movement (sagittal plane view)

As illustrated in Figure 11a, the uncompensated accelerometer estimate of $-\hat{g}^S$ (used as the vertical direction of the IMMS reference frame) causes an IMMS inclination error θ_a in q_{SF} proportional to the magnitude and direction of a^S. Estimation of a^S using a DAC method is thus highly desirable for improving orientation estimates. By including *a priori* information, namely the assumption of pendulum motion for the thigh segment, the acceleration of the thigh IMMS can be expressed in terms of the acceleration of the center-of-rotation (CoR) a_O and the radial and tangential accelerations a_r and a_t as in (14). By assuming that ${a_O}^S$ is negligible for the pelvis during cycling, (14) can be rewritten in terms of the angular velocity of the thigh and the CoR of the IMMS r^S as in (15).

$$a^S(t) = {a_O}^S(t) + {a_r}^S(t) + {a_t}^S(t) \tag{14}$$

$$= \frac{\mathrm{d}\omega^S}{\mathrm{dt}} \times r^S + \omega^S \times (\omega^S \times r^S) \quad (15)$$

Since the estimate $\hat{\omega}^S$ can be obtained from the PCF all that is required to make an estimate for a^S is an estimate of $\hat{r}^S$:

$$\hat{a}^S = \frac{\mathrm{d}\hat{\omega}^S}{\mathrm{dt}} \times \hat{r}^S + \hat{\omega}^S \times (\hat{\omega}^S \times \hat{r}^S) \quad (16)$$

The vector $\hat{r}^S$ was estimated in this study using a simple calibration procedure in which the subject, after standing still for 3 seconds in a single leg standing position, performed a repeated hip joint excursion for 5 seconds (see Figure 11b).

The key to the calibration is that it is also possible to track a^S by rearranging (16) into the form of (13). It is then possible to estimate the gravity vector g^S in (17) using (18).

$${a_{cal}}^S = y_A + \hat{g}^S \quad (17)$$

$$p(\hat{g}^S) = \hat{q} \otimes p(\hat{g}^S) \otimes \hat{q}^* \quad (18)$$

Here, $\hat{q}^*$ is a conjugated quaternion. Since the accelerometer signal y_A and the gravity vector in the global frame g^G in (17) are known, all that is needed to calculate $\hat{r}^S$ in (16) is the orientation $\hat{q}$ of the sensor during the movement in (18). Due to the short duration of the calibration, $\hat{q}$ can be estimated with sufficient accuracy by solving (9) using the orientation at standstill q_0 (calculated using FQA) and substituting y_G for ω. Thus, using gyroscope integration ${a_{cal}}^S$ was tracked in (17-18) and used to solve for $\hat{r}^S$ in (16). Furthermore, due to sensor noise a least squares algorithm was employed to optimize $\hat{r}^S$. In this study, a global grid search was employed to find the three elements of $\hat{r}^S$, and a MAE cost function E was chosen to be minimized as in (19).

$$E = \sum^t \| {a_{cal}}^S(t) - \hat{a}^S(t) \| \quad (19)$$

It should be noted that ${a_R}^S$ is highly corrupted by high frequency noise due to the numerical differentiation of ω^S in (14). Various filtering methods were attempted to attenuate the noise, and eventually a low-pass filter with a cut-off frequency of 15 Hz was chosen to smooth ${a_R}^S$.

2.2.4. Data analysis

The optimum gain values for the PCF and Pendulum Filters are given in Table 1. As expected, the optimal filter gain values decrease with increasing dynamic acceleration. It is clear from the higher Pendulum Filter gains that the Pendulum Filter weights q_{SF} more heavily and is thus more resilient to dynamic accelerations.

Table 1: Optimal filter gains

Filter	Slow	Medium	Fast
Passive	0.2	0.17	0.14
Pendulum	0.5	0.4	0.3

To compare Vicon measurements of $\hat{q}$ with the IMMS results it was necessary to align the reference frames for the two systems. The quaternion $q_{L\to I}$, representing the transformation between the laboratory and the IMMS frames, was obtained after a five minute stationary period using the average orientation output of the Xsens Kalman filter over one minute (assuming zero-mean static error) as in (20).

$$q_{L\to I} = {q^*}_{cluster} \otimes q_{kalman} \tag{20}$$

The Vicon marker trajectories were high pass filtered using the Vicon Woltring filter routine with an MSE setting of 20. Hip joint angles were defined, according to the Plug-in-Gait model conventions, as the orientation of the anatomical coordinate frame (ACF) of the distal femur relative to the ACF of the pelvis. Unlike in optical motion capture where the ACFs are defined by markers placed on anatomical landmarks, IMMS are unable to directly measure in the ACFs. IMMS-to-segment orientation $q_{S\to B}$ was calculated during a static pose calibration from q_S and an ACF orientation q_B as in (21).

$$q_{S\to B} = {q^*}_S \otimes q_B \tag{21}$$

Rather than assume the calibration values for q_B, both the pelvis and thigh segments $q_{S\to B}$ values were calculated using the Vicon Plug-in-Gait ACF orientations during two static trials: one standing in a T-pose position and the other sitting upright on the bike. The hip joint angles were then calculated using (22):

$$q_B = q_S \otimes {q^*}_{B\to S} \tag{22}$$

Furthermore, hip joint angles were also calculated using the Vicon marker trajectories and the Plug-in-Gait model in two ways. The first was the standard method of using the markers placed on the skin. The second involved the virtual reconstruction of the skin marker positions based on their relationship to the Vicon coordinate system attached to the segment IMMS. This allows for a more direct comparison between the filter tracking results by ensuring that the STA is the same for both systems. Hip joint angles were calculated in Euler angles for intuitive interpretation.

2.3. Results

2.3.1. IMMS orientation tracking

The accuracy of the PCF, Pendulum Filter and Xsens filter, defined as the combined MAE for all three axes (CMAE), is presented in Figure 12 for the slow, medium and fast trials.

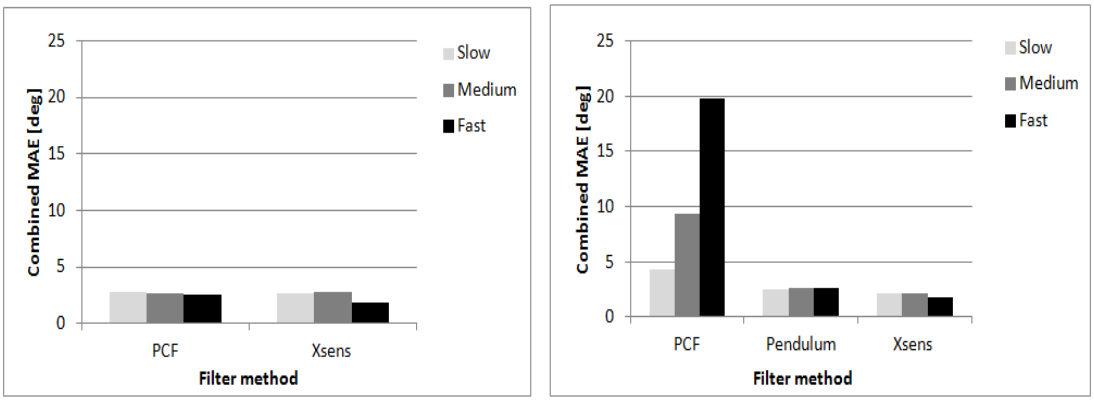

(a) (b)

Figure 12: Comparison of filter performances at different pedaling speeds for the (a) pelvis and (b) thigh IMMSs

It should be noted that the Pendulum Filter is only applicable to the thigh IMMS since the pelvis IMMS does not fulfill the assumption of pendulum motion. It can be seen from Figure 12a that the PCF performed very well in all three speed conditions for the pelvis IMMS, with CMAEs of 2.8°, 2.7° and 2.5° for slow, medium and fast pedaling. The Xsens filter performed within the MTw accuracy specifications with CMAEs of 2.7°, 2.6° and 1.9°. Figure 12b shows the average of the left and right thigh IMMS CMAEs. The PCF performed relatively well during slow pedaling (CMAE = 4.3°), with the errors then more than doubling for medium pedaling speed

(CMAE = 9.4°) and then more than doubling again for the fast trial (CMAE = 19.8°). The Pendulum Filter in Figure 12b, on the other hand, notably outperformed the PCF with CMAEs of 2.1°, 2.6° and 2.6° for the three trials respectively. This was only marginally higher than the Xsens filter, which produced CMAEs of 2.1°, 2.1° and 1.8° for slow, medium and fast pedaling. This equates to an average MAE < 1° for the three individual IMMS axes, which is very low and approaching the accuracy thresholds of both the IMMSs and Vicon validation method due to white noise.

2.3.2. Hip joint angle tracking

Since the Pendulum Filter accuracy was consistent across a range of dynamics, the effect of pedaling rate on hip joint angle accuracy was assumed negligible. Therefore, for the sake of brevity, the hip joint angles for the sagittal, frontal and transverse planes are only reported here for the fast pedaling trial (worst STA scenario). The hip angles were calculated with and without skin marker STA for the Vicon model, and using the sitting and standing segment calibrations for the IMMSs. Figure 13 shows hip joint angle curves for a representative pedal revolution chosen in the last minute of the trial. This allows for a visual illustration of the various factors affecting the accuracy of the results.

The difference between the IMMS results (shown in grey in Figure 13), which are calculated using the same sensor orientations, is predominantly influenced by the differences in STA during sitting and standing calibrations. This is attested by the constant offset between the curves. The dissimilarity between the two Vicon results (shown in black in Figure 13), on the other hand, is a result of the different STA effects local to the IMMS sensor (No STA condition) and the Vicon skin markers (STA condition). As would be expected, these manifest in more variable curve deformations due to differences in STA local to the IMMS and skin markers. Interestingly, the effects of skin marker STA are more pronounced near the bottom of the pedal stroke (minimum hip flexion), likely due to muscle contractions and movement of the ilio-tibial band when the leg is near full extension. Besides the effect of calibration pose on IMMS results and that of STA on the Vicon results, comparisons can also be made between Vicon and IMMS hip angle outputs. Quite clearly, the sitting calibration is more accurate (similar to the Vicon outputs) in comparison to the standing calibration, as evidenced by the solid grey curve being closer to the black curves.

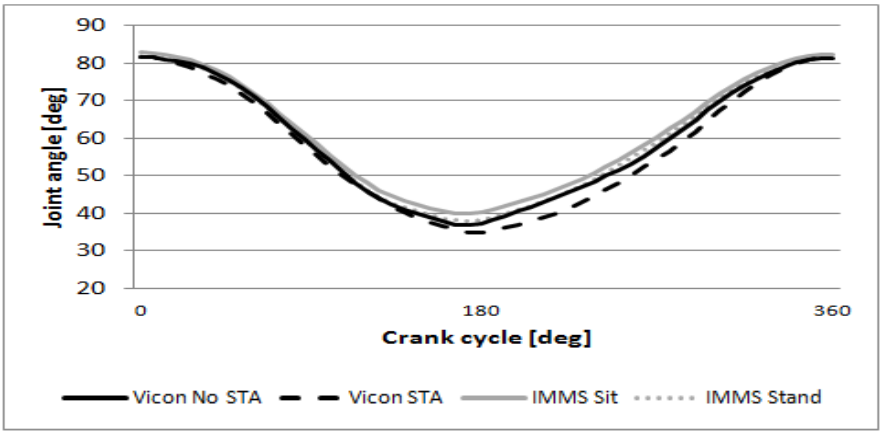

(b)

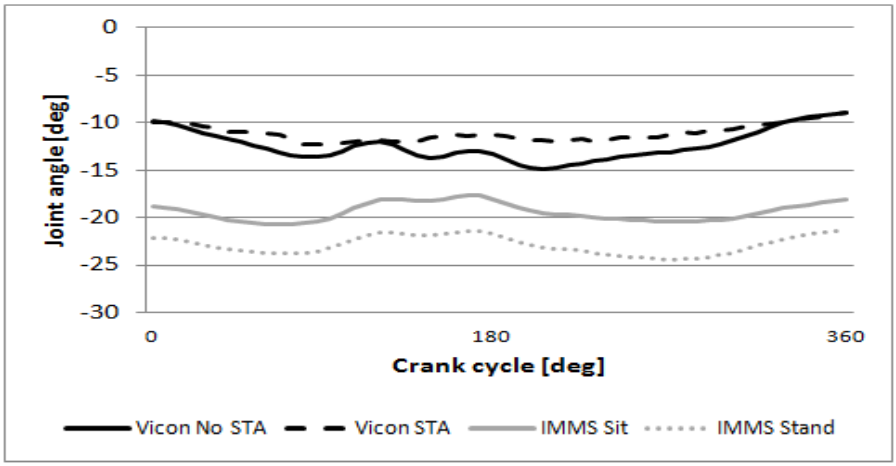

(b)

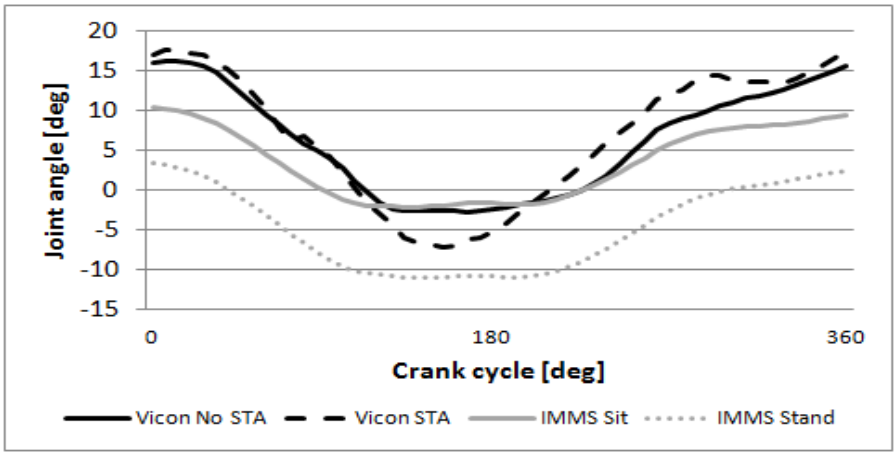

(c)

Figure 13: Representative hip (a) sagittal plane flexion (b) frontal plane abduction and (c) transverse plane rotation angles (internal rotations positive) for a crank cycle

Intuitively, the No STA curve shapes are also more similar to the IMMS shapes than the STA curves as they share a common STA locality on the IMMS. Nevertheless, a true comparison of the Vicon and IMMS systems would be between the IMMS standing and Vicon STA data. In addition to the comparison of Vicon and IMMS data, it is also of interest to investigate the effects of errors on the three different planes of motion of the hip. The dominant hip motion during cycling is flexion in the sagittal plane, demonstrated by the large hip flexion range of motion (>40°). Interestingly, however, hip flexion shows the least variation due to calibration pose amongst the three planes, which can be seen by the similarities in shape. Differences in absolute values, in contrast, are not clear from Figure 13 due to axis scaling. To provide more detail on shape and absolute errors, Table 2 and Table 3 give the squared correlation coefficients and MAEs between all four conditions.

Table 2: Hip angle squared correlation coefficients

	VICON		**IMMS**	
	No STA	**STA**	**Sit**	**Stand**
SAGITTAL PLANE (r^2)				
Vicon No STA		0.9832	0.9981	0.9980
Vicon STA			0.9875	0.9873
IMMS Sit				1.0000
IMMS Stand				
FRONTAL PLANE (r^2)				
Vicon No STA		0.9168	0.6054	0.6315
Vicon STA			0.7203	0.7287
IMMS Sit				0.9710
IMMS Stand				
TRANSVERSE PLANE (r^2)				
Vicon No STA		0.9539	0.9542	0.9605
Vicon STA			0.9703	0.9724
IMMS Sit				0.9984
IMMS Stand				

Table 3: Hip angle MAEs

	VICON		IMMS	
	No STA	**STA**	**Sit**	**Stand**
SAGITTAL PLANE (deg)				
Vicon No STA		2.1	2.2	0.8
Vicon STA			3.6	2.4
IMMS Sit				1.4
IMMS Stand				
FRONTAL PLANE (deg)				
Vicon No STA		1.2	6.9	10.5
Vicon STA			8.0	11.6
IMMS Sit				3.6
IMMS Stand				
TRANSVERSE PLANE (deg)				
Vicon No STA		2.9	2.2	9.9
Vicon STA			4.7	11.3
IMMS Sit				8.1
IMMS Stand				

The r^2 and MAE values in Table 2 and Table 3 can be used to compare the proportion of the errors due to STA on the Vicon results alone (top left block for each plane), to IMMSs calibrations alone (bottom left block), to STA between the systems (top to bottom of four top right blocks) and calibration between the systems (left to right). The analysis confirms that the IMMS hip flexion tracking was especially accurate compared to the Vicon STA results (all $r^2 > 0.98$ and MAE < 4°). As expected, the frontal and transverse plane tracking was less accurate than for the sagittal plane. CMAEs for both planes were over 10° for standing IMMS. However, both also showed improved MAEs when STA was made common and a sitting calibration was used. These improvements were cumulative, resulting in a reduction in both the frontal (MAE = 6.9°) and transverse (MAE = 2.2°) planes. Interestingly, while all transverse plane curve shapes were very similar ($r^2 > 0.95$), correlations were only moderate in the frontal plane between systems (0.6 - 0.73). Nevertheless, intra-system comparisons for the Vicon ($r^2 \approx 0.91$) and IMMS ($r^2 \approx 0.97$) and small inter-system differences suggest that the lower inter-system values are due to factors other than

STA or calibration. These factors remain unclear, but may be related to non-linear effects introduced by the Vicon Plug-in-Gait model's definition of the femur. Unlike the IMMS system, Vicon femur orientation is tracked using hip centers estimated from the pelvis skin marker positions. Another plausible reason is that the frontal plane hip range of motion is relatively small compared to errors between systems.

2.4. Discussion

This study successfully implemented the two key features required for tracking three-dimensional hip joint angles during cycling using IMMSs: IMMS tracking using complementary filtering and IMMS-to-segment calibrations using an optical motion capture system. Overall the results confirm a significant improvement in IMMS tracking using a novel adaptation to the PCF. The results also serve to validate the wireless MTw IMMS from Xsens, which performed within specifications. Furthermore, the study reports good accuracy in hip angle tracking compared to a gold-standard optical system. The analysis investigated the intra- and inter-system differences in hip angle outputs for all three anatomical joint planes of motion due to STA and calibration poses. One key finding was that the intra-system variability due to STA and calibration was in the same order of magnitude as the inter-system variability.

The IMMS tracking results highlight the influence of movement dynamics on filter performance when there is no DAC. Predictably, due to the low intensity of pelvis movement during cycling, the PCF performed very well for this segment at all speeds as well as for the thigh in the low pedaling speed trial. However, the medium and fast speeds violate the PCF's 'weak acceleration' assumption for the thigh IMMSs leading to large tracking errors. The Pendulum Filter tracking errors, on the other hand, were low and independent of pedaling dynamics. This demonstrates the efficacy of the CoR estimates from the dynamic calibration and the robustness of the DAC method. Moreover, with performance comparable to the advanced Xsens Extended Kalman filter, the Pendulum Filter supports claims that CFs can be implemented as successfully as EKFs [26].

Despite good IMMS tracking accuracy, the hip angle results demonstrate that the impact of segment calibration and STA on joint kinematics accuracy can be almost an order of magnitude larger than IMMS tracking errors. As is the case with most motion capture applications, the sagittal plane results were the most robust to changes

in calibration and STA, with negligible differences between systems. The errors in the other two planes, however, were both over 10° for the standing calibration pose, which is significant, although the curves display very similar shapes. The reduction in error using the sitting calibration pose suggests that the sensor to segment relationship changed between sitting and standing. This suggests, intuitively, that large STA errors may be introduced when the calibration pose is different to the movement pose - this is another noteworthy emphasis of the study. While the true effect of STA cannot be known either for Vicon or IMMS tracking without another gold-standard measurement (such as fluoroscopy), the results indicate that the STA for the two different systems was not significantly different in terms of CMAE. However, the shape of the graphs for the Vicon skin markers was different to the STA compensated Vicon outputs. This suggests that the sensor-to-segment orientation changed dynamically during the pendulum motion, changing the shape while still possibly maintaining a low MAE. This may affect the accuracy of analysis using variables such as range of motion.

The main contribution made by this study is that it describes a novel DAC method which is performed in the sensor frame, in contrast to the usual inertial frame approaches. The system utilizes a simple complementary filter structure which demonstrates that more complex Kalman filtering is not always necessary to achieve good results. The novel calibration method for finding the CoR is also an addition to other methods used to estimate joint centers in the upper limbs [36]–[38]. Clearly, the CoR for the thigh segment can add valuable information about segment inclination which might be exploited in any filtering algorithm and perhaps for other human movements besides cycling, such as walking and running. However, the Pendulum Filter works best when the hip joint center acceleration ${a_O}^S(t)$ in equation 10 is either negligible or known. In movements where the pelvis translates and ${a_O}^S(t)$ is not negligible it can still be estimated and compensated for if the pelvic orientation is accurately measured and gravity is removed. The CoR can also be estimated using a quick and simple dynamic calibration protocol that does not require any other instrumentation, making it suitable to implement in most testing conditions. The study also presents hip angle tracking for cycling using IMMS, which is currently sparse in the literature. The challenge of IMMS sensor-to-segment calibration is also highlighted, especially for the pelvis.

Nevertheless, the study has several limitations. Firstly, the IMMSs used were of a high quality, meaning that the sensor outputs are corrupted with less measurement

noise and thus subject to less drift error than genuine low-cost IMMSs. However, informal gyroscope integration tests revealed that drift error for the Xsens IMMSs is still large after more than 30 seconds. Even so, work with less expensive IMMSs would necessitate retuning of the filter gains and may result in different levels of accuracy. Secondly, further testing should be conducted with more subjects, on different bicycles and at higher speeds (> 100 rmp) to determine the sensitivity of the tracking accuracy to different levels of STA, movement and magnetic interference due to ferrous components. Furthermore, since the testing was performed indoors to facilitate the Vicon validation, the testing conditions excluded bicycle dynamics on the road. Further work thus needs to be done to understand the effects of accelerations due to a moving bicycle, which would require outdoor testing.

There is a clear need for developing innovative IMMS segment calibration methods which take the pose of the movement into account in order to reduce STA as well as modeling errors. The inherent limitations of static calibrations in which the segment pose is assumed could perhaps be overcome by the use of aiding technologies such as portable cameras, which could be used to provide segment poses on site similarly to the use of the Vicon in this study. It may also be beneficial to explore the optimization of IMMS placement to reduce both STA and accelerations due the CoR length.

2.5. Conclusion

This study presents a non-linear complementary filter with a novel DAC method applicable to tracking the orientation of an IMMS attached to the thigh during cycling. This method is based upon the assumption of pendulum motion for the thigh segment and was shown to drastically improve IMMS tracking for the same filter, especially with increasing pedaling cadences. Furthermore, while the DAC method is implemented in the sensor frame, it has very similar performance to the proprietary and industry-leading Xsens DAC method implemented in the inertial frame. The tracking of IMMSs on the pelvis and thigh of a cyclist allows for the calculation of useful biomechanical variables such as hip joint angles. Validation results proved that the IMMS hip joint outputs were highly accurate in the sagittal plane, and moderately so in the frontal and transverse planes. Factors affecting these errors were discussed; specifically the calibration methods used to align IMMSs to body segments and the inevitable STA. Nevertheless, it is shown that the hip joint angle accuracy in the

sagittal and transverse planes is sufficient to be used for biomechanical studies. Future work will expand the Pendulum Filter to a full lower body model.

2.6. References

[1] S. A. Jobson, A. M. Nevill, S. R. George, A. E. Jeukendrup, and L. Passfield, "Influence of body position when considering the ecological validity of laboratory time-trial cycling performance," *J. Sports Sci.*, vol. 26, no. 12, pp. 1269–1278, 2008.

[2] S. A. Jobson, A. M. Nevill, G. S. Palmer, A. E. Jeukendrup, M. Doherty, and G. Atkinson, "The ecological validity of laboratory cycling: Does body size explain the difference between laboratory- and field-based cycling performance?" *J. Sports Sci.*, vol. 1, no. 25, pp. 3–9, 2007.

[3] A. Jones and J. Doust, "A 1% treadmill grade most accurately reflects the energetic cost of outdoor running," *J. Sports Sci.*, vol. 14, no. 4, pp. 321–327, 1996.

[4] K. Baert *et al.*, "Technologies for highly miniaturized autonomous sensor networks," *Microelectron. J.*, vol. 37, no. 12, pp. 1563–1568, 2006.

[5] D. Gouwanda and S. M. N. A. Senanayake, "Emerging trends of bodymounted sensors in sports and human gait analysis," in *Proc. 4th Kuala Lumpur Int. Conf. Biomed. Eng., 2008*, Kuala Lumpur, Malaysia, pp. 715–718.

[6] D. Roetenberg, "Inertial and magnetic sensing of human motion," Ph.D. dissertation, Biomedical Technology Inst., Univ. Twente, Enschede, The Netherlands, 2006.

[7] C. Verplaetse, "Inertial proprioceptive devices: Self-motion-sensing toys and tools," *IBM Syst. J.*, vol. 35, nos. 3–4, pp. 639–650, 1996.

[8] E. Foxlin, "Motion tracking requirements and technologies," in *Handbook of Virtual Environment Technology*. Mahwah, NJ, USA: Lawrence Erlbaum Assoc., 2002, ch. 8, pp. 163–210.

[9] D. Roetenberg, H. Luinge, and P. Slycke. (2009, Apr.). *Xsens Homepage*

[Online]. http://www.xsens.com/images/stories/PDF/MVN_white _paper.pdf [Accessed 10 January 2010].

[10] R. Harle, "A survey of indoor inertial positioning systems for pedestrians," *IEEE Commun. Surv. Tuts.*, vol. 15, no. 3, pp. 1281–1293, Jul. 2013.

[11] A. Cutti, A. Ferrari, P. Garofalo, M. Raggi, A. Cappello, and A. Ferrari, "'Outwalk': A protocol for clinical gait analysis based on inertial and magnetic sensors," *Med. Biol. Eng. Comput.*, vol. 48, no. 1, pp. 17–25, 2010.

[12] K. Altun, B. Barshan, and O. Tunçel, "Comparative study on classifying human activities with miniature inertial and magnetic sensors," *Pattern Recognit.*, vol. 43, no. 10, pp. 3605–3620, 2010.

[13] H. Zhou and H. Hu, "Human motion tracking for rehabilitation—A survey," *Biomed. Signal Process. Control*, vol. 3, no. 1, pp. 1–18, 2008.

[14] O. J. Woodman, "An introduction to inertial navigation," Comput. Lab., Univ. Cambridge, Cambridge, U.K., Tech. Rep. 696, 2007.

[15] A. M. Sabatini, "Estimating three-dimensional orientation of human body parts by inertial/magnetic sensing," *Sensors*, vol. 11, no. 2, pp. 1489–1525, 2011.

[16] J. L. Crassidis, F. L. Markley, and Y. Cheng, "Survey of nonlinear attitude estimation methods," *J. Guid., Control, Dyn.*, vol. 30, no. 1, pp. 12–28, 2007.

[17] D. Simon, "A comparison of filtering approaches for aircraft engine health estimation," *Aerosp. Sci. Technol.*, vol. 12, no. 4, pp. 276–284, 2008.

[18] W. T. Higgins, "A comparison of complementary and Kalman filtering," *IEEE Trans. Aerosp. Electron. Syst.*, vol. AES-11, no. 3, pp. 321–325, May 1975.

[19] M. D. Hua, G. Ducard, T. Hamel, R. Mahony, and K. Rudin, "Implementation of a nonlinear attitude estimator for aerial robotic vehicles," *IEEE Trans. Control Syst. Technol.*, vol. 22, no. 1, pp. 201–213, Jan. 2014.

[20] R. Mahony, T. Hamel, and J. M. Pflimlin, “Nonlinear complementary filters on the special orthogonal group,” *IEEE Trans. Autom. Control*, vol. 53, no. 5, pp. 1203–1218, Jun. 2008.

[21] X. N. Y. L. Q. Zhang, Y. Cheng, and C. Shi, “Observability analysis of non-holonomic constraints for land-vehicle navigation systems,” *J. Global Position. Syst.*, vol. 11, no. 1, pp. 80–88, 2012.

[22] J. Pusa, “Strapdown inertial navigation system aiding with nonholonomic constraints using indirect Kalman filtering,” M.S. thesis, Dept. Math., Faculty of Science and Environmental Engineering, Tampere Univ. Technol., Tampere, Finland, 2009.

[23] H. J. Luinge, P. H. Veltink, and C. T. M. Baten, “Ambulatory measurement of arm orientation,” *J. Biomech.*, vol. 40, no. 1, pp. 78–85, 2007.

[24] V. T. van Hees *et al.*, “Separating movement and gravity components in an acceleration signal and implications for the assessment of human daily physical activity,” *PLOS ONE*, vol. 8, no. 4, pp. e61691, 2013.

[25] H. J. Luinge and P. H. Veltink, “Inclination measurement of human movement using a 3-D accelerometer with autocalibration,” *IEEE Trans. Neural Syst. Rehabil. Eng.*, vol. 12, no. 1, pp. 112–121, Mar. 2004.

[26] R. Mahony, M. K. J. Euston, P. Coote, and T. Hamel, “A non-linear observer for attitude estimation of a fixed-wing unmanned aerial vehicle without GPS measurements,” *Trans. Inst. Meas. Control*, vol. 33, no. 6, pp. 699–717, 2011.

[27] H. J. Luinge and P. H. Veltink, “Measuring orientation of human body segments using miniature gyroscopes and accelerometers,” *Med. Biol. Eng. Comput.*, vol. 43, no. 2, pp. 273–282, 2005.

[28] P. Rizun, “Optimal Wiener filter for a body mounted inertial attitude sensor,” *J. Navigat.*, vol. 61, no. 3, pp. 455–472, 2008.

[29] J. K. Lee, E. J. Park, and S. N. Robinovitch, “Estimation of attitude and external acceleration using inertial sensor measurement during various dynamic conditions,” *IEEE Trans. Instrum. Meas.*, vol. 61, no. 8, pp. 2262–2273, Aug. 2012.

[30] J. Cockcroft, “An evaluation of inertial motion capture technology for use in the analysis and optimization of road cycling kinematics,” M.S. thesis, Dept. Mech. Mechatronic Eng., Stellenbosch Univ., Stellenbosch, South Africa, 2011.

[31] S. J. Cockcroft and C. Scheffer, “Determining the feasibility of measuring outdoor road cycling kinematics using inertial motion capture technology,” *SAIEE Africa Res. J.*, vol. 102, no. 1, pp. 31–39, 2011.

[32] R. Marin-Perianu *et al.*, “A performance analysis of a wireless bodyarea network monitoring system for professional cycling,” *Personal Ubiquitous Comput.*, vol. 17, no. 1, pp. 197–209, 2013.

[33] W. H. K. De Vries, H. E. J. Veeger, C. T. M. Baten, and F. C. T. Van Der Helm, “Magnetic distortion in motion labs, implications for validating inertial magnetic sensors,” *Gait Posture*, vol. 29, no. 4, pp. 535–541, 2009.

[34] Y. Xiaoping, E. R. Bachmann, and R. B. McGhee, “A simplified quaternion-based algorithm for orientation estimation from earth gravity and magnetic field measurements,” *IEEE Trans. Instrum. Meas.*, vol. 57, no. 3, pp. 638–650, Mar. 2008.

3. Paper 2: A Complementary Filter for Tracking Bicycle Crank Angles using Inertial Sensors, Kinematic Constraints, and Vertical Acceleration Updates

Abstract: *In-field tracking of crank angles is important for analyzing outdoor cycling biomechanics, but current encoder-based methods are expensive and time-consuming. Inertial and magnetic measurement systems (IMMSs) have the potential for minimally-invasive crank angle tracking, although errors due to magnetic interference and static calibration hinder performance. This paper presents a nonlinear complimentary filter, called the Constrained Rotational Acceleration and Kinematics (CRANK) filter, which estimates crank angles without magnetometer measurements or a static calibration for the crank arm IMMS. The CRANK filter removes drift errors by exploiting constraints on the kinematics of the crank arm relative to the bicycle frame. Three five minute cycling tests were conducted using stereophotogrammetry and two IMMSs; a slow (approximately 80 rpm) and medium (90 rpm) cadence test on a level surface and a fast cadence test (100 rpm) with the bicycle inclined at 20° to the ground. A novel two-segment methodology for collecting ground truth data with an optical motion capture system is presented. We also provide analysis of CRANK filter performance for simulated outdoor dynamics (lateral tilt and roll). The CRANK filter achieved absolute errors (AEs) of 0.9 ± 0.6°, 1.7 ± 1.4° and 1.8 ± 1.2° for the slow, medium and fast tests, outperforming a commercial Kalman filter which produced AEs of approximately 10°. Under simulated outdoor conditions the CRANK filter was only slightly less accurate (AEs ≈ 3°). The CRANK filter is shown to be accurate, drift-free, easy to implement and robust against magnetic disturbances, sensor positioning, bicycle inclination and bicycle frame dynamics.*

Citation:

J. Cockcroft, J. H. Muller and C. Scheffer, "A complementary filter for tracking bicycle crank angles using inertial sensors, kinematic constraints and vertical acceleration updates," *IEEE Sensors J.* , vol. 15, no. 8, pp. 4218 - 4225, 2015

3.1. Introduction

An important aim in sports technology innovation is accurate in-field monitoring of athlete performance [1]. This is being achieved through the design of compact, non-invasive portable systems capable of providing the desired outcomes [2], [3]. These

systems typically contain miniaturized hardware such as inertial sensors which can be attached to athletes in their competitive environment or integrated with their sporting equipment [4]. One application of this type of system is in the field of cycling biomechanics [5], where a number of studies have investigated the use of wireless inertial sensor systems for real-time outdoor analysis of key outcomes [6]–[11]. Nonetheless, comprehensive in-field analysis of cycling biomechanics using inertial sensors has not yet been achieved. One important variable in cycling biomechanics is the angular position of the crank arm with respect to the bicycle frame. The crank angle is used when analyzing a range of biomechanical outcomes such as pedaling efficiency [12], bicycle fitting [13], muscle activation patterns [14] and joint angle kinematics [15] and kinetics [16]. Nevertheless, current methods of crank angle tracking have several disadvantages.

Previous studies conducted in controlled laboratory environments relied on ergometers or instrumented bicycles fitted with encoders or potentiometers to track the crank angle, see [17], [18]. However, despite accurate crank angle outputs, ergometers reduce the ecological validity of the testing and encoders require costly, time-consuming and cumbersome modifications to the bicycle which are undesirable when testing subjects in succession or with expensive bicycles. Optical motion capture systems have also been employed to estimate the crank angle using reflective markers attached to the bicycle [19]. The realism of testing is improved with this method, although it presents other barriers to in-field use. Firstly, cameras are typically required to be stationary, making it unfeasible for tracking a bicycle on the road. Secondly, the proximity of the cyclist to the crank arm can compromise marker tracking due to camera occlusions. Lastly, since the state of the art is to only place markers on the crank arm, there is also an absence in the literature of a rigorous method for defining and capturing the crank angle relative to a bicycle frame orientation. Nevertheless, optical systems are highly accurate and thus useful for benchmarking the accuracy of new in-field methods. Therefore, one aim of this study was to present a thorough method of acquiring reliable ground truth estimates of crank angles using stereophotogrammetry.

Besides encoder- and camera-based approaches, inertial and magnetic measurement systems (IMMSs) - containing accelerometers, gyroscopes and magnetometers - have the potential of in-field crank angle tracking [20]. IMMSs are ideal for many sporting analysis applications due to their small size, low cost and proprioceptive motion sensing capabilities [21], [22]. However, one of the primary disadvantages of

orientation tracking using an IMMS is that the vector observations used to solve for the sensor orientation are subject to interference which leads to drift errors [23]. The inclination reference vector, an estimate of the gravity vector extracted from accelerometer measurements and used to determine roll and pitch angles, is easily corrupted by the occurrence of indistinguishable dynamic acceleration. Similarly, magnetic field measurements from the magnetometer are usually used as the heading reference vector, which is unreliable within a non-homogenous magnetic field. These disadvantages are relevant to the tracking of the crank arm orientation as cycling involves relatively large and persistent dynamic accelerations and variable magnetic interference due to ferromagnetic materials [6], [7]. Moreover, this compromises the ability of static calibration methods to provide the sensor-to-body rotations required to track the crank arm coordinate system (frame) using measurements in the sensor frame [24]. In efforts to overcome reference vector interference and drift error, researchers have proposed methods exploiting domain constraints [20], including updates for zero velocity, zero-attitude and zero-integrated heading rate at appropriate points in time [25] and various kinematic constraints [26]–[28].

In line with this approach, this study proposes a novel IMMS method of tracking the crank angle which does not use gravity and magnetic field reference vectors for the crank arm IMMS, and which does not require a sensor-to-segment calibration for the crank arm. Instead, this method is based on two algorithms developed to exploit domain constraints between the bicycle frame and the crank arm: a Vertical Acceleration Update (VAU) algorithm and a Kinematic Constraint Rotation (KCR) algorithm. The VAU assumes that the sum of the gravitational and radial acceleration vectors measured by a crank arm sensor would reach a maximum or minimum when the crank arm position is vertical i.e. aligned with gravity. The KCR, on the other hand, applies a simple hinge joint constraint to the crank arm rotation – effectively assuming that the crank arm has the same roll and yaw angle as the bicycle frame. In addition, both these domain constraints apply directly to the crank arm body frame and not the sensor frame, foregoing the need for static calibrations of the crank arm. The VAU and kinematic constraint were implemented within the nonlinear passive complementary filter (PCF) proposed by Mahony [29]. The PCF is simpler than the Kalman filter (KF), requires the tuning of only two scalar gains, is capable of online compensation for gyroscope bias and has shown comparable performance to the KF [30].

The aim of this study was to test the hypothesis that the VAU and KCR can be successfully employed to accurately estimate bicycle crank angles. This was done by conducting cycling experiments in a motion analysis laboratory whilst simultaneously tracking the crank angle with IMMSs and an optical motion capture system to provide ground truth data. A modified PCF, called the Constrained Rotational Acceleration and Kinematics (CRANK) filter, was developed to estimate the crank angle using the VAU and KCR, and its performance was compared to that of a commercial KF and the standard PCF which both use the traditional gravity and magnetic field estimates and static calibrations. The CRANK filter was also tested under simulated outdoor conditions (tilt and roll of the bicycle frame). The second aim was to propose a two-segment (crank and frame) method of defining and capturing the crank angle using optical motion capture systems.

3.2. Methods

3.2.1. Data collection

One subject was tested pedaling on a standard mid-range mountain bike attached to a stationary trainer in an indoor laboratory. The subject pedaled at a self-selected slow (cadence ≈78 rpm), medium (≈88 rpm) and fast (≈97 rpm) rotation speed for three consecutive 5-minute periods respectively. For the slow and medium cadence tests, the bicycle was positioned level with the laboratory floor (zero bicycle frame inclination angle), whereas the bicycle setup was changed for the fast test by securing the front wheel at a raised height such that the inclination of the bicycle was 20°. Two wireless IMMSs (MTw Development Kit, Xsens, B.V. Technologies, Enschede, Netherlands) were used to track the crank angle. The IMMSs were rigidly attached to the bicycle: one on the seat post and the other on the right surface of the left crank arm (the crank IMMS could not be placed on the lateral side of the crank arm due to foot obstructions). The crank angle was also estimated using a gold-standard optoelectronic motion analysis system (Vicon MX T-series, Vicon Motion Systems Ltd, U.K.) and reflective markers attached to the bicycle. The crank arm IMMS could not be tracked directly using markers as it had to be attached to the inside surface of the crank arm and markers would therefore not have been visible to the cameras. The IMMS and stereophotogrammetry data was collected synchronously at 120Hz.

3.2.2. Crank angle definition

In the absence of a formal mathematical definition in the literature, the crank angle was defined in this study using the relative orientation between two right-handed frames: one representing a bicycle body frame F and the other representing a crank arm body frame C (Figure 14). The axis X_F was chosen as the forward direction of the bike i.e. parallel to the line joining both wheel centers. Note that X_F does not necessarily lie parallel to the top bar or the ground if the wheels are not grounded (as with a stationary trainer). The perpendicular axis Z_F was defined as lying in the plane containing the longitudinal axes of the seat tube and X_F. Therefore, the crank arm C rotates in the XZ_F plane about the third orthogonal axis Y_F. Y_C is also perpendicular to the XZ_F plane and the YZ_C plane was defined as the plane containing Y_C and the longitudinal axis of the crank arm. The third crank axis X_C is defined, trivially, as the third orthogonal direction.

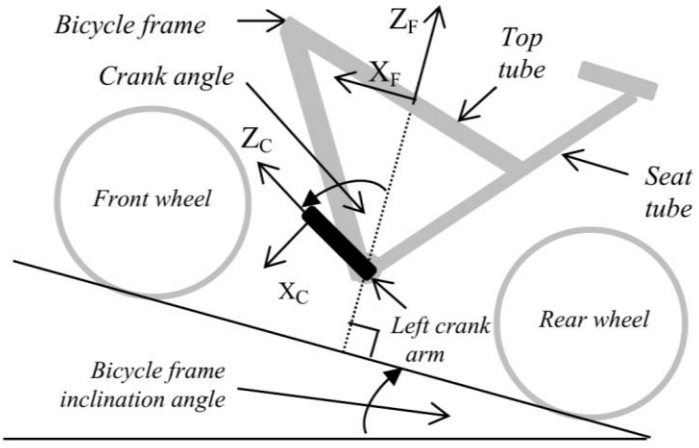

Figure 14: Side view showing crank angle as defined by the bicycle frame and crank arm axes.

In this study, the orientation of a rigid segment's body frame (B) relative to a global frame (G) is expressed in quaternion format according to the Hamiltonian convention in (23):

$$q_{segment}^{B\to G} = [s\ \boldsymbol{v}] \tag{23}$$

where s is a scalar and $\boldsymbol{v}$ is a three-element vector. The relative orientation $q_{CF}^{B\to B}$ between the body (B) frames F and C in Figure 14 is thus calculated using (24).

$$q_{CF}^{B\to B} = {q^*}_C^{B\to G} \otimes q_F^{B\to G} \tag{24}$$

Here, the superscript $*$ implies a conjugated quaternion and $\otimes$ represents a quaternion multiplication. This can be used to calculate the Euler angles as in (25):

$$f_{Q\to E}(q_{CF}^{B\to B}) = [A_Z \quad A_X \quad A_Y] \tag{25}$$

where $f_{Q\to E}$ is a standard function converting quaternions into Euler angles using a 3-1-2 rotation sequence. In this study, A_Z and A_X were assumed to be mechanically constrained to zero and A_Y was considered as the crank angle. Therefore, crank angle tracking relies on accurate tracking of $q_F^{B\to G}$ and $q_C^{B\to G}$.

3.2.3. Reference data from stereophotogrammetry

To track the crank angle using an optical motion capture system, the positions of reflective markers attached to the bicycle were measured with respect to a global laboratory frame L (Figure 15). The crank orientation $q_C^{B\to L}$, was tracked using a pedal marker M_{pedal} and a marker placed on the left and right centers of rotation of the crank hub (M_{right} and M_{left}). The line from M_{right} and M_{left} defined the primary axis Y_C, and the secondary axis Z_C was defined as perpendicular to Y_C in the plane formed by a marker attached to the end of the pedal shaft M_{pedal}, M_{right} and M_{left}. Due to mechanical constraints of planar crank arm motion relative to the bicycle frame, the lateral axis Y_F was taken to be parallel to Y_C - and was thus also taken as the primary axis of $q_F^{B\to L}$, running from M_{right} to M_{left}. The perpendicular axis X_F was defined using the vector running from M_{back} to M_{front}. M_{back} and M_{front} were placed on the end of rear and front wheel skewers to represent the height of the wheel center.

It was found that M_{right}^C and M_{left}^C were not clearly visible to the cameras during pedaling due to occlusions by the body. To overcome this problem, an additional marker M_{top}^B was attached to the bicycle frame (see Figure 15a). Assuming constant relative positions for markers attached to a rigid body, the position of M_{right} and M_{left} could be reconstructed during the dynamic tests using M_{top}, M_{front} and M_{back} and standard static calibration techniques (refer to Section 3.2.8 of the methodology for details). The reconstruction of M_{right} and M_{left} for the crank arm orientation estimate is based upon the assumption that these markers are attached to the axis of rotation of the crank hub and therefore in effect rigidly attached to both the bicycle frame and the crank arm.

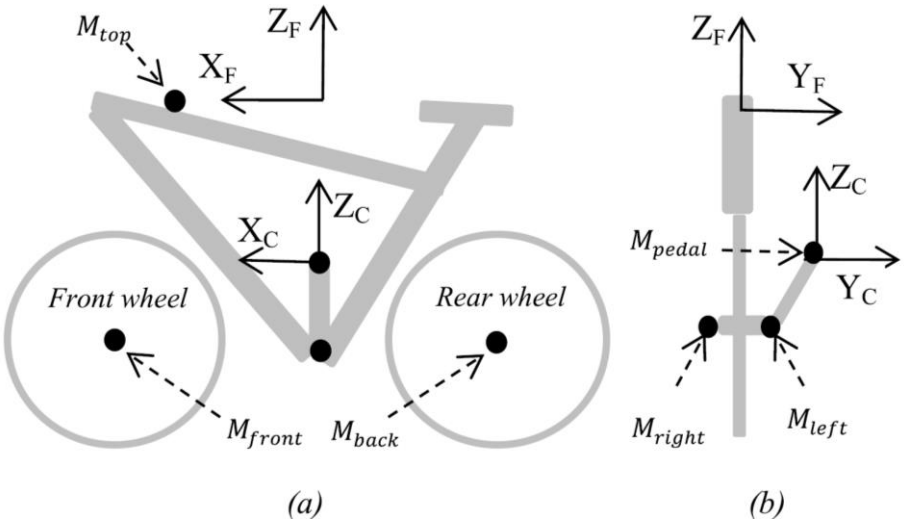

Figure 15: Marker placements used to track the bicycle and crank arm coordinate systems during stereophotogrammetry testing.

3.2.4. PCF structure

A nonlinear passive complementary filter (PCF) was used to track the orientation of the bicycle frame relative to an inertial north-east-up frame *I* [29]. The sensor inputs to the PCF were the three-dimensional measurements from the IMMS gyroscope, accelerometer and magnetometer; designated y_G^F, y_A^F and y_M^F respectively. The sensor models used were:

$$y_G^F(t) = \omega_F^S(t) + b_F^S(t) \tag{26}$$

$$y_A^F(t) = -g_F^S(t) + a_F^S(t) \tag{27}$$

$$y_M^F(t) = m_F^S(t) + d_F^S(t) \tag{28}$$

The superscript *S* refers to quantities expressed in the IMMS sensor frame and t is a discrete point in time at which measurements were taken. The first terms represent parameters of interest for the IMMS attached to the bicycle frame *F*; ω_F^S represents the angular velocity, g_F^S the gravitational component of acceleration and m_F^S the local magnetic field intensity. The second terms represent noise; a_F^S is the dynamic acceleration, b_F^S is the gyroscope bias and d_F^S is the disturbances to the local magnetic field intensity. As shown in Figure 16, the output of the PCF is the bicycle frame orientation $\hat{q}_B^{B\to I}$ – where the accent symbol ^ represents an estimated quantity. This is

obtained by rotating the orientation estimate $\hat{q}_F^{S\to I}$ using a static sensor-to-body frame calibration quaternion $\hat{q}_B^{S\to B}$ (see Chapter 3.2.8 for details).

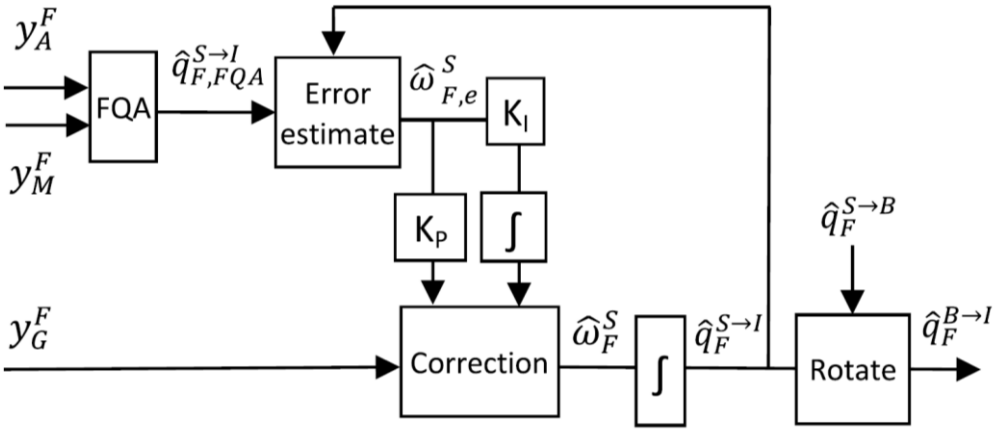

Figure 16: The PCF tracks the bicycle sensor frame orientation $\hat{q}_F^{S\to I}$ and then rotates it to obtain bicycle body frame orientation $\hat{q}_F^{B\to I}$

The PCF tracks $q_F^{S\to I}$ by estimating and integrating ω_F^S (Figure 16). This is done using the differential equation in (29) for rigid body kinematics relating $q_F^{S\to I}$ to ω_F^S:

$$\dot{q}_F^{S\to I}(t) = \frac{1}{2} q_F^{S\to I}(t-1) \otimes p(\omega_F^S(t)) \tag{29}$$

where $p(\omega_F^S) = [0 \quad \omega_F^S]$. It thus follows that

$$q_F^{S\to I}(t) = q_F^{S\to I}(t-1) + T\dot{q}_F^{S\to I}(t) \tag{30}$$

where T is the time between samples. The estimation of ω_F^S is achieved in the PCF by filtering noise from the gyroscope signal y_G^F in a correction step. The gyroscope error correction is implemented using an error feedback loop containing measurement error $\hat{\omega}_{F,e}^S$ as in (31) and (32).

$$\hat{\omega}_F^S(t) = y_G^F(t) - \hat{b}_F^S(t-1) + K_P\hat{\omega}_{F,e}^S(\mathrm{t}) \tag{31}$$

$$\hat{b}_F^S(t) = \hat{b}_F^S(t) + K_I\hat{\omega}_{F,e}^S(\mathrm{t}) \tag{32}$$

In (31), a proportional gain K_P is used as well as compensation for gyroscope bias b_F^S. The gyroscope bias was updated in (32) by integrating measurement error $\hat{\omega}_{F,e}^S$ using

integral feedback gain K_I. To calculate the error term $\hat{\omega}_{F,e}^{S}$, an error quaternion $\hat{q}_e$ is calculated using an orientation estimate $\hat{q}_{F,aux}^{S\to I}$, obtained from auxiliary sensors:

$$\hat{q}_e(t) \quad = \hat{q}_F^{S\to I}(t) \otimes \hat{q}_{F,aux}^{S\to I}(t) \tag{33}$$

The PCF converts the components of the error quaternion in (33) into an angular velocity feedback error $\hat{\omega}_{F,e}^{S}$ using (34).

$$\hat{\omega}_{F,e}^{S}(t) = 2s_e(t)\boldsymbol{v}_e(t) \tag{34}$$

In this study, the Factored Quaternion Algorithm (FQA) was used to estimate $\hat{q}_{F,aux}^{S\to I}$ in (33) using y_A^F and y_M^F [31]. In Figure 16, this is shown as $\hat{q}_{F,FQA}^{S\to I}$.

3.2.5. CRANK filter structure

The CRANK filter in Figure 17 is a modification of the PCF in Figure 16. It is designed to estimate the crank arm orientation $\hat{q}_C^{B\to I}$ directly, without magnetometer measurements as an input or a sensor-to-body frame rotation step at the end. Instead of the FQA, the CRANK filter uses a novel Vertical Acceleration Update (VAU) algorithm to provide the auxiliary estimate in (33). See Chapter 3.2.6 for details on the VAU. Similarly, the gyroscope signal y_G^C is transformed from the crank sensor frame to the crank body frame using a Kinematic Constraint Rotation (KCR) algorithm (see Chapter 3.2.7 for details). Therefore, the estimate $\hat{q}_{C,VAU}^{B\to I}$ of crank arm orientation is used to calculate the feedback error term $\hat{\omega}_{C,e}^{B}$. This is used to correct the rotated gyroscope signal $\hat{\omega}_{C,KCR}^{B}$.

The filter gain K_I was set at a value twenty times smaller than the proportional gain K_P for both the PCF and the CRANK filter. Tuning of K_P was performed for the filters using a grid search from 0 to 5 at a resolution of 0.1. The optimal K_P was the value which minimized errors with reference to ground truth data. For the crank arm tracking, this produced K_P values of 0.1 and 3.4 for the PCF and CRANK filter respectively. A value of 0.6 was obtained for optimal bicycle frame tracking. Crank arm tracking was implemented for the CRANK filter, the PCF and the Xsens KF, to allow for comparison. Only the PCF and Xsens KF were used for the bicycle frame tracking as the VAU and KCR do not apply.

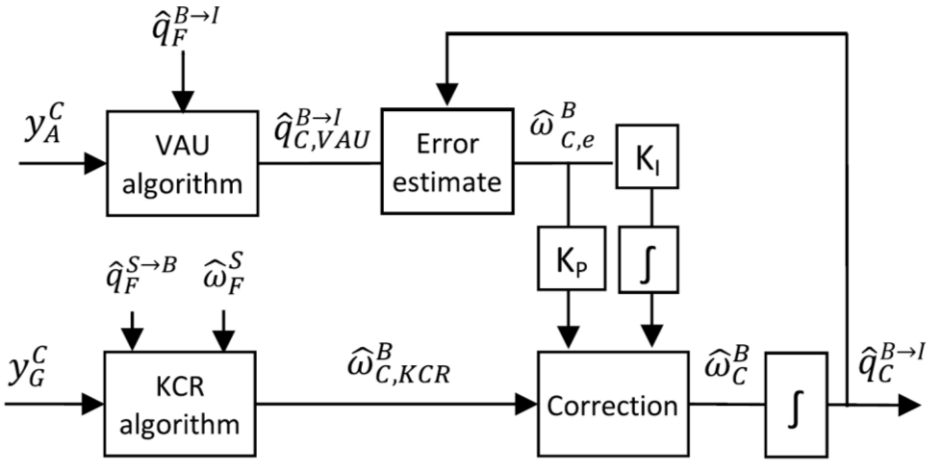

Figure 17: The CRANK filter uses the KCR and VAU algorithms to track the crank arm orientation without a magnetometer or rotations

3.2.6. The VAU algorithm for the CRANK filter

The VAU algorithm in Figure 17 operates on the magnitude of the crank IMMS acceleration smoothed with a 4th order low-pass Butterworth filter (cut-off frequency 10Hz). As shown in Figure 18, this acceleration consists of two dominant vector components: centripetal and gravitational acceleration.

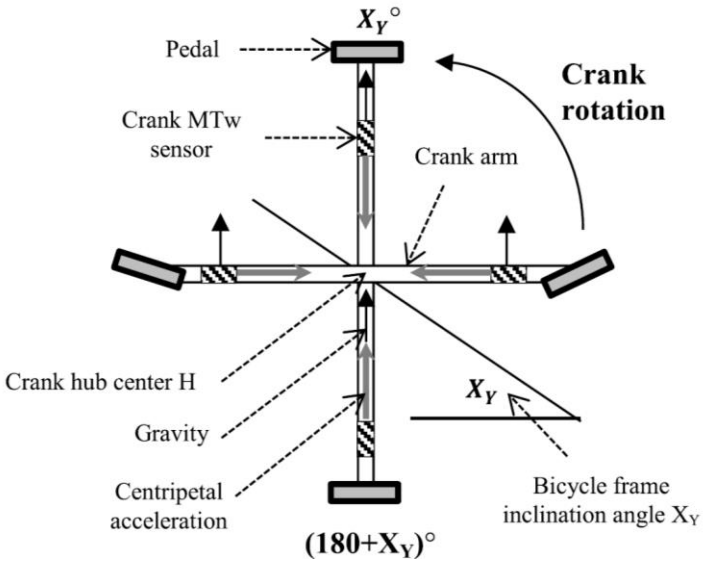

Figure 18: Direction of primary acceleration components measured by the crank IMMS at various crank angles (as viewed from the side).

The direction of the centripetal acceleration is constant in the sensor frame, while the gravity vector direction is variable in the sensor frame. Therefore, the magnitude of the accelerometer signal is sinusoidal in nature, peaking when the centripetal acceleration is vertical and reaching a minimum when the centripetal acceleration points down (Figure 19).

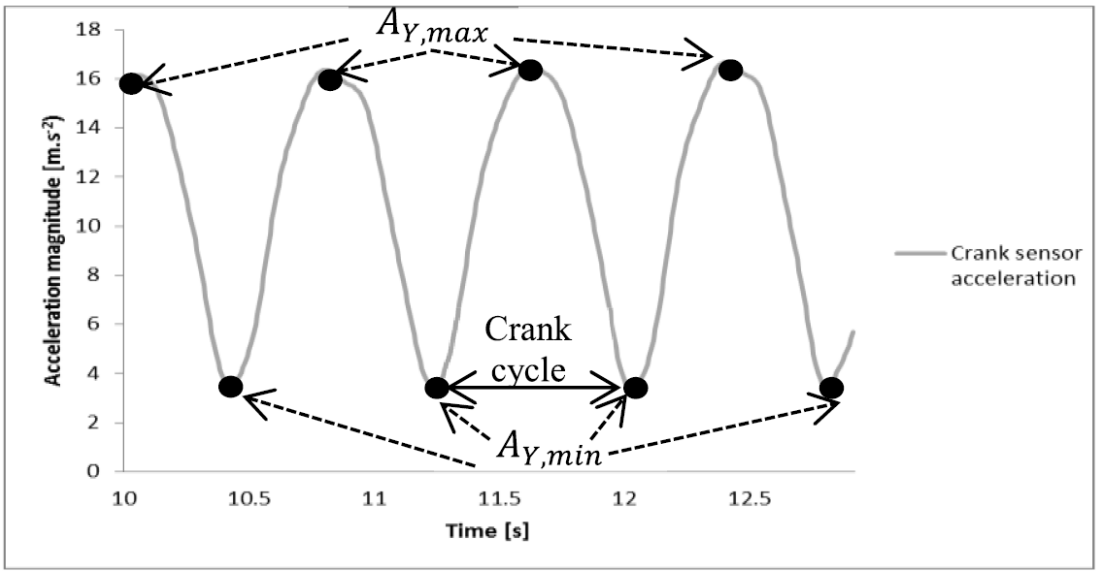

Figure 19: The maxima and minima of the acceleration magnitude of the crank arm IMMS correspond to known crank angles.

The VAU algorithm assumes that crank angle A_Y in (25) is equal to (180-X_Y)° when these two acceleration components are positively aligned and X_Y° when in opposite directions:

$$\hat{A}_{Y,max} = 180 + \hat{X}_Y \quad (35)$$

$$\hat{A}_{Y,min} = \hat{X}_Y \quad (36)$$

where the $\hat{x}_Y$ is the bicycle frame inclination angle from

$$f_{Q\to E}(\hat{q}_F^{B\to I}) = [\hat{X}_Z \quad \hat{X}_X \quad \hat{X}_Y] \quad (37)$$

Values for $\hat{A}_{max}$ and $\hat{A}_{min}$ are substituted into (38) to calculate the crank arm orientation relative to the bicycle frame, and then into (39) to obtain $\hat{q}_{C,VAU}^{B\to I}$ (Figure 17).

$$\hat{q}_{CF}^{B\to B} = f_{E\to Q}([0 \quad 0 \quad \hat{A}_Y]) \tag{38}$$

$$\hat{q}_{C,VAU}^{B\to I} = \hat{q}_F^{B\to I} \otimes \hat{q}_{CF}^{B\to B} \tag{39}$$

The zero values in (38) enforce the kinematic constraint in the crank arm motion. It is important to note that the VAU algorithm only estimates $\hat{q}_{C,VAU}^{B\to I}$ at the maxima and minima in Figure 19. At all other points in time, $\hat{\omega}_{C,e}^{B}$ is set equal to zero i.e. the CRANK filter implements gyroscope integration.

3.2.7. The KCR algorithm for the CRANK filter

As shown in Figure 17, the KCR algorithm receives input $\hat{\omega}_F^S$ using $\hat{q}_F^{S\to B}$ (see Section 3.2.8 on how this was calculated) and first estimates the angular velocity of the bicycle body frame as in (40):

$$\hat{\omega}_F^B = [\hat{\omega}_{F,X}^B \quad \hat{\omega}_{F,Y}^B \quad \hat{\omega}_{F,Z}^B] \tag{40}$$

Similarly to (40), the angular velocity of crank arm body frame this can be written as:

$$\omega_C^B = [\omega_{C,X}^B \quad \omega_{C,Y}^B \quad \omega_{C,Z}^B] \tag{41}$$

However, unlike $\hat{\omega}_F^B$, ω_C^B in (41) could not be estimated from the gyroscope signal y_G^C without a calibration quaternion $q_C^{S\to B}$. Instead, the KCR algorithm output $\hat{\omega}_{C,KCR}^B$ is an approximation of $\omega_{C,Y}^B$ – the only component of ω_C^B which influences the crank angle - obtained by exploiting several kinematic constraints between $\hat{\omega}_F^B$ and $\hat{\omega}_C^B$.

Firstly, the kinematic constraints of the system imply that there is zero relative angular velocity between the bicycle and crank arm body frames about the X- and Z-axes. Therefore, the crank vector magnitude $\left\|[\hat{\omega}_{C,X}^B \quad \hat{\omega}_{C,Z}^B]\right\|$ can be taken as equal to the bicycle vector magnitude $\left\|[\hat{\omega}_{F,X}^B \quad \hat{\omega}_{F,Z}^B]\right\|$. Secondly, since the Y-axis is shared (Figure 14), we know that the angular velocity vector $[\hat{\omega}_{F,X}^B \quad 0 \quad \hat{\omega}_{F,Z}^B]$ is perpendicular to the crank rotation rate $\omega_{C,Y}^B$. Lastly, since the crank arm IMMS is rigidly attached to the crank body frame, the magnitude of the gyroscope signal $\|y_G^C\|$ can be used to estimate the magnitude of $\|\omega_C^B\|$. Combining the above three inferences leads to:

$$\|y_G^C\| \approx \left\|\omega_{C,X}^B \quad \omega_{C,Y}^B \quad \omega_{C,Z}^B\right\|$$

$$\approx \sqrt{\left\|\hat{\omega}_{C,Y}^{B}\right\|^{2} + \left\|\left[\hat{\omega}_{C,X}^{B} \quad \hat{\omega}_{C,Z}^{B}\right]\right\|^{2}}$$

$$\approx \sqrt{\left\|\hat{\omega}_{C,Y}^{B}\right\|^{2} + \left\|\left[\hat{\omega}_{F,X}^{B} \quad \hat{\omega}_{F,Z}^{B}\right]\right\|^{2}} \tag{42}$$

Solving for $\hat{\omega}_{C,Y}^{B}$ in (42) yields

$$\hat{\omega}_{C,Y}^{B} = \sqrt{(\|y_G^C\|)^2 - \left\|\left[\hat{\omega}_{F,X}^{B} \quad 0 \quad \hat{\omega}_{F,Z}^{B}\right]\right\|^{2}} \tag{43}$$

The KCR algorithm estimates an effective angular velocity $\hat{\omega}_{C,KCR}^{B}$ for the crank arm body frame (Figure 17) as in (44), which ensures that the crank angle rotation rate $\hat{\omega}_{C,Y}^{B}$ is preserved for integration in (29) and (30) while assuming that the other two unknown components are zero.

$$\hat{\omega}_{C,KCR}^{B} = [0 \quad \hat{\omega}_{C,Y}^{B} \quad 0] \tag{44}$$

This enables the integration of the gyroscope in the crank body frame to track the crank angle without the need for a static calibration. The VAU assumption of negligible $\hat{\omega}_{C,X}^{B}$ and $\hat{\omega}_{C,Z}^{B}$ does not affect the crank angle estimate, and is corrected by the kinematic constraints implemented.

3.2.8. Static calibrations

Static calibrations were required for tracking the bicycle body frame $\hat{q}_F^{B\to I}$ (see Figure 16), since the orientation of the bicycle frame sensor relative to the frame $\hat{q}_F^{S\to B}$ was not known *a priori*. Therefore, the bicycle was positioned in an upright position on the laboratory floor and held in place by the stationary trainer for the static test. Data was captured and processed through the PCF in order to obtain $\hat{q}_F^{S\to B}$ and then $\hat{q}_F^{S\to B}$ was calculated using the ground truth orientation $q_F^{B\to L}$ (to allow dynamic comparisons to ground truth) as in (45):

$$\hat{q}_F^{S\to B} = q_F^{B\to L^*} \otimes q_F^{S\to I} \tag{45}$$

The performance of the PCF was compared to Xsens KF for the tracking of the bicycle frame, and therefore the $q_C^{S\to I}$ output from each filter was used to calculate a unique calibration value as well. Similarly, the results of the CRANK filter were compared to the performance of the Xsens onboard KF and the PCF which use direct heading and inclination referencing from the gravitational and magnetic fields.

Therefore, these filters required a static calibration for tracking the crank body frame. This required calculation of

$$\hat{q}_C^{S\to B} = q_C^{B\to L^*} \otimes q_C^{S\to I} \tag{46}$$

using an estimate of the static sensor orientation $q_C^{S\to I}$ from the Xsens and PCF filters, and the ground truth value of the crank arm quaternion $q_C^{B\to L}$ from the camera system.

3.2.9. Data analysis

Analysis of filter performance was conducted using mean absolute error (AE). AE was calculated for each filter relative to the ground truth data provided by the camera system. The mean AE (MAE) and standard deviation in AE (SDAE) over the five minute trial were used to quantify filter performance.

We also tested filter performance under simulated environmental noise due to typical movements of the bicycle frame in outdoor conditions. We assumed negligible yaw rates (slow changes in direction and no slippage of the wheels), since normal outdoor cycling does not comprise sustained sharp turns. We assumed a sinusoidal pitch rate (continuous inclination changes every ten pedal strokes), and fast lateral tilt about the X-axis of the bicycle body frame (Figure 14). Lateral tilt was assumed to be sinusoidal in nature with a frequency driven by the pedaling cadence. We simulated two tilt conditions: a sinusoidal angular velocity about the frame X-axis equivalent to a 20° lateral tilt (representing a seated position) and another equivalent to a 40° lateral tilt (pedaling in a standing position) over the crank cycle. Moreover, random noise was added to each sinusoid equal to 5% of the amplitude. This represented additional vibrations due to an irregular road surface. We also modeled the resultant accelerations from the bicycle frame angular velocity using a simple inverted pendulum model. The pendulum lengths for the bicycle frame and crank arm sensors were approximated as 1m and 0.3m (estimated height above the ground in upright position). The noisy sinusoid representing each simulated outdoor situation was added to the angular velocity measurement of the bicycle frame gyroscope. This was done by rotating the body frame sinusoid into the sensor frame. Similarly, the same sinusoid signal was rotated and added to the crank arm sensor gyroscope.

3.3. Results

The MAEs in bicycle frame estimates for the Xsens KF and the PCF were in the order of 1° or less, and SDAEs were in the order of 0.5° (Table 4).

Table 4: Mean absolute errors in bicycle frame tracking

	Xsens KF AE [deg] (mean (SD))			**PCF AE [deg] (mean (SD))**		
Cadence	*Roll*	*Pitch*	*Yaw*	*Roll*	*Pitch*	*Yaw*
Slow	0.6 (0.2)	0.4 (0.1)	0.9 (0.3)	0.6 (0.1)	0.5 (0.2)	1.1 (0.4)
Medium	0.7 (0.4)	0.8 (0.3)	1.0 (0.5)	0.6 (0.3)	0.9 (0.2)	0.9 (0.5)
Fast (inclined)	0.8 (0.3)	0.6 (0.3)	0.8 (0.5)	0.7 (0.4)	0.7 (0.2)	1.0 (0.6)

For the crank arm tracking, the CRANK filter produced similar errors (approximately 1°), but the KF and PCF performance was notably degraded (Table 5).

Table 5: Mean absolute errors in crank frame tracking

	Xsens KF AE [deg] (mean (SD))			**PCF AE [deg] (mean (SD))**			**CRANK AE [deg] (mean (SD))**		
Cadence	*Roll*	*Pitch*	*Yaw*	*Roll*	*Pitch*	*Yaw*	*Roll*	*Pitch*	*Yaw*
Slow	6.1 (3.2)	9.9 (6.3)	9.0 (7.1)	7.1 (3.4)	9.9 (8.7)	9.5 (6.9)	0.3 (0.1)	0.5 (0.2)	0.76 (0.3)
Medium	9.8 (4.4)	9.3 (9.9)	11.5 (8.5)	10.7 (4.5)	12.8 (11.0)	11.6 (8.1)	0.4 (0.3)	0.9 (0.2)	0.8 (0.2)
Fast (inclined)	10.2 (5.9)	9.8 (9.1)	13.1 (8.5)	13.4 (5.5)	12.1 (11.1)	13.2 (8.2)	0.5 (0.3)	0.7 (0.2)	0.9 (0.4)

The CRANK filter produced markedly lower AEs in crank arm angles relative to the bicycle frame than the Xsens KF and PCF for all tests (Figure 20). The CRANK filter AEs in the crank angle (relative pitch angle) were 0.9 ± 0.6°, 1.7 ± 1.4° and 1.8 ± 1.2° for the Slow, Medium and Fast tests respectively. The Xsens KF produced MAEs and SDAEs of approximately 10° and 5° respectively. The PCF was even more inaccurate, ranging between 10-15° in MAE with SDAEs of up to 10°. CRANK filter AEs for the other two relative angles between the bicycle frame and crank arm – roll angle A_X and yaw angle A_Z in (3) – were below 0.5° for all tests, while those using the Xsens KF and PCF were markedly higher (MAEs between 5-15°, SDAEs between 5-10°).

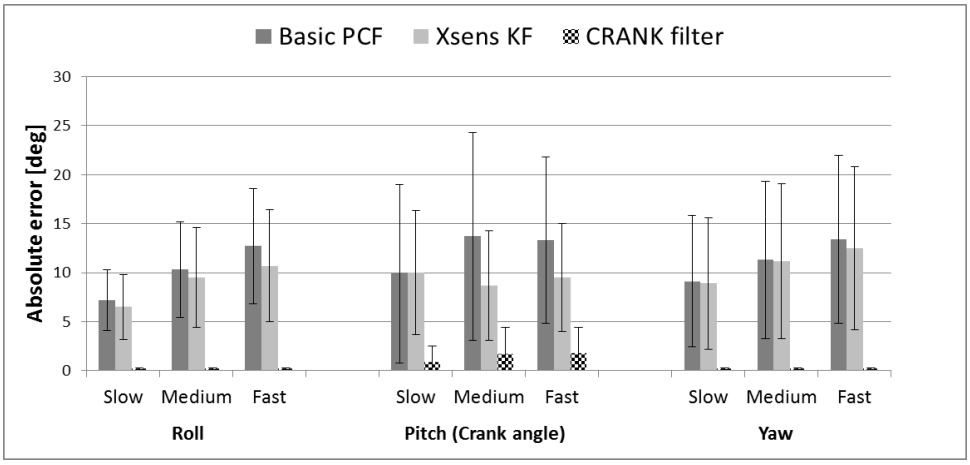

Figure 20: Crank angle tracking performance for the CRANK filter during testing compared to the Xsens KF and PCF. Bar graphs represent the MAE, error bars represent the SDAE.

CRANK filter performance for simulated motion of the bicycle frame (see Section 3.2.9 under Methods for details) was only slightly less accurate than under controlled laboratory conditions (Figure 21). With the simulated environmental noise, the AEs increased slightly to 1.6 ± 1.2°, 1.9 ± 1.3° and 2.4 ± 1.8° for 20° pitch and lateral tilt and to 2.6 ± 1.9°, 2.8 ± 1.7° and 3.6 ± 2.7° for 40° pitch and tilt.

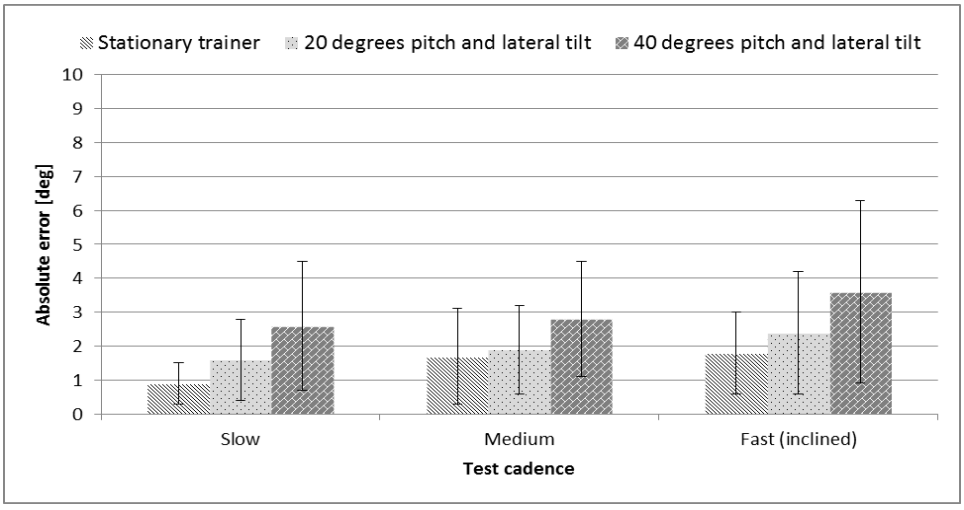

Figure 21: Performance of the CRANK filter under ideal conditions and with simulated bicycle frame motion.

3.4. Discussion

This study presents a novel complementary filter for tracking the crank angle using two IMMSs. The proposed CRANK filter achieved MAEs of less than 2° in ideal laboratory conditions and below 3° under simulated motion of the bicycle frame. This suggests that the CRANK filter is able to operate in outdoor conditions, although this should be verified with future field tests. The CRANK filter is robust; its accuracy was not degraded by the inclination of the bicycle, and it does not require a magnetometer for the crank sensor, making it resistant to magnetic interference. It is also easy to use since it does not require the sensors to be attached at specific positions or orientations relative to the bicycle. Furthermore, it can be implemented relatively quickly as it does not involve complicated Kalman filtering or calibration methods which are time-consuming and prone to error.

According to the authors' knowledge only one other study, by Kitawaki and Oka [32], has attempted to estimate bicycle crank angles using wireless inertial sensors. They report errors of 0.339 ± 0.115° for their system, which is very low. However, their study limited their tests to only 25 seconds and the crank angle appears to have been tracked using basic integration of the gyroscope signal. This method can therefore not track the crank angle for periods longer than a few seconds due to gyroscope drift error, as Kitawaki and Oka [32] offer no filtering method for removing the gyroscope bias using vector observations. Their methodology also relies on precise alignment of the axes of crank sensor with the crank arm, which may be time-consuming and difficult. Furthermore, their collection of ground truth data using an optical motion capture system did not include bicycle frame orientation and used only two markers for the crank arm tracking. The main advantages of the present study with respect to the approach proposed by Kitawaki and Oka [32] are that it presents a more thorough ground truth data collection method, incorporates a filtering algorithm which provides drift-free estimates of crank angle over extended periods of time and does not require alignment of the crank sensor with the crank segment.

The CRANK filter outperformed the Xsens KF and the PCF, both of which made use of classical IMMS vector observations and required a static calibration procedure. The Xsens KF is known to operate with less than 1° error in magnetically undisturbed environments. However, ferrous metal components in the bicycle resulted in a severely corrupted heading reference vector during the calibration and during

pedaling. This produced both offset and drift errors in the orientation output of the KF (and PCF). The CRANK filter makes no use of the magnetometer in the crank IMMS and was thus unaffected by the magnetic disturbances. It should be noted that the error in crank angle estimates is the combination of several errors for a two-segment model: frame IMMS tracking error (PCF errors), frame calibration error, crank IMMS tracking (errors in the KCR and VAU algorithms) and crank sensor-to-body calibrations (for crank angle tracking using the Xsens KF and PCF). Errors in the frame IMMS tracking were shown to contribute very little to crank angle error for both the PCF and KF, although kinematic constraints were violated with these filters and it is likely that magnetic disturbances during the static calibrations contributed largely to these errors. In contrast, the near zero relative roll and yaw errors for the CRANK filter demonstrate the effectiveness of the VAU kinematic constraints.

The main limitation of the CRANK filter is that it requires sustained forward pedaling. The VAU does not work at low cadences as it requires centripetal accelerations to work. Also, the KCR algorithm operates on scalar values and thus cannot distinguish between forward and backward pedaling. The CRANK filter also relies on a relatively fast sampling rate. For example, a sampling rate of 120 Hz implies that the resolution of the sensor data is 3° of crank rotation per sample at a slow cadence of 60 rpm. Therefore, at faster pedaling rates, the VAU could be inaccurate by several degrees for a single observation. Nevertheless, the CRANK filter produced errors below 3° even at a cadence of 100 rpm – suggesting that time-resolution errors average out closer to zero over time.

3.5. Conclusion

This study presents a novel method of accurately estimating the angle of a bicycle crank arm with IMMS over an extended period of time without needing a magnetometer or a static calibration procedure. This approach highlights the possibility of overcoming inertial and magnetic interference using innovative domain constraints instead of vector observations. Simulation results indicate that the CRANK filter is robust against even large movements of the bicycle frame.

3.6. References

[1] N. Davies, E. H. Chi, G. Borriello, and G. Hunt, “Guest editors’ introduction: Pervasive computing in sports technologies,” *IEEE Pervasive Comput.*, vol. 4, no. 3, pp. 22–25, Jul. 2005.

[2] C. Cummins, R. Orr, and C. West, “Global positioning systems (GPS) and microtechnology sensors in team sports: A systematic review,” *Sports Med.*, vol. 43, no. 10, pp. 1025–1042, Oct. 2013.

[3] E. H. Chi, “Sensors and ubiquitous computing technologies in sports,” in *Computers in Sport*, P. Dabnichki and A. Baca, Eds. Boston, MA, USA: WIT Press, 2008, pp. 249–268.

[4] A. Baca, P. Dabnichki, M. Heller, and P. Kornfeind, “Ubiquitous computing in sports: A review and analysis,” *J. Sports Sci.*, vol. 27, no. 12, pp. 1335–1346, Oct. 2009.

[5] R. R. Bini and F. P. Carpes, Eds., *Biomechanics of Cycling*. New York, NY, USA: Springer, 2014.

[6] J. Cockcroft and C. Scheffer, “Determining the feasibility of measuring outdoor road cycling kinematics using inertial motion capture technology,” *SAIEE Africa Res. J.*, vol. 102, no. 2, pp. 31–39, Jun. 2011.

[7] S. J. Cockcroft, “An evaluation of inertial motion capture technology for use in the analysis and optimization of road cycling kinematics,” M.S. thesis, Dept. Mech. Mechatron. Eng., Univ. Stellenbosch, Stellenbosch, South Africa, 2011.

[8] J. Cockcroft, J. H. Muller, and C. Scheffer, “A novel complimentary filter for tracking hip angles during cycling using wireless inertial sensors and dynamic acceleration estimation,” *IEEE Sensors J.*, vol. 14, no. 8, pp. 2864–2871, Aug. 2014.

[9] R. Marin-Perianu *et al.*, “A performance analysis of a wireless body-area network monitoring system for professional cycling,” *Pers. Ubiquitous Comput.*, vol. 17, no. 1, pp. 197–209, Jan. 2013.

[10] J. Y. Xu, X. Nan, V. Ebken, Y. Wang, G. J. Pottie, and W. J. Kaiser, “Integrated inertial sensors and mobile computing for real-time cycling performance guidance via pedaling profile classification,” *IEEE J. Biomed. Health Informat.*, vol. 19, no. 2, pp. 440–445, Mar. 2015.

[11] Y. Zhang, K. Chen, and J. Yi, "Rider trunk and bicycle pose estimation with fusion of force/inertial sensors," *IEEE Trans. Biomed. Eng.*, vol. 60, no. 9, pp. 2541–2551, Sep. 2013.

[12] R. R. Bini, P. A. Hume, and A. Cerviri, "A comparison of cycling SRM crank and strain gauge instrumented pedal measures of peak torque, crank angle at peak torque and power output," in *Proc. Eng.*, vol. 13. Apr. 2011, pp. 56–61.

[13] V. Ferrer-Roca, A. Roig, P. Galilea, and J. García-López, "Influence of saddle height on lower limb kinematics in well-trained cyclists: Static vs. dynamic evaluation in bike fitting," *J. Strength Conditioning Res.*, vol. 26, no. 11, pp. 3025–3029, Nov. 2012.

[14] F. Hug and S. Dorel, "Electromyographic analysis of pedaling: A review," *J. Electromyography Kinesiol.*, vol. 19, no. 2, pp. 182–198, Apr. 2009.

[15] S. J. Elmer, P. R. Barratt, T. Korff, and J. C. Martin, "Joint-specific power production during submaximal and maximal cycling," *Med. Sci. Sports Exerc.*, vol. 43, no. 10, pp. 1940–1947, Oct. 2011.

[16] R. R. Bini, P. A. Hume, and J. Croft, "Cyclists and triathletes have different body positions on the bicycle," *Eur. J. Sport Sci.*, vol. 14, no. 1, pp. S109–S115, Mar. 2014.

[17] S. Dorel, J.-M. Drouet, A. Couturier, Y. Champoux, and F. Hug, "Changes of pedaling technique and muscle coordination during an exhaustive exercise," *Med. Sci. Sports Exerc.*, vol. 41, no. 6, pp. 1277–1286, Jun. 2009.

[18] A. R. Chapman, B. Vicenzino, P. Blanch, and P. W. Hodges, "Patterns of leg muscle recruitment vary between novice and highly trained cyclists," *J. Electromyography Kinesiol.*, vol. 18, no. 3, pp. 359–371, Jun. 2008.

[19] G. Ettema, H. Lorås, and S. Leirdal, "The effects of cycling cadence on the phases of joint power, crank power, force and force effectiveness," *J. Electromyography Kinesiol.*, vol. 19, no. 2, pp. e94–e101, Apr. 2009.

[20] O. J. Woodman, "An introduction to inertial navigation," Comput. Lab., Cambridge Univ., Cambridge, U.K., Tech. Rep. UCAM-CL-TR-696, Aug. 2007.

[21] E. Foxlin, "Motion tracking requirements and technologies," in *Handbook of Virtual Environments: Design, Implementation, and Applications*, K. S. Hale and K. M. Stanney, Eds. Boca Raton, FL, USA: CRC Press, 2002, pp. 163–210.

[22] C. Verplaetse, "Inertial proprioceptive devices: Self-motion-sensing toys and tools," *IBM Syst. J.*, vol. 35, nos. 3–4, pp. 639–650, 1996.

[23] A. M. Sabatini, "Estimating three-dimensional orientation of human body parts by inertial/magnetic sensing," *Sensors*, vol. 11, no. 2, pp. 1489–1525, Jan. 2011.

[24] D. Roetenberg, H. Luinge, and P. Slycke. (Apr. 8, 2009). *Xsens MVN: Full 6DOF Human Motion Tracking Using Miniature Inertial Sensors*. [Online]. Available: http://www.xsens.com/images/ stories/PDF/MVN_white_paper.pdf

[25] R. Harle, "A survey of indoor inertial positioning systems for pedestrians," *IEEE Commun. Surveys Tuts.*, vol. 15, no. 3, pp. 1281–1293, Jul. 2013.

[26] H. J. Luinge, P. H. Veltink, and C. T. M. Baten, "Ambulatory measurement of arm orientation," *J. Biomech.*, vol. 40, no. 1, pp. 78–85, 2007.

[27] J. Pusa, "Strapdown inertial navigation system aiding with nonholonomic constraints using indirect Kalman filtering," M.S. thesis, Dept. Math., Tampere Univ. Technol., Tampere, Finland, 2009.

[28] Y. Li, X. Niu, Q. Zhang, Y. Cheng, and C. Shi, "Observability analysis of non-holonomic constraints for land-vehicle navigation systems," *J. Global Positioning Syst.*, vol. 11, no. 1, pp. 80–88, Oct. 2012.

[29] R. Mahony, T. Hamel, and J.-M. Pflimlin, "Nonlinear complementary filters on the special orthogonal group," *IEEE Trans. Autom. Control*, vol. 53, no. 5, pp. 1203–1218, Jun. 2008.

[30] R. Mahony, M. Euston, J. Kim, P. Coote, and T. Hamel, "A non-linear observer for attitude estimation of a fixed-wing unmanned aerial vehicle without GPS measurements," *Trans. Inst. Meas. Control*, vol. 33, no. 6, pp. 699–717, Aug. 2011.

[31] X. Yun, E. R. Bachmann, and R. B. McGhee, “A simplified quaternionbased algorithm for orientation estimation from earth gravity and magnetic field measurements,” *IEEE Trans. Instrum. Meas.*, vol. 57, no. 3, pp. 638–650, Mar. 2008.

[32] T. Kitawaki and H. Oka, “A measurement system for the bicycle crank angle using a wireless motion sensor attached to the crank arm,” *J. Sci. Cycling*, vol. 1, no. 2, pp. 13–19, 2013.

4. Paper 3: Accurate Bicycle Crank Angle Tracking using Wireless Inertial and Magnetic Measurement Systems and Two Novel Functional Calibrations

Abstract: *An important outcome when analyzing cycling biomechanics is the crank angle. Minimally invasive technologies such as wireless inertial and magnetic measurement systems (IMMSs) have the potential to measure crank angles quickly and affordably – even outdoors. However, magnetic field disturbances around the crank arm and large centripetal accelerations during pedaling introduce calibration and tracking errors. This study presents a novel passive complementary filter designed to track the crank angle using sensor data from two IMMSs; one attached to the bicycle frame and the other to the crank arm. The filter includes dynamic acceleration compensation (DAC) and a heading constraint (HC) algorithm which allows for tracking of the crank arm IMMS heading without magnetometer data. We also propose two functional methods of sensor-to-body frame alignment which are based on kinematic constraints and do not require magnetometer measurements. We validated the filter during three five-minute tests at a self-selected slow, medium and fast cadence using an optical motion capture system. The filter produced low and consistent absolute errors (AEs) of 1.3 ± 0.9° or less in all three tests for both frame alignment methods. In contrast, large and variable AEs were found (11.6 ± 7.6°, 14.2 ± 10.7° and 14.0 ± 10.2° respectively) with the DAC and HC algorithms disabled and using a relative pose calibration that relies on magnetometer data. This filter is simple and cost-effective to implement, and its performance demonstrates that it is robust against typical errors caused by continuous dynamic motion and time-varying magnetic interference near the crank.*

Submitted: *IEEE Sensors J.* Journal (10 December 2014)

4.1. Introduction

Inertial sensor technology has advanced considerably in accuracy and portability over the past two decades [1]. This has resulted in a prolific expansion of their usage for human analytics in fields such as healthcare and sports [2, 3]. In particular, wireless inertial and magnetic measurement systems (IMMSs) have introduced opportunities to perform non-invasive human motion analysis in novel environments. However, variability in movement task dynamics and local magnetic field conditions often present context-specific challenges to accurate IMMS tracking [4]. Tracking a moving IMMS requires knowledge of the alignment between two coordinate systems

(frames): a frame representing the measurement axes (the sensor frame) and another representing the reference (inertial) frame [5]. Estimating sensor-to-inertial frame alignment typically involves solving Wahba's problem with vector matching techniques [6, 7]. The solution is then combined with strapdown integration of the gyroscope data in a sensor fusion scheme to filter out measurement errors [8]. IMMS vector matching relies on measurements of the gravitational and magnetic field vectors by accelerometers and magnetometers respectively. This means that dynamic accelerations and disturbances to the local magnetic field are a source of error – especially in applications involving sustained rigorous motion or exposure to variable magnetic interference [9, 10]. Therefore, methods of compensating for these disturbances are often developed using additional domain constraints which apply to the specific application [5].

Besides sensor-to-inertial frame alignment, a second source of error in IMMS tracking is estimation of the alignment between the sensor frame and the frame in which body motion is analyzed (body frame). For instance, in the field of gait analysis, measurements in the sensor frame attached to a bone segment are transformed to the anatomical body frame representing segment morphology [11, 12]. As a result, reliable IMMS tracking also depends upon accurately determining the static alignment between the sensor frame and desired body frame. There are three primary methods of performing sensor-to-body frame alignment: manual, relative pose and functional methods. Manual alignment, the most basic approach, involves precise placement of the sensor frame on the tracking object in order to produce a predetermined alignment to the body frame. This can be both time-consuming and subject to significant human error, especially when dealing with complex body geometries with uneven contact surfaces. Relative pose methods involve a stationary body frame pose in which the simultaneous sensor-to-inertial and body-to-inertial frame alignments are assumed known [13]. Static pose calibrations thus suffer both from orientation estimation errors for the sensor and incorrect positioning of the body in the inertial frame. Functional methods exploit constraints to the kinematics of the body frame (such as planar motion) during a dynamic calibration movement while the same motion is measured in the sensor frame [14]. Dynamic methods fail if the kinematic constraints assumed for the system are violated, or if sensor measurements are inaccurate. Therefore, similarly to sensor-to-inertial tracking, accurate sensor-to-body frame alignment techniques are often context-specific and remain actively researched in a number of fields.

The aim of this study was to develop a method of tracking bicycle crank angles accurately using wireless IMMSs. The crank angle is an important variable in studies investigating cycling performance, and simple portable measurement systems such as IMMSs are desirable for in-field data collection. However, disturbances to the magnetic field near the bicycle crank arm are commonplace, rendering the measurements from a magnetometer on the crank arm unreliable for vector matching techniques [15, 16]. Since these disturbances are permanent and yet variable during crank motion, they cannot be removed using normal magnetic mapping techniques [9] and thus hinder dynamic sensor-to-inertial alignment tracking. Furthermore, since the interference cannot be removed temporarily for a static pose calibration, this also degrades estimation of sensor-to-body frame alignment. The study objective was thus to develop a method of performing the sensor-to-inertial and sensor-to-body frame alignments for the crank arm without magnetometer measurements. We accomplished this by exploiting a kinematic constraint between the crank arm body frame and the body frame of the bicycle in a nonlinear complementary filter structure. This novel method also includes a dynamic acceleration compensation (DAC) method for improving gravity estimates, and was successfully validated using an optical motion capture system.

4.2. Methods

4.2.1. Data collection

An experiment was conducted with a subject riding a road bicycle indoors on a stationary trainer positioned on a level floor. The subject was tested cycling at three self-selected cadences: slow (≈80 rpm), medium (≈90 rpm) and fast (≈100 rpm). Each test lasted for a period of five minutes. In order to track the crank angle, one wireless IMMS (MTw Development Kit, Xsens, B.V. Technologies, Enschede, Netherlands) was rigidly attached to the seat post of the bicycle frame and another on the right-facing surface of the left crank arm (the crank IMMS cannot be placed on the outside lateral surface of the crank arm due to foot obstructions). For validation purposes, the crank angle was measured simultaneously using an optoelectronic motion analysis system (Vicon MX T-series, Vicon Motion Systems Ltd, UK) and reflective markers were placed on the frame and crank arm according to the protocol described in [17]. Markers could not be placed on the crank IMMS as it was on the inside of the crank arm which made the markers invisible to the cameras. Data was collected synchronously at 120 Hz for both systems.

4.2.2. Crank angle tracking

In this study we describe the orientation of any generic frame *CS1* relative to another generic frame *CS2* using the Hamiltonian quaternion notation in (47):

$$q^{\mathrm{CS2}\rightarrow\mathrm{CS1}} = [s\ \boldsymbol{v}] \tag{47}$$

where s is a scalar and $\boldsymbol{v}$ is a three-dimensional vector. This allows for the transformation of a three-dimensional vector x^{CS2} expressed in *CS2* to *CS1* by

$$p(x^{CS1}) = q^{\mathrm{CS2}\rightarrow\mathrm{CS1}} \otimes p(x^{CS2}) \otimes q^{*\mathrm{CS2}\rightarrow\mathrm{CS1}} \tag{48}$$

The symbol $\otimes$ represents a quaternion multiplication, the superscript $*$ denotes a conjugated quaternion and $p(x^{CS2}) = [0\ p(x^{CS2})]$. The bicycle crank angle at any time t was defined as the orientation of a chosen body frame (B) for the crank arm (C) relative to one for the bicycle frame (F):

$$q_{CF}^{B\rightarrow B}(t) = q^{*I\rightarrow B}_{C}(t) \otimes q_{F}^{I\rightarrow B}(t) \tag{49}$$

where I is the inertial reference frame. The relevant crank angle A_Y, expressed in Euler angles, is shown in Figure 22 and can be calculated from $q_{CF}^{B\rightarrow B}$ in (49) using

$$f_{Q\rightarrow E}(q_{CF}^{B\rightarrow B}) = [A_Z \quad A_X \quad A_Y] \tag{50}$$

where $f_{Q\rightarrow E}$ is a standard conversion from Hamiltonian quaternions to Euler angles using a ZXY rotation sequence. Therefore, any bicycle crank angle measurement method requires tracking of $q_F^{I\rightarrow B}$ and $q_C^{I\rightarrow B}$ to calculate $q_{CF}^{B\rightarrow B}$.

Figure 22 also shows the Vicon marker positions used to define the axes of the body frames required for ground truth data. The bicycle and crank arm body frames were defined with a common primary axis $\mathrm{Y^I}$ (coming out of the page) about which the crank arm rotates relative to the bicycle frame. The secondary axis $\mathrm{X_F^I}$ was defined using the line joining the two wheel centers, while the secondary axis $\mathrm{Z_C^I}$ was defined using the line joining the pedal marker and the crank hub marker [17].

We estimated the crank angle using measurements from the IMMS attached to the bicycle frame and the IMMS attached to the crank arm. Each IMMS produces sensor measurements from a three-dimensional gyroscope, accelerometer and magnetometer. These were designated y_G, y_A and y_M respectively, and modeled as:

$$y_G(t) = \omega^S(t) + b^S(t) \quad (51)$$

$$y_A(t) = -g^S(t) + a^S(t) \quad (52)$$

$$y_M(t) = m^S(t) + d^S(t) \quad (53)$$

where ω^S is the angular velocity of the IMMS in the sensor frame, g^S is the gravitational acceleration and m^S is the magnetic field intensity. Environmental noise components b^S, a^S and d^S represent the gyroscope bias, dynamic acceleration of the IMMS and the local magnetic field disturbances respectively. The superscript S indicates quantities expressed in the IMMS sensor frame.

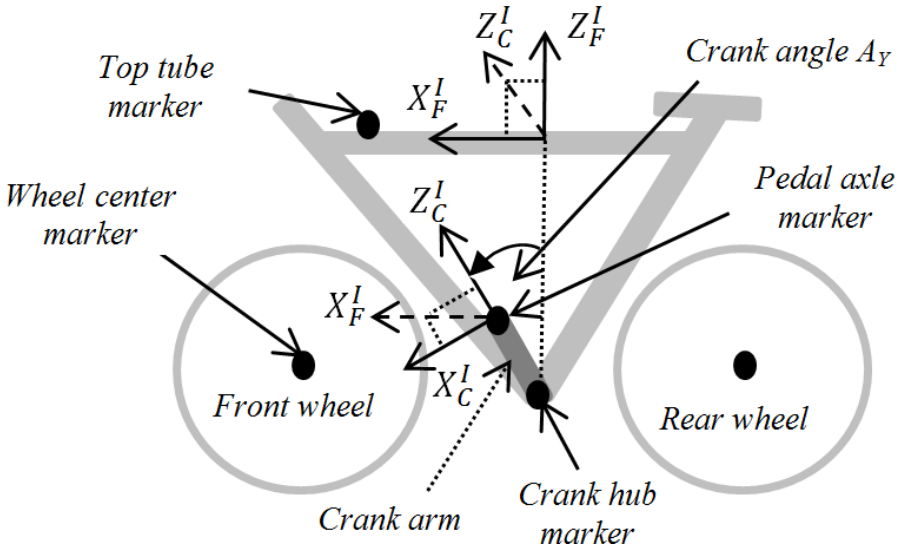

Figure 22: Body frame definition for crank angle tracking. Marker placement is shown for data collection using an optical motion capture system

4.2.3. Functional sensor-to-segment frame calibration

To express any measured or estimated quantities in the desired body frame, it is necessary to obtain the coordinate system transformation $q_F^{S\to B}$. For example, this enables the transformation in (54):

$$q^{I\to B}(t) = q^{I\to S}(t) \otimes q^{S\to B^*} \quad (54)$$

Note that $q_F^{S\to B}$ is not time-dependent as the sensor and body frames were both rigidly attached to the crank arm. A functional frame alignment procedure (Dynamic_FA)

was developed in order to estimate sensor-to-segment transformations $q_C^{S\to B}$ and $q_F^{S\to B}$ for the crank arm and bicycle frame IMMSs respectively (Figure 23).

The first functional calibration involved steady rotation of the crank arm (by hand with subject off the bicycle) for five revolutions while the bicycle frame was held stationary (Figure 23a). The dynamic acceleration components measured by the crank arm IMMS during this movement can be interpreted using the principles of angular kinematics. Relative to the crank hub center the crank IMMS rotates with angular velocity ω_C . This induces a radial acceleration a_r which has a constant direction in the sensor frame along the radius of rotation r_C . Changes in ω_C also lead to tangential acceleration of the IMMS a_t. Since the crank IMMS measures accelerations relative to the inertial frame, it also senses the linear acceleration of the crank hub a_L. The second calibration involved repeated lateral tilting of the bicycle frame (from side to side) while otherwise stationary (Figure 23b). Similarly, the IMMS attached to the bicycle frame experiences linear, radial and tangential accelerations as it rotates at angular velocity ω_F about radius r_F from the floor.

The functional calibration movements in Figure 23 both involve rotation about a single body frame axis. By keeping the bicycle frame stationary, the angular velocity vector ω_C in Figure 23a can be measured with the crank IMMS gyroscope and used to define the leading Y_C axis for the crank body frame in the sensor frame. Similarly, the X_F axis of the bicycle frame can be estimated using the bicycle IMMS gyroscope signal in Figure 23b. The secondary axes of the bicycle and crank body frames – Y_F and X_C - were defined as perpendicular to the radii of rotation r_F and r_C respectively. This is based on the assumption that during the calibration r_F lies in the XZ-plane of the bicycle body frame and r_C lies in the YZ-plane of the crank arm body frame (refer to Figure 22 and Figure 23). Trivially, the third axis for each body frame is defined as perpendicular to the other two. Therefore, it was possible to calculate the body frame relative to the sensor frame for both IMMSs using the well-known TRIAD method [18]. This ensures that the secondary axes are perpendicular to the primary axes even though r_F and r_C are not.

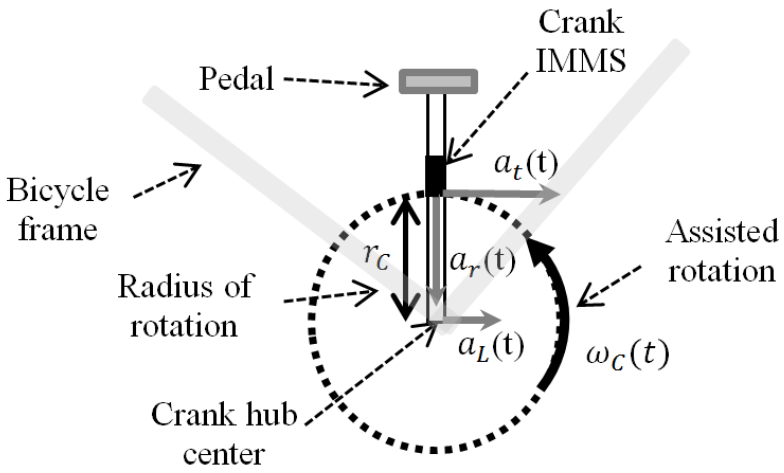

(a) Crank rotation calibration for crank arm IMMS (side view)

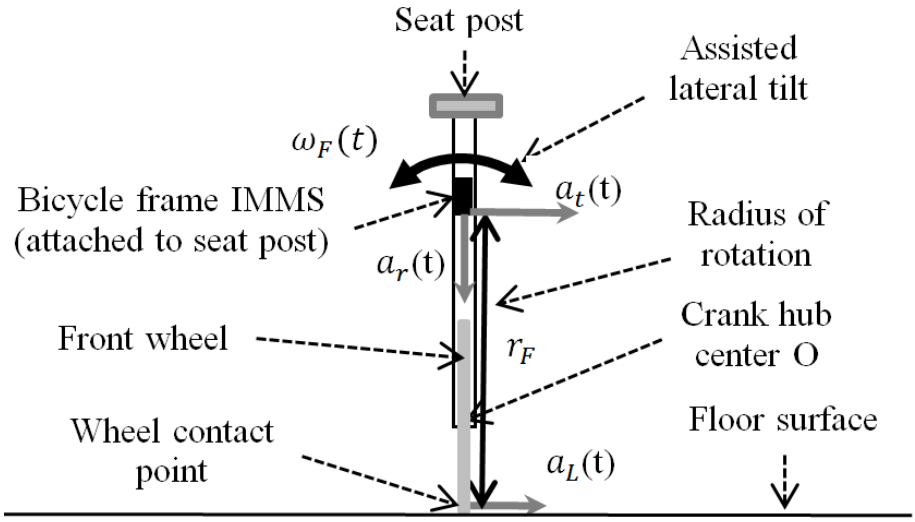

(b) Lateral tilt calibration for bicycle IMMS (front view)

Figure 23: Functional calibration movements with a single body axis rotation for (a) the crank arm IMMS and (b) the bicycle frame IMMS showing radii of IMMS rotation and components of acceleration.

4.2.4. Radius of rotation estimation

This section provides detail on the estimation of radii of rotation r_F and r_C which are required for the functional calibration method described in Chapter 4.2.3. Referring to

(52) and Figure 22, the dynamic acceleration of the bicycle and crank IMMSs can be defined as in (55):

$$a^S(t) = {a_o}^S(t) + {a_r}^S(t) + {a_t}^S(t) \tag{55}$$

where ${a_o}^S$ is the acceleration of the crank hub center due to translation and rotation of the bicycle frame relative to the ground, ${a_r}^S$ is the radial acceleration due to crank angular velocity and ${a_t}^S$ is the tangential component due to angular acceleration of the crank. The functional calibrations in Figure 22 were designed in such a way that the linear acceleration ${a_o}^S$ is negligible. Therefore, the dynamic acceleration of the IMMSs could be approximated as purely rotational acceleration:

$$\begin{aligned} a_{rot}^S(t) &\approx {a_r}^S(t) + {a_t}^S(t) \\ &= \frac{\mathrm{d}\omega^S(t)}{\mathrm{dt}} \times r^S + \omega^S(\mathrm{t}) \times (\omega^S(\mathrm{t}) \times r^S) \end{aligned} \tag{56}$$

where the symbol $\times$ designated a cross-product multiplication. Therefore, it can be seen that solving for r^S in (56) requires *a priori* knowledge of a_{rot}^S and ω^S. Assuming negligible gyroscope bias values (only for this calibration), an estimate of ω^S can be obtained from the IMMS gyroscope signal y_G in (51). Similarly, an estimate of a_{rot}^S can be obtained using the accelerometer measurement and an estimate of the gravitational acceleration vector by rearranging (52):

$$\hat{a}_g^S(t) = \mathrm{y}_A(t) + \hat{g}^S(t) \tag{57}$$

The gravity estimate was first obtained for each IMMS while stationary immediately preceding the functional calibration. This is a trivial case of (57) where the dynamic acceleration is considered to be zero. During the calibration movement, the gravity vector in (57) was tracked using gyroscope integration:

$$\hat{g}^S(t) = \hat{g}^S(t-1) + \hat{g}^S(t-1) \times y_G(t) \tag{58}$$

The period between the start time t_1 and end time t_2 of the calibrations was chosen to be five seconds, which was considered too short to induce notable gyroscope drift in (58). We solved for r^S by minimizing the mean error between $\hat{a}_{rot_{t_1 \to t_2}}^S$ in (56) and $\hat{a}_{g\ t_1 \to t_2}^S$ in (57) using a grid-search.

4.2.5. PCF with DAC for tracking the bicycle frame

Tracking of the bicycle frame sensor orientation $q_F^{I\to S}$ was performed using the passive complementary filter (PCF) described by Mahoney *et al.* [19]. In summary, the PCF receives the IMMS sensor signals as inputs and then estimates the IMMS angular velocity ω_F^S (Figure 24). This is then integrated to track orientation according to the following differential equation describing rigid body kinematics:

$$\dot{\hat{q}}_F^{I\to S}(t) = \frac{1}{2}\hat{q}_F^{I\to S} \otimes p(\hat{\omega}_F^S) \tag{59}$$

The accent symbol ^ represents an estimated quantity and the single dot accent a time derivative. The estimate $\hat{\omega}_F^S$ is obtained by filtering out errors from the gyroscope signal y_F^S in a correction step. The correction step involves an error feedback loop in which $\hat{q}_F^{I\to S}$ is compared to the PCF output from the previous time step. The Factored Quaternion Algorithm (FQA) was used to obtain an auxiliary estimate of the IMMS orientation $\hat{q}_{F,FQA}^{I\to S}$ using a gravity estimate and magnetometer measurements [18]. The DAC step substitutes the radius of rotation and the gyroscope signal into (52) to estimate the dynamic acceleration, which can be used to estimate the gravity vector by manipulating (52). The FQA estimate is then used to estimate an angular velocity error $\hat{\omega}_e^S$:

$$\hat{q}_e(t) = \hat{q}_F^{I\to S}(t-1) \otimes \hat{q}_{F,FQA}^{I\to S}(t) = [s_e(t) \quad \boldsymbol{v}_e(t)] \tag{60}$$

$$\hat{\omega}_e(t) = 2s_e(t)\boldsymbol{v}_e(t) \tag{61}$$

The angular velocity error from (61) is used for proportional and integral gain feedback correction in order to estimate $\hat{\omega}_F^S$ using

$$\hat{\omega}_F^S(t) = y_F^S(t) - \hat{b}(t) + K_P\hat{\omega}_e(t) \tag{62}$$

The online bias update is provided by integrating $\hat{\omega}_e^S$:

$$\dot{\hat{b}}(t) = -K_I\hat{\omega}_e(t) \tag{63}$$

Lastly, the PCF's IMMS orientation estimate was rotated into the body frame using an estimate of the sensor-to-body frame alignment $\hat{q}_F^{S\to B}$ as in (54).

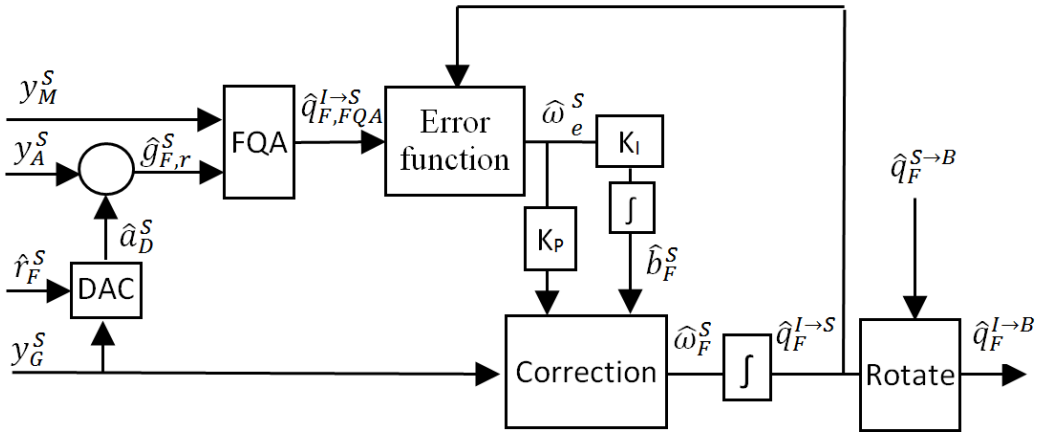

Figure 24: The PCF filter tracks the orientation of the bicycle frame sensor by correcting and then integrating the gyroscope signal. A rotation step is then used to transform this to the bicycle body frame.

4.2.6. PCF with DAC for tracking the crank arm

Due to magnetic disturbances caused by the pedals and bicycle drive train, the PCF in Figure 24 was adapted to track the crank arm body frame orientation $q_C^{I\to B}$ without measurements from the crank arm IMMS magnetometer. This adapted PCF performs the sensor-to-body frame rotation before the error function and correction steps, and thus directly estimates the body frame angular velocity and orientation (Figure 25). Instead of using the crank IMMS magnetometer measurement and FQA (as with the PCF in Figure 24), a heading constraint (HC) algorithm was developed to provide an auxiliary measurement $\hat{q}_{C,HC}^{I\to B}$ of the crank body frame orientation. The HC exploits the mechanical constraints of the crank arm body frame relative to the bicycle body frame so that the heading of the crank body frame can be inferred from the bicycle body frame heading (calculated using the bicycle frame IMMS magnetometer).

The HC is implemented using rotation matrix notation, giving bicycle body frame axes in the inertial frame as in (64):

$$\begin{aligned} R_F^{I\to B} &= f_{q\to R}(q_F^{I\to B}) \\ &= [X_F^I\ Y_F^I\ Z_F^I] \\ &= [X_F^B\ Y_F^B\ Z_F^B]^T \end{aligned} \tag{64}$$

where symbol R represents a direction cosine matrix and $f_{Q\to R}$ is a standard function converting Hamiltonian quaternions to rotation matrices. Similarly, the crank arm body frame axes which the HC estimates are given in (65):

$$R_C^{I\to B} = [X_C^B\ Y_C^B\ Z_C^B]^T \tag{65}$$

The HC step exploits the fact that the crank arm axis of rotation (Y_C^I) is defined as coincident with the lateral axis of the bicycle body frame (Y_F^I), implying that the plane XZ_F is parallel to plane XZ_C. Therefore, the bicycle heading vector X_F^B also lies in the plane XZ_C– perpendicular to the rotation axis (refer to Figure 22).

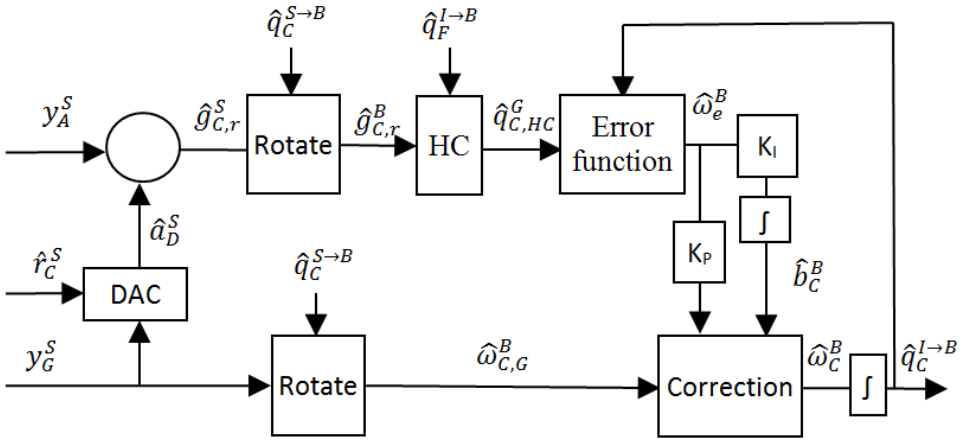

Figure 25: The PCF_HC filter which tracks the crank arm without magnetometer measurements or disturbances due to dynamic acceleration. A DAC step is performed in the sensor frame followed by a rotation to the body frame. Heading information is then inferred from the bicycle frame orientation before the standard PCF filtration.

This allows the perpendicular Y_C^B to be calculated using Z_C^B and X_F^B:

$$Y_C^B = Z_C^B \times X_F^B \tag{66}$$

where X_F^B was obtained from (64) using the PCF's bicycle body frame estimate. Z_C^B was estimated as in (67) from the normalized DAC gravity estimate and the crank arm frame alignment:

$$Z_C^B = g_C^S/\|g_C^S\|.R_C^{S\to B^T} \tag{67}$$

Finally, the crank arm heading was found trivially using (68):

$$X_C^B = Y_C^B \times Z_C^B \tag{68}$$

4.2.7. Alternative IMMS sensor-to-body calibrations

We compared the functional calibration technique Dynamic_FA (described in Chapter 4.2.3) to two other methods of sensor-to-body frame alignment. The first was a standard static pose method (Static_FA) in which the bicycle and crank arm body frames were manually positioned at known orientations. The second was a novel mixed calibration method (Mixed_FA), which is a combination of the Static_FA and Dynamic_FA methods. For the Static_FA method, the bicycle frame alignment $\hat{q}_{F,static}^{S\to B}$ was obtained by taking IMMS measurements while holding the bicycle frame in a stationary upright position. The PCF was used to estimate orientation measurement $\hat{q}_{F,static}^{I\to S}$ and the assumed bicycle frame orientation was $\hat{q}_{F,static}^{I\to B} = [1\ 0\ 0\ 0]$. Manipulation of (54) allows:

$$\hat{q}_{F,static}^{S\to B}(t) = \hat{q}_{F,static}^{I\to B\ *} \otimes \hat{q}_{F,static}^{I\to S}(t) \tag{69}$$

Similarly, the crank arm frame alignment $\hat{q}_{C,static}^{S\to B}$ was estimated by manually positioning the crank arm at a zero crank angle for the Static_FA recording. Therefore, the orientation of the crank body frame $\hat{q}_{C,static}^{I\to B} = [1\ 0\ 0\ 0]$ was used in (69) together with $\hat{q}_{C,static}^{I\to S}$. Note that for Static_FA the IMMS orientation $\hat{q}_{C,static}^{I\to S}$ was estimated by the PCF in Figure 24 (which includes a magnetometer) and not by the filter in Figure 25. The Mixed_FA was developed to estimate the sensor-to-segment alignment of the crank arm IMMS without a magnetometer and without solving for the radius of rotation necessary for Dynamic_FA. Instead, Mixed_FA solves the alignment problem using Davenport's Q-method [20], a vector matching technique which determines the relative orientation of two frames using two or more vectors observable in both frames:

$$q_C^{CS1\to CS2} = f_{Q\_METHOD}(v_1^{CS1}, v_2^{CS1}, v_1^{CS2}, v_2^{CS2}) \tag{70}$$

The two vectors observable in both frames were the crank arm angular velocity and the gravity vector, such that

$$\hat{q}_{C,mixed}^{S\to B} = f_{Q\_METHOD}(\hat{g}_C^S, \hat{\omega}_C^S, \hat{g}_C^B, \hat{\omega}_C^B) \tag{71}$$

For Mixed_FA, the gravity vector was measured in the sensor frame using the accelerometer during the stationary Static_FA trial.

$$\hat{g}_C^S = -y_{A,static}^C \tag{72}$$

It was also rotated into the body frame during a static pose using the known gravity vector in the inertial frame and the assumed crank arm orientation as in (73):

$$p(\hat{g}^B_{C,static}) = \hat{q}^{I\rightarrow B}_{C,static}{}^{*} \otimes p([0\ 0\ -\hat{g}^I]) \otimes \hat{q}^{I\rightarrow B}_{C,static} \quad (73)$$

The angular velocity vectors in (71) were obtained from the Dynamic_FA trial described in Figure 23a. The angular velocity in the sensor frame was estimated using the crank arm gyroscope measurement i.e. $\hat{\omega}^S_C = y^C_{G,dynamic}$. The planar motion between the crank arm and bicycle body frames implies that all of the angular velocity measured by the crank arm IMMS occurs about the crank arm Y-axis i.e. $\hat{\omega}^B_C = [0\ ||y^C_{G,dynamic}||\ 0]$.

4.2.8. Outcomes and data analysis

To compare the accuracy of the different frame alignment methods, we tracked the crank angle during the three trials using the PCF and PCF_HC filters (Figure 24 and Figure 25) with frame alignments Static_FA, Mixed_FA and Dynamic_FA. Furthermore, to assess the influence of the DAC and HC algorithms, we also assessed crank angle errors obtained without them by tracking both body frames using the PCF in Figure 24 with DAC disabled (the dynamic acceleration estimate assumed to be zero). We also assessed the effectiveness of the DAC by analyzing crank angle errors for the PCF and PCF_HC with and without the DAC step at different filter gain values (different weighting of the gravity estimate). We analyzed the performance of each of these filter configurations using the mean absolute error (AE) calculated from the ground truth data provided by the optical motion capture system. The mean AE (MAE) and standard deviation in AE (SDAE) for each trial were then calculated.

Tuning of the proportional filter gain K_P for each filter configuration was done using reference data recorded by the optical motion capture system for a separate cycling trial. An automated grid search through the K_P values from 0 to 5 was performed to find the gain which produced the lowest MAE. As a result, the proportional feedback gain K_P was set to a value of 1 for the PCF in Figure 24 when tracking the bicycle body frame, as noise terms a^S_F in (52) and d^S_C in (53) were low and the FQA estimate could be weighted fairly heavily. As mentioned above, the PCF filter was also used to track the crank arm for comparison to the PCF_HC: here the magnetic interference and dynamic accelerations were much higher, resulting in a lower tuned K_P value of 0.5. In contrast, due to the heading constraint and dynamic acceleration compensation of the PCF_HC reducing errors in gravity and heading estimates, the performance of

this filter was far less sensitive to the K_P value. A higher K_P value of 1.5 was obtained for the PCF_HC. The integral feedback gain K_I was set in all filter implementations to a value of $0.01K_P$.

4.3. Results

The Static_FA method produced appreciably higher errors in crank angle estimates compared to Mixed_FA and Dynamic_FA for all cadences (Figure 26).

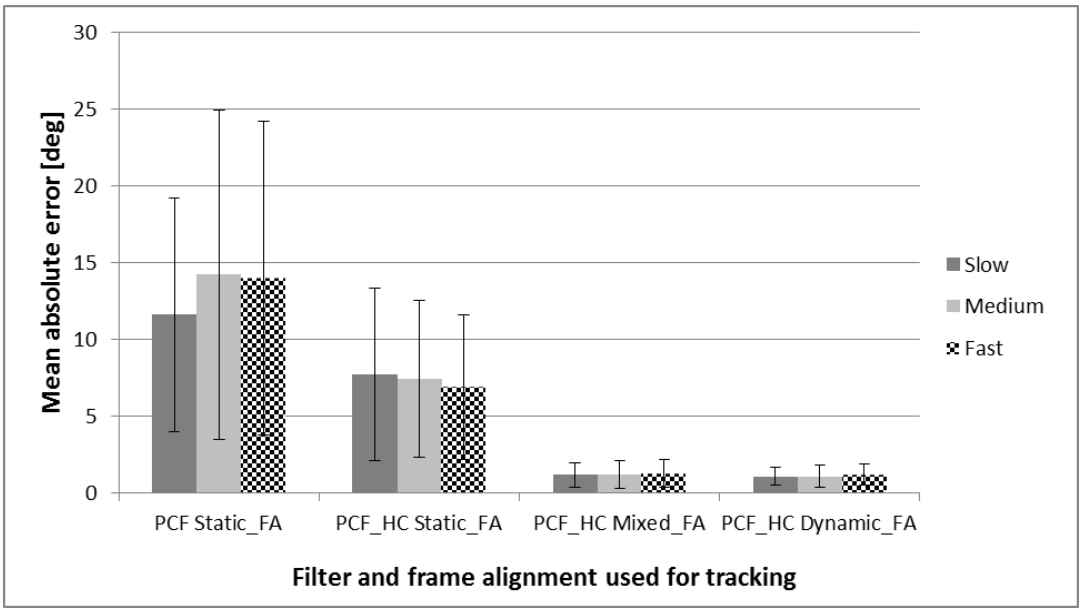

Figure 26: Errors in crank angle estimates for the PCF and PCF_HC using different frame alignment methods in comparison to Vicon reference measurements. Bar values indicate the average of the absolute errors and error bars designate the standard deviation in absolute error.

When tracking both body frames using the bicycle frame PCF, Static_FA produced large errors (MAE > 10°) and significant variability in error (SDAE ≈ 10°). MAEs and SDAEs decreased appreciably for Static_FA using the PCF_HC. Much lower errors were found using Mixed_FA and Dynamic_FA with the PCF_HC. MAEs were very similar and negligibly affected by cadence. The MAEs for Mixed_FA were 1.2 ± 0.9°, 1.2 ± 0.9° and 1.3 ± 0.9° for the slow, medium and fast tests respectively. The Dynamic_FA results were 1.1 ± 0.6°, 1.1 ± 0.7° and 1.2 ± 0.7° for the three tests respectively.

Figure 27 demonstrates the difference in PCF_HC performance (using Dynamic_FA) at different gain values with and without DAC. In both cases, for gain values lower

than 0.5 and approaching zero the effectiveness of the feedback correction is reduced and MAEs increased rapidly due to integration drift. However, the performance of the PCF_HC was largely insensitive to filter gain values from 0.5 to 5 with DAC enabled, whereas MAEs increased sharply with the gain value without the DAC. Moreover, performance did not deteriorate with faster pedaling when using the DAC, whereas errors increased with high cadences when DAC was disabled. This demonstrates that the DAC was effective in removing accelerations due to crank arm rotation.

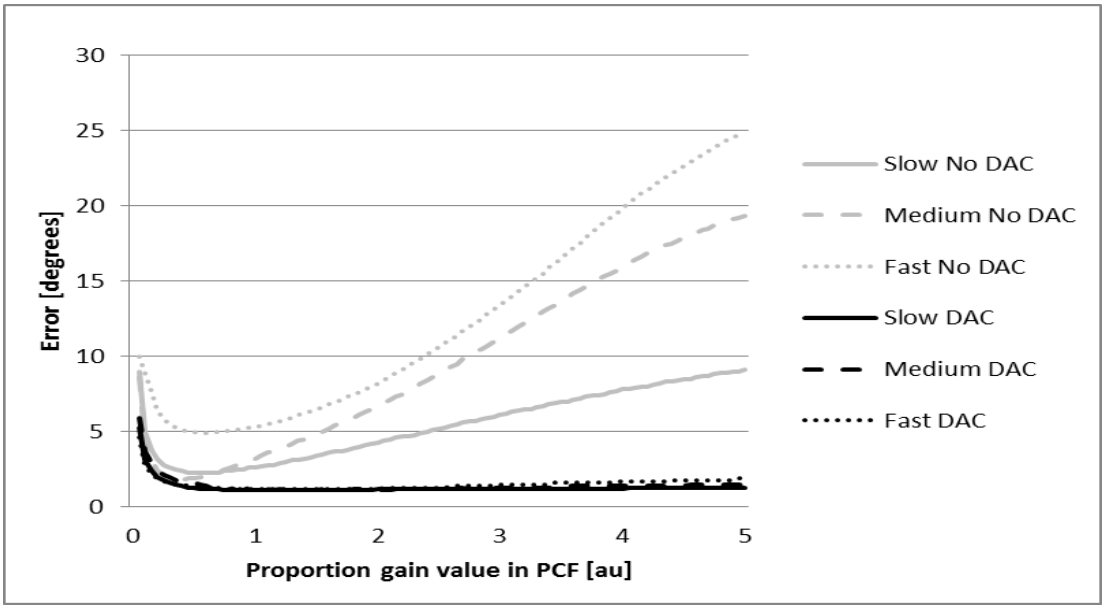

Figure 27: Absolute errors in crank angle estimates using PCF_HC with Dynamic_FA at different filter gain values.

An analysis of the magnetic field intensity measured by the bicycle frame IMMS and crank arm IMMS revealed that there were significant magnetic disturbances near the crank arm that were not present near the bicycle frame IMMS (Figure 28). The mean and SD of the magnetic field intensity was not significantly affected by cadence, but the variability in the crank magnetometer data indicates that it was affected by the crank angle. The average magnetic field intensity around the bicycle frame IMMS was 7-9% above normal (a value of one), and the SD was 1.1%. The crank arm IMMS field intensity was much larger, with a 41±18% deviation from normal. As expected, disturbances due to dynamic acceleration were also much higher for the crank arm and increased with cadence. However, DAC removed the majority of the disturbances from the crank IMMS accelerometer measurements (Figure 28).

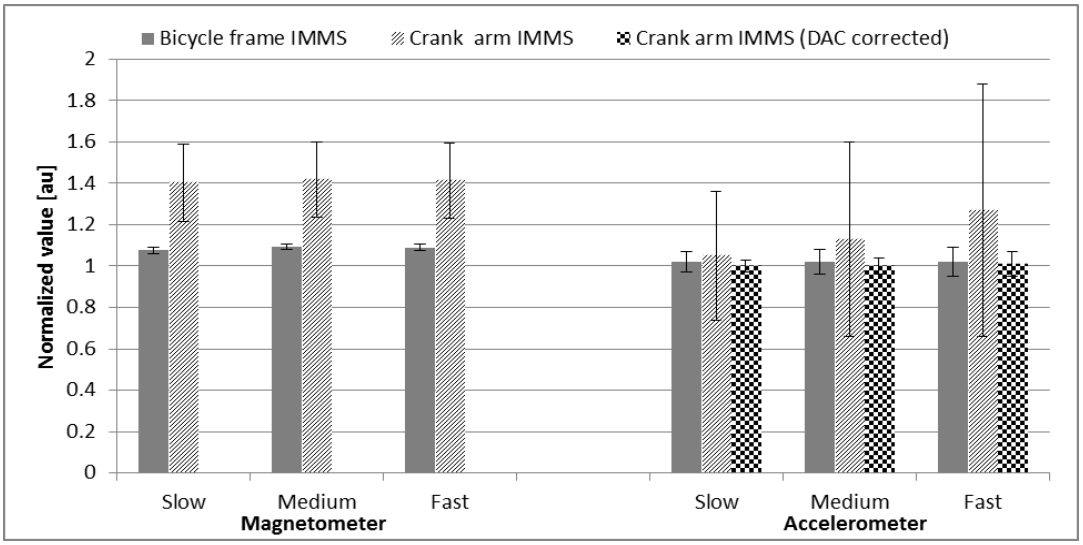

Figure 28: Comparison of magnetometer measurements and acceleration measurements (with and without DAC) for the IMMSs. Data normalized to a value of 1 for the undisturbed magnetic and gravitational fields respectively. Bar values give the mean value for each test and error bars indicate the SD.

4.4. Discussion

In this study we present a nonlinear passive complementary filter (PCF_HC) for tracking the bicycle crank angle using two wireless IMMSs attached to the crank arm and bicycle frame. The PCF_HC is robust against commonly-found disturbances to the magnetic and gravitational field vectors measured by the crank arm IMMS. To solve the problem of magnetic field interferences, we propose two magnetometer-free sensor-to-body calibration methods and a heading constraint algorithm, which exploit the planar motion of the crank arm relative to the bicycle frame. The PCF_HC also incorporates a dynamic acceleration compensation method to improve estimates of the gravity vector during rigorous pedaling. Validation tests for the PCF_HC were conducted with an optical motion capture system at three pedaling speeds. The results show that the PCF_HC performed with absolute errors of $1.3 \pm 0.9°$ or better at all cadences using both Mixed_FA and Dynamic_FA despite continuous and variable magnetic and gravitational field disturbances. This was superior to crank angle tracking using the magnetometer data, which produced mean absolute errors greater than 10°. These findings demonstrate that the heading constraint and proposed frame alignment techniques can be used successfully to track bicycle crank angles despite magnetic interferences which can cause magnetometer-based methods to fail.

While there has been a recent increase in inertial sensor applications for cycling analysis [21-24], the authors are aware of only two studies focusing on crank angle tracking [25, 17]. In the first study, Kitawaki and Oka measured bicycle crank angles using wireless inertial sensors [25]. They report lower MAE values than this study (0.339 ± 0.115°), but only used gyroscope integration limited to a short 25 second test. They present no filtering method for gyroscope bias estimation or drift error minimization using measurement updates from auxiliary sensors e.g. inclination updates using an accelerometer. Their protocol also requires a manual alignment of the axes of crank sensor with the crank arm body frame, which can lengthen the testing time and may suffer from sensor positioning errors. Our study allows for arbitrary placement of the sensors on the bicycle, and can operate drift-free over an extended period using measurement updates. The MAEs in this study were similar to those reported in the second study using the so-called CRANK filter [17]. However, the PCF_HC overcomes a limitation of the CRANK filter in that it requires dynamic accelerations to work, and can thus only compensate for gyroscope drift error during normal forward pedaling. The PCF_HC filter performs acceleration updates using the gravity vector (it eliminates dynamic accelerations), meaning that it operates drift-free even when the crank arm is stationary or when pedaling backwards.

The Static_FA results for the PCF and PCF_HC (Figure 26) illustrate the typical error effects due to dynamic accelerations and magnetic interference. The reduced error variability for the PCF_HC shows that the heading constraint improved the stability of the PCF filter by removing significant noise introduced by the magnetometer measurements. On the other hand, mean errors were still appreciably higher for the PCF_HC using Static_FA than with Mixed_FA and Dynamic_FA. This can be explained by the fact that Static_FA uses the magnetometer in the crank arm IMMS to obtain the sensor heading, whereas as the other two frame alignments do not. Unlike the well-known Static_FA method, the Mixed_FA method is unaffected by magnetic field disturbances. However, these two methods are still both susceptible to human error when the crank arm is positioned at a prescribed crank angle during the static pose. Therefore, Dynamic_FA may be preferable in terms of reducing both human error and time spent on a static calibration procedure.

As shown in Figure 27 and Figure 28, the DAC method was particularly effective at removing dynamic accelerations from the crank arm IMMS. This allows for a wide range of filter gains to produce similar performance. The DAC effectively removes high frequency errors in gravity estimation related to the pedaling frequency i.e. with

DAC the auxiliary measurement system can track the faster changes in crank angle. This allows the filter to have a higher cross-over frequency between the gyroscope integration system and the auxiliary measurement system. The increased gain reduces the settling time required for orientation and bias estimation, especially if the filter needs to re-initialize for some reason during active pedaling. Without DAC, the optimal gain region is very narrow and the minimum error is higher. Figure 28 illustrates the extent of environmental disturbances which are possible with a bicycle. It is quite possible that some bicycles may have much lower or higher magnetic interference levels near the crank arm. This variability makes it essential that crank angle tracking methods are not susceptible to magnetic field disturbances. Although we used two bicycle IMMS magnetometers for heading observations, the HC algorithm ensures that interference in these measurements does not affect crank angle accuracy significantly because the effect is duplicated for both body segments to preserve the constraint. The accelerometer signal analysis illustrates the increasing disturbances of dynamic accelerations on gravity estimation. It should be noted that the standard deviation in measured acceleration – roughly 0.6g for the fast cadence trial – equates to approximately one quarter of the range of acceleration i.e. 2.4g. This implies that the dynamic acceleration is larger than the gravitational acceleration during fast pedaling.

We have made three contributions towards eventual field testing of cycling using IMMSs. Firstly, we have developed two simple, magnetometer-free methods of performing sensor-to-body frame alignment. Secondly, we have presented a method of tracking the heading of the crank arm IMMS using the bicycle frame magnetometer using the HC algorithm. Lastly, we have developed a method of estimating the radius of rotation for both body frames and compensating for the rotational accelerations. Nevertheless, future work is required to determine the accuracy of the PCF_HC (especially the DAC) during very long periods of cycling as well as under outdoor conditions. While the results of this study are only directly applicable to indoor use, the methodology proposed is quicker, easier and more cost-effective to implement in a laboratory setting than other approaches such as optical motion capture. It can thus already be used for indoor applications as an alternative.

4.5. Conclusion

This study validated two sensor-to-body frame alignment methods for tracking the angular crank arm position using wireless IMMSs. Unlike standard static pose

calibrations, these methods are unaffected by the common magnetic field disturbances commonly found near bicycle pedals. A nonlinear complementary filter is also presented which implements novel heading constraint and dynamic acceleration compensation algorithms that enables highly accurate crank angle tracking, improve filter responsiveness and are resistance to magnetic field interferences.

4.6. References

[1] A. M. Hasan, K. Samsudin, A. R. Ramli, R. S. Azmir and S. A. Ismaeel, "A review of navigation systems (integration and algorithms)," *Aust. J. Basic Appl. Sci.*, vol. 3, no. 2, pp. 943-959, 2009.

[2] A. Baca, P. Dabnichki, M. Heller and P. Kornfeind, "Ubiquitous computing in sports: A review and analysis," *J. Sports Sci.*, vol. 27, no. 12, pp. 1335-1346, 2009.

[3] A. Avci, S. Bosch, M. Marin-Perianu, R. Marin-Perianu and P. Havinga, "Activity recognition using inertial sensing for healthcare, wellbeing and sports applications: A survey," in *Architecture of computing systems (ARCS), 2010 23rd international conference on*, VDE, 2010.

[4] H. Zeng and Y. Zhao, "Sensing movement: Microsensors for body motion measurement," *Sensors*, vol. 11, no. 1, pp. 638-660, 2011.

[5] O. J. Woodman, "An introduction to inertial navigation," University of Cambridge Computer Laboratory, Cambridge, 2007.

[6] M. D. Shuster and S. D. Oh, "Three-axis attitude determination from vector observations," *J. Guid. Control Dynam.*, vol. 4, no. 1, pp. 70-77, 1981.

[7] F. L. Markley and D. Mortari, "How to estimate attitude from vector observations," in *Proceedings of the AAS/AIAA Astrodynamics Specialist Conference*, 1999.

[8] A. M. Sabatini, "Estimating three-dimensional orientation of human body parts by inertial/magnetic sensing," *Sensors*, vol. 11, no. 2, pp. 1489-1525, 2011.

[9] W. H. K. De Vries, H. E. J. Veeger, C. T. M. Baten and F. C. T. Van Der Helm, "Magnetic distortion in motion labs, implications for validating inertial magnetic sensors," *Gait Posture*, vol. 29, no. 4, pp. 535-541, 2009.

[10] D. Roetenberg, "Inertial and Magnetic Sensing of Human Motion," University of Twente, 2006.

[11] D. Roetenberg, H. Luinge, and P. Slycke. (2009, Apr.). *Xsens Homepage* [Online]. http://www.xsens.com/images/stories/PDF/MVN_white _paper.pdf [Accessed 10 January 2010].

[12] H. Luinge, P. Veltink and C. Baten, "Ambulatory measurement of arm orientation," *J. Biomech.*, vol. 40, pp. 78–85, 2007.

[13] L. Morton, L. Baillie and R. Ramirez-Iniguez, "Pose calibrations for inertial sensors in rehabilitation applications," in *Wireless and Mobile Computing, Networking and Communications (WiMob), 2013 IEEE 9th International Conference on*, Lyon, 2013.

[14] J. Favre, R. Aissaoui, B. M. Jolles, J. A. De Guise and K. Aminian, "Functional calibration procedure for 3D knee joint angle description using inertial sensors," *J. Biomech.*, vol. 42, no. 14, pp. 2330-2335, 2009.

[15] J. Cockcroft and C. Scheffer, "Determining the feasibility of measuring outdoor road cycling kinematics using inertial motion capture technology," SAIEE Africa Research Journal, vol. 102, no. 1, pp. 31 – 39, 2011.

[16] J. Cockcroft, "An evaluation of inertial motion capture technology for use in the analysis and optimization of road cycling kinematics," University of Stellenbosch, Stellenbosch, 2011.

[17] J. Cockcroft, J. H. Muller and C. Scheffer, "A novel complementary filter for tracking bicycle crank angles using inertial sensors, kinematic constraints and vertical acceleration updates," *IEEE Sensors J.*, vol. 15, no. 8, pp. 4218 - 4225, 2015.

[18] Y. Xiaoping, E. R. Bachmann and R. B. & McGhee, "A simplified quaternion-based algorithm for orientation estimation from earth gravity and magnetic field

measurements," *Instrumentation and Measurement, IEEE Transactions on*, vol. 57, no. 3, pp. 638-650, 2008.

[19] R. Mahony, T. Hamel and J. M. Pflimlin, "Nonlinear complementary filters on the special orthogonal group," *Automatic Control, IEEE Transactions on*, vol. 53, no. 5, pp. 1203-1218, 2008.

[20] J. Keat, "Analysis of Least-Squares Attitude Determination Routine DOAOP," Computer Sciences Corporation, Maryland, 1977.

[21] R. Marin-Perianu, M. Marin-Perianu, P. Havinga, S. Taylor, R. Begg, M. Palaniswami and D. Rouffet, " A performance analysis of a wireless body-area network monitoring system for professional cycling," *Pers. Ubiquit. Comput.*, vol. 17, no. 1, pp. 197-209, 2013.

[22] J. Y. Xu, X. Nan, V. Ebken, Y. Wang, G. J. Pottie, and W. J. Kaiser, "Integrated inertial sensors and mobile computing for real-time cycling performance guidance via pedaling profile classification," *IEEE J. Biomed. Health Informat.*, vol. 19, no. 2, pp. 440–445, Mar. 2015.

[23] Y. Zhang, K. Chen and J. Yi, "Rider trunk and bicycle pose estimation with fusion of force/inertial sensors," *IEEE T. Bio-Med. Eng.*, vol. 60, no. 9, pp. 2541-2551, 2013.

[24] J. Cockcroft, J. Muller and C. Scheffer, "A novel complimentary filter for tracking hip angles during cycling using wireless inertial sensors and dynamic acceleration estimation," *IEEE Sensors J.*, vol. 14, no. 8, pp. 2864 - 2871, 2014.

[25] T. Kitawaki and H. Oka, "A measurement system for the bicycle crank angle using a wireless motion sensor attached to the crank arm," *J. Sci. Cycling*, vol. 1, no. 2, pp. 13–19, 2013.

5. Paper 4: A Descriptive Study of Step Alignment and Foot Positioning Relative to the Tee by Professional Rugby Union Goal Kickers

Abstract: *This study describes foot positioning during the final two steps of the approach to the ball amongst professional rugby goal kickers. An optical motion capture system was used to test 15 goal kickers performing 10 goal kicks. The distance and direction of each step, as well as individual foot contact positions relative to the tee, were measured. The intra- and inter-subject variability was calculated as well as the correlation (Pearson) between the measurements and participant anthropometrics. Inter-subject variability for the final foot position was lowest (placed 0.03 ± 0.07 m behind and 0.33 ± 0.03 m lateral to the tee) and highest for the penultimate step distance (0.666 ± 0.149 m), performed at an angle of 36.1 ± 8.5° external to the final step. The final step length was 1.523 ± 0.124 m, executed at an external angle of 35.5 ± 7.4° to the target line. The intra-subject variability was very low; distances and angles for the 10 kicks varied per participant by 1.6–3.1 cm and 0.7–1.6°, respectively. The results show that even though the participants had variability in their run-up to the tee, final foot position next to the tee was very similar and consistent. Furthermore, the inter- and intra-subject variability could not be attributed to differences in anthropometry. These findings may be useful as normative reference data for coaching, although further work is required to understand the role of other factors such as approach speed and body alignment.*

Citation:

J. Cockcroft, D. van den Heever, " A descriptive study of step alignment and foot positioning relative to the tee by professional rugby union goal kickers ," *J. Sports Sci.*, "In-press", 2015

5.1. Introduction

The majority of points in a game of rugby union are scored by goal kickers. Consequently, accurate and reliable goal kicking is a crucial skill in the sport and goal kickers spend several hours during a training session refining their goal kicking technique [1]. A goal kick is a complex series of motions involving an angled approach to the ball, planting of the support foot beside the ball and a sequential transfer of momentum from the pelvis to the foot segment of the kicking leg [1-3].

Elite rugby union goal kickers can achieve success rates of over 80% in a season (www.goalkickers.co.za), despite diversity in their goal kick execution.

The understanding of these different movement strategies has been restricted by a lack of research on optimal goal kicking biomechanics up to date [1, 4-6]. It is thus probable that further scientific analysis of goal kicking technique will yield improvements to goal kicking success rates through better coaching and training methods. Only a few studies of rugby union goal kicking have been conducted, with most focusing on factors influencing foot and ball velocity. Baktash *et al.* [1] investigated the effect of different instep foot positions on resultant ball velocity in goal kicking. Four different foot positions relative to the kicking tee were marked and the three university male kickers each performed three good trials of each condition. The results suggested no significant differences in velocities across the different conditions within each participant. Padulo *et al.* [6] investigated the relationship between four different run-up types to the goal–kick, kinematic variables and the average ball velocity. The participants in the study were six senior athletes playing at national level. The study reports significant differences in run time and ball velocity for the different run-ups with a longer run-up resulting in higher ball velocities.

Zhang *et al.* [5], using a novel velocity decomposition method, examined the contributions of individual body segments to the final foot velocity during rugby goal kicking. Seven male university kickers participated in the study. The results showed that knee flexion/extension made the biggest contribution to final foot velocity, followed by hip flexion, pelvis velocity and pelvis rotation. A proximal-to-distal sequential motion pattern of body segments were consistently observed, indicating the important role of interaction between adjacent segments during the rugby goal kicking movement. Bezodis *et al.* [4] studied the contribution of the non-kicking-side arm during a rugby goal kick. Five experienced male kickers performed trials with an accuracy requirement. They found greater angular momentum in the non-kicking-side arm for skilled kickers. They also showed that the center of mass of the kicking leg was closer to the stance ankle in the mediolateral direction for accurate kickers. In a study by Ball *et al.* [7] four elite rugby league goal kickers (the goal kick is similar to rugby union goal kick) performed between five and 15 goal kicks on their usual training ground from 40 m in front of the goalposts. Body lean, body alignment to the target and center of mass (CM) velocity at ball contact was investigated. The results showed that all players leaned away from the ball, body alignment angles were non-

zero (indicating that the kickers were not square to the target at ball contact) and they moved their CM towards the target.

However, the groups tested in these studies were very small (three to seven participants), and covered varying levels of skill. There is thus a need for larger studies analyzing goal kicking technique in an elite population.

Many more biomechanical studies have been conducted on kicking movements similar to rugby union goal kicking [1]. According to Lees *et al.* [8], the nature of the approach to the ball appears to be important in soccer instep kicking. An important factor in maximal kicking is the length of the last stride. A longer last stride has been reported for longer kicks in soccer [9, 10]. Furthermore, Ball [11] also reports on the importance of the last stride in punt kicking in Australian Rules football. Other important factors include the position of the support foot relative to the ball and the support leg kinematics during the punt kick [11, 12]. Notably, the placement of the support foot has received little attention in research even though it is believed to be important to the outcome of the kick [8]. Overall, it is generally believed that elite athletes display less mechanical variability and greater temporal proximity of these kicking movement components compared to less skilled players [3]. It is therefore important to understand the influence and interdependence of the step lengths and foot positions relative to the tee in rugby goal kicking, as well as the intra- and inter-participant variability of these outcomes within different age-groups and skill levels. Moreover, since step length is highly correlated with leg length in normal walking, group variability in step lengths and foot positioning during the approach to the ball in goal kicking may be influenced by body dimensions [13]. Therefore, it would be helpful to understand how the inter-participant variability in factors such as anthropometrics influences variability in measurement outcomes.

This study presents a description of foot position relative to the tee in the approach to the ball by elite rugby goal kickers. The aim was to capture baseline data from a skilled player population in order to improve biomechanical knowledge of this movement. We also wanted to investigate the relationship between participant body size and the step and foot position parameters. In particular, the objectives were to describe:

a) The average distance and angle of the final two steps and associated foot positions relative to the tee, as well as the inter-participant variability

b) The average intra-participant variability (inconsistency) for the step and foot position parameters, as well as the inter-participant variability in inconsistency

c) The correlation between participant anthropometry (height and leg length) and the inter- and intra-participant variability in step and foot position parameters

This was achieved by measuring the foot positions of professional rugby union goal kickers during a battery of consecutive kicks using an advanced three-dimensional motion capture system.

5.2. Methods

5.2.1. Participants

The study was conducted at the motion analysis laboratory at the University of Stellenbosch and included fifteen professional rugby union goal kickers. At the time of the study each participant was competing at either national or international level and gave informed consent for the testing. Ethical approval for the research was obtained from the Human Research Ethics Committee of Stellenbosch University. The participant population had an average age of 26.4 years (range: 20-32), average height of 1.79 m (1.72 – 1.91) and average weight of 87 kg (82.4 – 93.3).

5.2.2. Data collection

Each participant performed ten consecutive goal kicks in the laboratory using their own kicking tee and a single pre-selected premier league Gilbert rugby ball. Due to the hard rubber flooring in the laboratory, participants performed the test kicks wearing running shoes. Participants were instructed to perform a complete goal kick (run-up and kick at self-selected speed and intensity) towards a target defined by two strips of tape simulating distant goal posts on the wall behind a steel framed net (Figure 29). Participants were instructed that the target was a mid-range (submaximal) distance away. The laboratory's 8-camera Vicon MX system was used to create a capture volume (L x W x H approximately 4m x 4m x 2m) covering the run-up area of the kicker, and the kicking tee was placed in the same predefined position to ensure that the non-kicking support leg (SL) foot landed on a Bertec force-plate imbedded in the floor. Data from these two systems was captured synchronously in the Vicon Nexus software (version 1.8.4) at 200 Hz and 1000 Hz respectively. The Vicon cameras were calibrated dynamically using the standard

dynamic 5-point wand waving procedure, and the force plate output was set to zero before the start of every test. Besides masking the cameras from environmental sources of infra-red reflection, it was also necessary to cover any reflective materials in the participant's shoes and clothing with tape to prevent false marker detections.

Standard passive-reflective Vicon markers (14 mm diameter) were placed on the left and right shoe points corresponding to the heel (heel marker) and end of the second metatarsal (toe marker). A marker was also placed at the back of the tee to mark its position. Each participant performed their own stretch and warm up routine before the marker placement. This was then followed by 5-10 practice kicks in order to acclimatize to the markers, the different floor surface and running shoes. The ten kicks were then recorded from 2s before the start of the run-up (determined by a verbal cue given by the participant) until 2s seconds after ball strike. After marker reconstruction and labeling, the Vicon Nexus Woltring filter algorithm (MSE value of 20 mm) was used to remove high frequency measurement noise from the foot marker trajectories. The foot marker trajectories were then exported to Matlab (version 8.2.0.701, R2013b) for analysis.

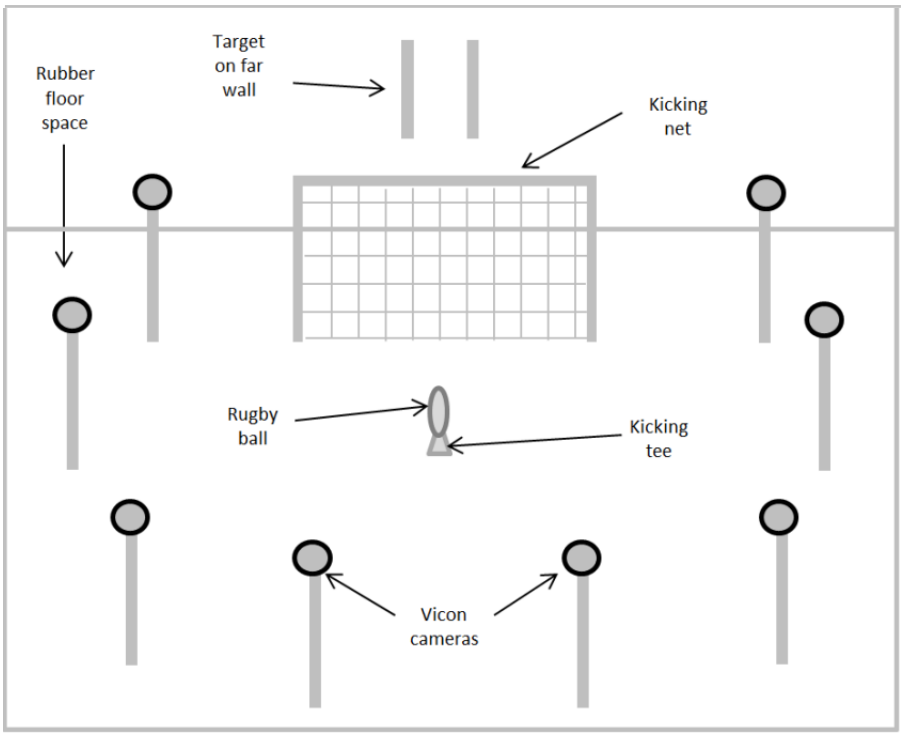

Figure 29: Schematic of test set up showing Vicon cameras positions relative to ball, net and target.

5.2.3. Data analysis

Data analysis consisted of two parts: a step analysis (Figure 30a) and a foot position analysis (Figure 30b). The step analysis focused on the final two steps in the approach to the ball. The penultimate step is from the SL to the kicking leg (KL) i.e. from a foot contact point on the SL (S1) to one on the KL (K1). This was named the 'ghost step' because of the typical drifting motion carried out by players executing it. The final step, between K1 and the SL foot contact (S2), was called the 'power step' because it is typically performed at a high intensity. The ghost step length was defined as the horizontal distance between the SL toe marker at time of S1 and the KL toe marker position at the time of K1. Similarly, the length of the power step was defined as the horizontal distance from the KL toe marker at K1 to the SL heel marker at the time of S2. Since the step length is a scalar value, the angular direction of each step was also analyzed to provide insight into the direction of approach during each step. The power step angle was defined as the external angle between the power step and the line between tee and target. The ghost step angle was taken as the external angle between the power step and ghost step. .

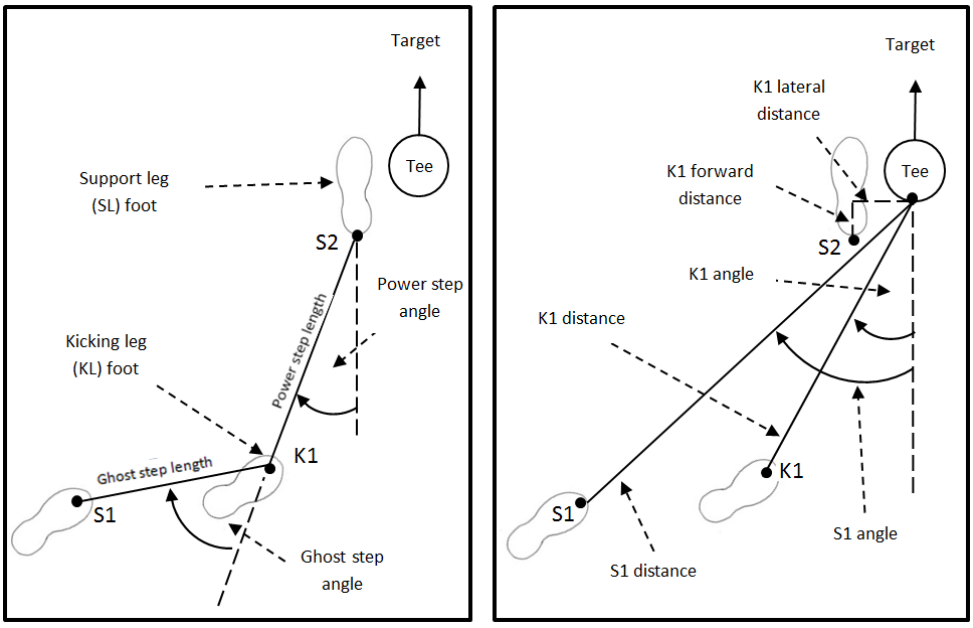

(a) (b)

Figure 30: A top view illustration (for a right-foot place-kick) of (a) the angle and distance of the ghost and power steps (b) the angle and distance to the tee of the S1 and S2 foot positions and the lateral and forward position of the SL foot at S2.

The ghost step and power step measurements both include the variability of two foot contact positions. Therefore, the second part of the analysis focused on the individual variability in foot positions at S1, S2 and K1 relative to the fixed position of tee (see Figure 30b). The distance to the tee and angle to the tee relative to the target line were calculated for the S1 and K1 toe marker positions. In contrast, the position of the SL heel marker was analyzed by taking the lateral distance (perpendicular distance from target line) and the forward distance (along the target line direction) relative to the tee marker. The kicking events (S1, K1 and S2) were detected automatically using a customized Matlab algorithm. S2 was detected when the vertical force of the force plate exceeded a minimum threshold of 30 N. Due to the higher sampling rate of the force plate, the algorithm chose the nearest Vicon camera sample as S2. The S1 event was defined as the peak acceleration corresponding to the lifting of the SL foot off of the ground at the beginning of the ghost step. This was chosen instead of the moment of foot contact as some players with a two-step run-up begin the approach to the ball with the SL foot on the ground. The K1 event was defined as the moment of peak acceleration after S1 corresponding to the foot contact on the ground. The anthropometric measurements included were participant height, kicking leg length and support leg length which were performed by a qualified physiotherapist.

For the group analysis, the mean and standard deviation (SD) of each parameter was calculated for the participants' ten kicks. The mean for a player's ten kicks was taken to be representative of the participant, and these means were then averaged to obtain a group mean and group SD for each parameter (Representative Data). The group mean for the Representative Data is thus the baseline average norm and the group SD of the Representative Data was taken to be the inter-participant variability of the norms. Secondly, the intra-participant SD for the ten kicks was taken as the intra-participant variability for the ten kicks (Inconsistency Data). Therefore, the group mean of the Inconsistency Data represents the baseline norm, and the group SD represents the inter-participant variability in inconsistency. Lastly, in order to assess the interdependence of the parameters and the effects of different body sizes, relationships between basic participant anthropometric measurements and the step and foot position parameters were examined using the Pearson correlation function for linear relationships. A 95% confidence limit was set with an alpha level of $P = 0.05$ for significance.

5.3. Results

The results for the Representative Data and Inconsistency Data analysis are given in Table 6. On average, the ghost step length was slightly less than half the length of the power step (44%). It was also more variable than the power step, especially as a percentage of its length (22.4% vs. 8.1%). In terms of foot position, the S1 distance to the tee was naturally the longest at 2.365 m. The S1 position also contained the highest dimensional variability (0.206 m), although this was even lower than the power step length variability as a percentage of length (8.7%). The least variable foot position between participants, proportional to length, was the K1 position (5.8%) with a length of 1.756 ± 0.101 m.

Table 6: Group means and SDs of representative data and the associated inconsistency

	REPRESENTATIVE DATA		INCONSISTENCY DATA	
	Group mean	**Group SD**	**Group mean**	**Group SD**
Distances [m]				
Ghost step	0.666	0.149	0.023	0.008
Power step	1.523	0.124	0.026	0.008
S1 to tee	2.365	0.206	0.031	0.010
K1 to tee	1.756	0.101	0.020	0.005
S2 lateral	0.330	0.031	0.016	0.004
S2 forward	-0.031	0.074	0.018	0.005
Angles [deg]				
Ghost step	36.1	8.5	1.6	0.5
Power step	35.5	7.4	1.0	0.4
S1 to tee	50.9	5.3	0.7	0.4
K1 to tee	43.6	6.2	0.7	0.4

The lowest dimensional inter-participant variability in the Inconsistency Data was for the S2 lateral distance to the tee. The SL foot was placed approximately 33 cm to the side of the ball with 3cm of variability, while the S1 forward distance variability was more than double this (7.4 cm). The negative 3 cm forward plant distance indicates that on average the heel was placed slightly behind the back of the tee. The angular measurements again show the ghost step to be the most variable (8.5°), although angular variability was consistent as this was only slightly more than the minimum angular variability of 5.3° which was found for the S1 foot position. The power step

angle was almost identical to the ghost step angle and, as would be expected, slightly smaller than the K1 angle since all players placed the SL foot lateral to the ball at S2. The participants employed a K1 foot position approximately diagonal to the tee (43.6°) with a moderate variability of 6.2°. The S1 angle was slightly larger than the K1 angle, which corroborates the positive ghost angle.

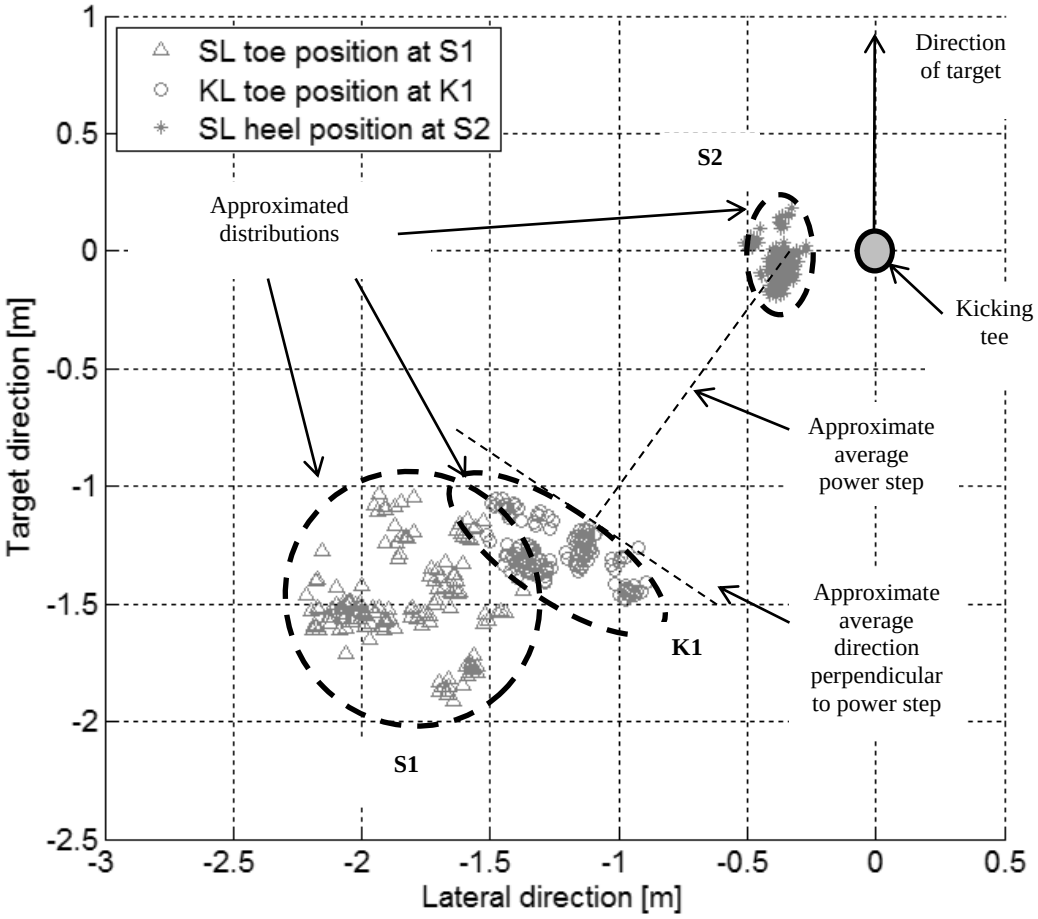

Figure 31: View from above of foot placements relative to the tee at S1, K1 and S2. The distributions are approximated by thick dashed lines illustrating the nature of foot placement variability.

In terms of the inconsistency data, the most consistent parameters were the S2 lateral and forward distances which varied by approximately 1-2 cm for the participants' 10 kicks. Of the longer distances, the K1 foot position was the most consistent (1.5 – 2.5 cm) and S1 was the most inconsistent (2-4 cm). The intra-participant variability in the angular measurements was slightly higher for the step parameters than the foot

positions relative to the tee, although by less than 1°. The distribution patterns of the foot positions are shown in Figure 31.

The S2 plant foot position was slightly more variable in the target direction compared to the lateral direction. The K1 toe positions were also significantly less variable in the direction of power step and more spread out perpendicular to the power step. It should be noted, therefore, that the variability in K1 foot position (SD 0.101 m) is largely due to the variability of the power step angle. The S1 position, on the other hand, approximates a more random circular distribution. While its variability perpendicular to the run-up is similar in size to the K1 position, the parallel variability is significantly larger than that of the K1 position – this explains the larger S1 distance inter-participant variability in Table 6. The average S1 position is also lateral to the average K1 position, which correlates with the positive ghost angle.

Table 7 shows the correlation coefficients for the participant anthropometric measurements and the different run-up parameters defined. It is evident that participant height is not a significant factor in determining step lengths or foot positions relative to the tee. None of the relationships between height and the biomechanical parameters showed any statistical significance. The strongest correlation between anthropometric measurements and biomechanical parameters were between leg length and S1 distance with a correlation of 0.55 for both legs.

Table 7: Correlation between participant anthropometric measurements and mean kick parameters

	Ghost step distance	**Power step distance**	**S1 distance**	**K1 distance**	**S2 lateral distance**	**S2 forward distance**	**Ghost step angle**	**Power step angle**	**S1 angle**	**K1 angle**
Height	-0.22	0.26	0.40	0.05	0.43	-0.06	-0.02	0.16	0.21	0.08
KL length	-0.22	0.42	0.55*	0.13	0.48	-0.22	-0.08	0.29	0.38	0.28
SL length	-0.25	0.42	0.55*	0.11	0.45	-0.23	-0.10	0.31	0.39	0.30

(* indicates a P value < 0.05)

Table 8 shows the correlation coefficients for the participant anthropometric measurements and the standard deviations in the kick parameters for their 10 kicks. Again there was no clear correlation between the data with only the S1 distance

variability showing moderate correlation with the kicking leg length of -0.54 ($P < 0.05$).

Table 8: Correlation between participant anthropometric measurements and standard deviations of kick parameters

	Ghost step distance	Power step distance	S1 distance	K1 distance	S2 lateral distance	S2 forward distance	Ghost step angle	Power step angle	S1 angle	K1 angle
Height	-0.29	-0.30	-0.47	-0.17	0.00	0.04	0.37	-0.19	-0.21	-0.32
KL length	-0.09	-0.23	-0.54*	-0.21	-0.03	0.04	0.32	-0.12	-0.11	-0.21
SL length	-0.09	-0.22	-0.50	-0.16	-0.06	0.00	0.31	-0.13	-0.10	-0.21

(* indicates a P value < 0.05)

5.4. Discussion

This study presents the first description of foot positioning during the approach to the ball amongst professional rugby-union goal kickers measured using a gold-standard three-dimensional motion capture system. The analysis focused on three key foot positions relative to the kicking tee which define the final two steps in the approach to the ball. The parameters included both the distance and direction of the steps and foot positions relative to the tee, as well as the intra-participant variability for 10 kicks. The results show that inter-participant variability was considerably higher than intra-participant variability for all parameters. Intra-participant variability was also consistent for the group, suggesting that while there may be appreciable differences in how successful goal kickers approach the ball these differences do not markedly affect the consistency of execution. We also found that the penultimate step direction varied considerably relative to the final step direction, and that the group variability decreased notably for each successive foot position during the run-up. This suggests that foot positioning next to the tee may be the most important foot position during the run-up, and perhaps also that sufficient emphasis on penultimate step technique may be lacking. Lastly, we found no significant correlation between the height and leg length of players and foot positioning, which would caution against the use of anthropometrics as a major basis of coaching run-up distance and angles. This study provides valuable and novel reference data and analyses for coaches and sport scientists interested in professional goal kicking technique. The breakdown of events

and step phases proposed in the analysis framework could also provide a useful starting point for future research aimed at improving coaching and training methods.

This study's finding of a 1.523 m (SD 0.124 m) mean power step length is very similar to that of Stoner and Ben-Sira [9], who report a last step length of 1.5m for medium range kicking in soccer. Lees *et al.* [8] suggest in a review of the biomechanics of kicking in soccer that the length of the last step is important in maximal kicking. Stoner and Ben-Sira [9] also found that professional soccer players executed a longer last step (1.69 m) when performing a long-range kick. Similarly, Ball [11] investigated the biomechanics of distance kicking in Australian rules football and found longer kick distances to be associated with larger last step distances. He reports last step distances in the region of 1.74 m for maximal punt kicking, which is understandably higher than those for the sub-maximal kicking tests in this study. It should also be noted that the slightly shorter step lengths could have been reported in this study due to the toe-to-heel calculation method used to measure the power step.

Similarly to the foot position analysis presented in this study, Baktash *et al.* [1] investigated the effects of different instep foot positions on ball velocity in goal kicking, but found no significant difference between positions. However, ball position relative to the support foot has been indicated as an important variable in soccer kicking, together with approach angle and last stride [2, 11, 14-16]. The findings of this study support this assertion, as it was found that players ensured highly repeatable placement of the SL foot at S2. Even with the variability in power step between participants the foot plant distances to the tee were consistent, especially in the lateral direction. Lateral distances for foot position at S2 were more consistent at a mean of 33 cm to the side of the ball with a group SD of 3 cm, compared to the forward target direction with a mean of -3 cm (heel placed behind the tee) with a group SD of 7 cm. This is in close agreement with McLean *et al.* [17], who report mean foot to ball distances for soccer drive kicking of 37.3 cm to the side and 8.1 cm behind the ball. However, they measured the distances from the center of the ball to a position on the foot a third of the distance from the heel to the toe. Scurr and Hall [18], investigating the effects of approach angle on penalty kick kinematics with recreational soccer players, found foot placements of 32.7 cm to the side and 9.7 cm behind the ball. They measured the distances from the center of the ball to the lateral aspect of the fifth metatarsal. This suggests that while the lateral plant distance is very similar in soccer, rugby goal kickers typically plant the foot closer to the

target relative to the tee. This may be due to the differences in direction of the ball spin which soccer players seek to impart to the ball compared to rugby goal kicking.

Descriptions and possible explanations of variability formed a key component of this study. The intra-participant variability (kicker inconsistency) was very low on average as well as consistent for the group, suggesting that professional rugby union goal kickers tend to reach similar high levels of repeatability from training. This means that the inconsistency results from this study (< 3 cm distance, < 2° direction) might be used as a basic guideline of the required consistency for skilled goal kicking when training young kickers. In contrast, inter-participant variability in the approach was notable. This suggests that the measurements from this study cannot be used directly as a guide for determining step lengths or step angles. However, the results may be useful as a normative reference data. Notably, it was found that participant anthropometry in general did not have a major influence on the inter-participant variability of distance parameters – although leg length and S1 distance showed moderate correlation. This differentiates goal kicking from movements such as walking, where step length generally increases proportionally with leg length [13]. It may be that the observed inter-participant variability was due to other factors such as approach speed. For instance, shorter players may execute a proportionally more aggressive power step in order to achieve similar kicking distances to taller players. They may also adopt a longer and faster run-up for this reason, increasing ghost step length accordingly. Participant anthropometry also did not correlate significantly with the inconsistency data. This may indicate that similar levels of motor control can be expected from kickers of different heights.

Both the intra- and inter-participant variability results show that control of foot position increases as players approach the ball. In terms of intra-participant variability, the S2 foot positions were remarkably consistent (almost twice so compared to the S1 position) and the second most consistent was the K1 position. Moreover, the S1 and K1 angles were twice as repeatable as the step angles. This suggests that the kickers were controlling the S2 and K1 positions relative to the tee by adjusting the step lengths and angles – rather than the other way around. This may also be due to the fact that kickers typically fix their gaze on the ball and tee during the run-up, rather than focusing on the S2 position. The inter-participant variability displays a similar trend to the intra-participant variability in that it decreases in the approach to the ball. It appears that participants adjusted their K1 and S1 foot positions in order to optimize S2 foot placement and perhaps other aspects of their

technique (speed and body alignment, for example) rather than converging on optimal step distances. This can be inferred from Figure 31 where S2 foot positions next to the tee were very similar despite greater variability at the preceding foot positions (S1 and K1). The higher inter-participant variability in S1 and K1 positions relative to the tee appears to be largely due to variability in step angles – although there was also variability in the step lengths, which is not directly affected by step angles. In fact, working backwards from S2, the inter-participant variability in S1 position can be seen as cumulative, containing the variability of both the ghost and power step lengths and angles. It is not immediately clear why the ghost step was taken in a different direction to the power step, or why it was so inconsistent, amongst the participants. This may have to do with inter-participant variability in the alignment of the pelvis and upper body to the target during the run-up. The variability in step length, however, could rather be due to variability in other linear parameters such as run-up momentum, speed and acceleration.

The limitations of this study relate mainly to factors affecting the ecological validity of testing. Due to the fact that data was collected in a laboratory setting, the rubber floor surface presented different footing conditions to the grass playing surface used in rugby games. This in turn required the use of different shoes (running shoes) compared to the boots typically used by the players when competing. While this should not have significantly affected step lengths and foot positioning, it may have altered the frictional forces during foot contact. To reduce this effect, players were allows multiple practice kicks until they felt comfortable in the new conditions. Another limitation was that the players were not able to kick towards their usual target (upright poles) in the laboratory and the distance and success of each kick could thus not be determined. We aimed to simulate the target appearance on the laboratory wall, and instructed the participant to perform a long distance (but submaximal) kick. The practice kicks were also important for familiarization with the target. On the other hand, it should be noted that this familiarization with the target may have affected the intra-participant variability of the results since players do not typically execute multiple kicks from the same field position in a game. However, changes in goal kicking technique are not necessarily necessary or desirable for different target distances and angles. Nevertheless, randomization of the target conditions may provide insight into the effect of this on variability. Lastly, further work is needed to understand the changes in the measured outcomes due to pressure and fatigue, as these were not considered for this study.

These findings constitute a valuable contribution to the understanding of the inter- and intra-participant variability in run-up geometry amongst professional rugby union goal kickers. Greater standard deviations for measured parameters are indicative of less consistent movement patterns, a trait associated with less skilled kickers [4, 19]. It would therefore be interesting to see how the intra-participant and inter-participant variability of unskilled players compares to those of the elite participants reported in this study, as well as how these groups respond to different coaching interventions aimed at reducing variability. Future research should thus include similar analysis conducted on young and unskilled adult populations. It is also necessary to document other related biomechanical aspects, such as body alignment relative to the target and approach speed, during the approach to the ball.

5.5. References

[1] S. Baktash, A. Hy, S. Muir, T. Walton and Y. Zhang, "The Effects of Different Instep Foot Positions on Ball Velocity in Place Kicking," *Int. J. Sports Sci. Eng.*, vol. 3, no. 2, pp. 85-92, 2009.

[2] M. Isokawa and A. Lees, "A biomechanical analysis of the instep kick motion in soccer," in *Science and Soccer*, 2nd ed., T. Reilly and M. Williams, Eds., London, Routledge, 1988, pp. 449-455.

[3] W. Barfield, D. Kirkendall and B. Yu, "Kinematic Instep Kicking Differences Between Elite Female and Male Soccer Players," *J. Sport Sci. Med.*, vol. 1, no. 3, pp. 72-79, 2002.

[4] N. Bezodis, G. Trewartha, C. Wilson and G. Irwin, "Contributions of the non-kicking-side arm to rugby place-kicking technique," *Sports Biomech.*, vol. 6, no. 2, pp. 171-186, 2007.

[5] Y. Zhang, G. Liu and S. Xie, "Movement sequences during instep rugby kick: a 3D biomechanical analysis," *Int. J. Sports Sci. Eng.*, vol. 6, no. 2, pp. 89-95, 2012.

[6] J. Padulo, G. Granatelli, B. Ruscello and S. D'Ottavio, "The place kick in rugby," *Sports Med. Phys. Fitness*, vol. 53, no. 3, pp. 224-231, 2013.

[7] K. Ball, D. Talbert and S. Taylor, "Biomechanics of goal kicking in rugby league," in *Science and Football VII*, New York, Routledge, 2013, pp. 47-52.

[8] A. Lees, T. Asai, T. Anderson, H. Nunome and T. Sterzing, "The biomechanics of kicking in soccer: A review," *J. Sports Sci.*, vol. 28, no. 8, pp. 805-817, 2010.

[9] L. Stoner and D. Ben-Sira, "Variation in movement patterns of professional soccer players when executing a long range and a medium range in-step soccer kick," in *Biomechanics VII-B: International series on Biomechanics*, A. Morecki, Ed., Baltimore, University Park Press, 1981, pp. 337-341.

[10] A. Lees and L. Nolan, "Three dimensional kinematic analysis of the instep kick under speed and accuracy conditions," in *Science and Football IV*, A. Murphy, T. Reilly and W. Spinks, Eds., London, Routledge, 2002, pp. 16-21.

[11] K. Ball, "Biomechanical considerations of distance kicking in Australian Rules football," *Sports Biomech.*, vol. 7, no. 1, pp. 10-23, 2008.

[12] K. Ball, "Loading and performance of the support leg in kicking," *J. Sci. Med. Sport*, vol. 16, pp. 455-459, 2013.

[13] A. L. Hof, "Scaling gait data to body size," *Gait Posture*, vol. 4, no. 3, pp. 222-223, 1996.

[14] J. Hay, "The biomechanics of sports techniques", 2nd ed., Englewood Cliffs: Prentice Hall, 1985.

[15] A. Harrison and A. Mannering, "A biomechanical analysis of the instep kick in soccer with preferred and non-preferred foot," in *XXIV ISBS Symposium*, Salzburg, 2006.

[16] C. Egan, M. Verheul and G. Savelsbergh, "Effects of experience on the coordination of internally and externally timed soccer kicks," *J. Mot. Behav.*, vol. 39, no. 5, pp. 423-432, 2007.

[17] B. McLean and D. Tumilty, "Left-right asymmetry in two types of soccer kick," *Br. J. Sports Med.*, vol. 27, no. 4, pp. 260-262, 1993.

[18] J. Scurr and B. Hall, “The effects of approach angle on penalty kicking accuracy and kick kinematics with recreational soccer players,” *J. Sport Sci. Med.*, vol. 8, pp. 230-234, 2009.

[19] S. Phillips, “Invariance of elite kicking performance,” in Biomechanics IX-B, D. Winter, R. Norman and R. Wells, Eds., Champaign, *Human Kinetics*, 1985, pp. 539-542.

6. Paper 5: Approach Speed, Acceleration and Deceleration Amongst Professional Rugby Goal Kickers: Does It Influence Foot Speed at Ball Contact?

Abstract: *Despite its prominence within rugby union, goal kicking in this sporting code remains under-researched. In particular, there is a lack of reference data for professional goal kicking biomechanics and uncertainty about the determinants of performance. The aim of this study was to provide novel data on approach speed amongst highly skilled kickers and to investigate whether approach speed is correlated to foot speed at ball impact. We recorded 10 kicks by fifteen professional rugby union goal kickers using an optical motion capture system. We analyzed approach speed, timing and acceleration during three movement phases: kicking leg loading, flight and support leg loading. One major finding was that despite notable variability in the approach kinematics – relative standard deviations (RSDs) were 10-30% - the group demonstrated relatively similar maximum foot speeds (RSD of 6%). Similarly, intra-participant variability was noticeably lower for maximum foot speed (2%) than for approach kinematics (5-18%). We also found that foot speeds were moderately correlated with approach speed, but not with deceleration before ball strike as previously reported. Conversely, decelerations during support leg loading may be a source of instability. These findings provide a basis for future research, and the novel dataset may be useful for developing evidence-based coaching methods.*

Submitted: UK *J. Sports Sci.* (27 May 2015)

6.1. Introduction

Approximately half of all points in rugby union games are scored through goal kicking [1]. The average goal kick success rate in international matches is approximately 70%, with top-ranked kickers converting close to 90% of goal kick attempts [1]. Therefore, skilled goal kickers are critical to the success of rugby union teams. However, due to a lack of data describing professional goal kicking biomechanics, the relationship between technique and performance in rugby union is not clearly understood. Moreover, studies of kicking in other sports [2, 3] may have limited applicability to rugby goal kicking due its unique ball geometry, ground placement, imparted spin and flight trajectory. Therefore, more research is required in order to develop evidence-based teaching and training methods.

All kicking performance is essentially determined by the foot-ball interaction during contact [4]. This is a brief and complex phenomenon influenced primarily by kicking biomechanics, ball properties and footwear design. Given specific ball and footwear conditions, optimal goal kicking technique ultimately moves the kicking foot along the correct trajectory at impact (to ensure accuracy) with enough momentum transfer to the ball (in order for it to reach the target). In rugby union goal kicking, where the ball sometimes needs to travel well over 50m, it is thus important that a kicker generates adequate foot speed at ball strike. However, foot speed at impact has not yet been reported for a group of professional rugby union goal kickers. It thus remains unclear how foot speeds in this population compare to amateur rugby-union kickers as well as kickers in other sports. Further investigations are also warranted in order to determine the mechanisms used to generate foot speed during this kicking movement – and how consistently these mechanisms can be executed by individual kickers [5].

Kickers typically generate foot speed by transferring angular momentum to the kicking foot in a proximal-to-distal kinematic sequence [6], a common strategy for generating high distal-segment speed in throwing, hitting and kicking movements [7]. Proximal-to-distal sequencing has also been observed in a study of rugby goal kicking, which found that knee flexion-extension plays a dominant role in generating foot speed [8]. However, the authors could not find any studies examining the influence of the run-up on the kinematic sequence. Higher approach speeds may contribute additional momentum at the beginning of the kinematic sequence, thereby increasing foot speed. On the other hand, excessive approach speed may result in reduced movement coordination. This suggests that there may be an ideal approach speed that optimizes the trade-off between kick distance and accuracy [6, 9], although this is not known for rugby union goal kicking.

Changes in speed may also be an important aspect of goal kicking technique. One soccer study found that a large deceleration of the center of mass just before ball strike may also assist in transferring momentum to the kicking foot [10]. This is consistent with the concept of momentum transfer in kinematic sequences. However, excessive deceleration during the non-kicking leg loading phase may lead to large forces which destabilize the center of mass, possibly reducing motor control and increasing the risk of injury [11]. Therefore, a description of the timing and magnitude of speed changes during the approach amongst professional kickers may provide useful information for both researchers and coaches.

In light of the aforementioned gaps in the literature, the purpose of this study was to report on foot speed and run-up kinematics amongst professional rugby union goal kickers, as well as the relationship between the two. Specifically, we aimed to use gold-standard optical motion capture technology to provide novel reference values for:

a) foot speed, approach speed, timing and acceleration at key points in the run-up

b) inter- and intra-participant variability

c) the correlations between foot speed, approach speed, acceleration and deceleration

6.2. Methods

Fifteen male professional rugby union goal kickers participated in the study (height: 1.79 m (1.72 – 1.91), age: 26.4 years (range: 20 – 32), and weight: 87 kg (82.4 – 93.3). All participants gave informed consent before testing. Ethical approval for the study was obtained from the institution's research committee.

Data was collected in an indoor laboratory using a three-dimensional optoelectronic motion capture system (Vicon MX T-series, Vicon Ltd, Vicon UK). Participants wore running shoes instead of rugby boots due to the hard flooring of the laboratory. One passive-reflective pelvic marker (14 mm diameter) was placed on the sacrum. Another two markers were placed on the non-kicking leg shoe at the midpoint of the heel (heel marker) and above the second metatarsal (toe marker). Four markers were placed on the kicking leg shoe: a heel marker, a toe marker, an ankle marker (placed on the lateral malleolus) and a lateral marker placed mid-way along the length and height of the shoe (reference marker). The additional ankle and reference markers on the kicking foot were required to track the kicking foot toe marker during the kick as it was not clearly visible in the Vicon cameras near impact with the ball. During a Vicon static calibration trial, the measured position of the toe marker relative to a coordinate system defined by the measured heel, ankle and technical marker was determined. Then, in the dynamic kicking trials the heel, ankle and reference markers were used to estimate the toe marker position, overcoming camera occlusions. Lastly, two markers – one placed on the left and right side of the ball so that the midpoint approximated the ball center – were used to determine the moment of impact with the ball.

Each participant participated in the testing using their own kicking tee but all tests were conducted with the same ball. Participants kicked the ball into a steel-framed net placed towards a target on the laboratory wall (Figure 32). A designated position for the kicking tee was used to ensure repeatability of the target direction relative to the Vicon coordinate system. Participants were allowed 5-10 practice kicks after marker placement to become accustomed to the testing environment, after which ten consecutive goal kicks were captured. To avoid minimal and maximal effort extremes, players were instructed to perform a mid-range kick assuming a 40 m distance to the target. The Vicon cameras were calibrated using the conventional 5-point wand waving procedure and marker data was captured at 200 Hz.

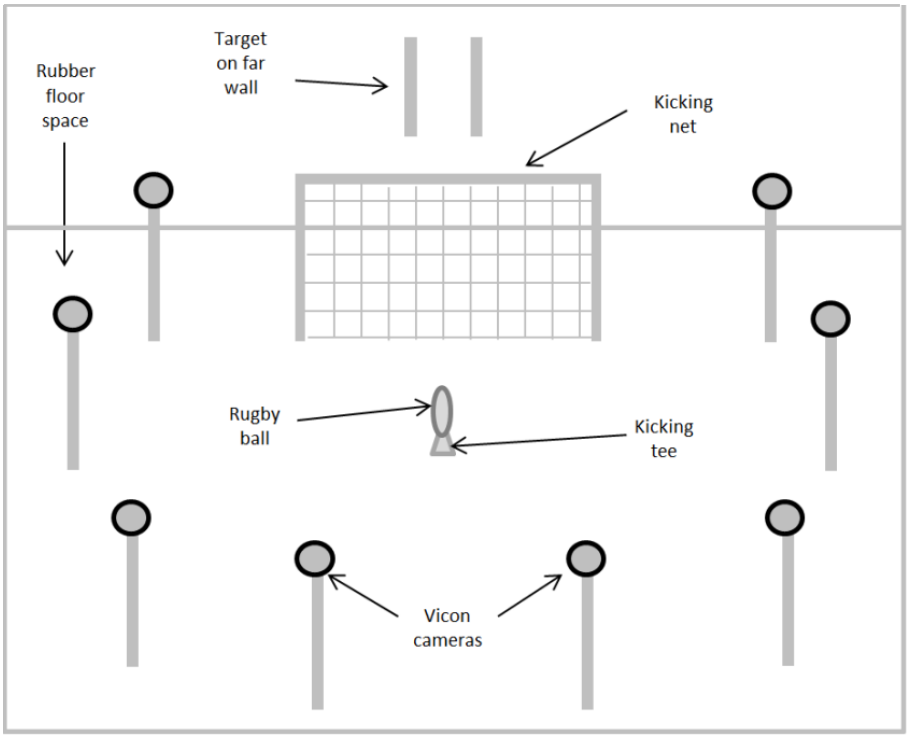

Figure 32: Schematic of test set up showing Vicon cameras positions relative to ball, net and target.

Marker trajectories were reconstructed and labeled using standard pipeline operations in the commercial Vicon Nexus software (version 1.8.4). Trajectory smoothing was performed for the body markers using a 4th-order zero-phase Butterworth filter. The ball markers were not smoothed, in order to avoid errors near impact due to smoothing. In this study we analyzed the last two steps during the approach to the

ball until foot contact with the ball. The movement was broken down into four phases (ghost, launch, flight and support) using five movement events (Figure 33a).

Two events were defined in relation to the support leg foot (S1 and S2) and three in relation to the kicking leg foot (K1, K2 and K3). S1 and K2 designate events where the foot loses contact with the ground and K1, S2 and K3 represent moments of initial foot contact with the ground or ball (Figure 33a). We designated the loading phase of the kicking leg before ball strike (K1 to K2) the 'launch' phase. This is followed by the flight phase (both feet in the air) which starts at K2 and ends with the support foot landing next to the tee (S2). Lastly, we designated a portion of the support leg loading phase – from initial contact (S2) until the kicking foot makes contact with the ball (K3) – as the support phase. We also assessed the time between when the non-kicking foot comes off the ground (S1) during the penultimate approach step to K1 (named ghost phase time). A negative ghost time indicates the presence of double support (walking) in the penultimate step, whereas positive ghost times indicate that the player was running during the penultimate step. A custom algorithm developed in Matlab (Release 2012b, The Mathworks, Inc.) was used to detect the time of the kick events from the ball, heel and toe marker kinematics (Figure 33b).

We defined the approach speed using the horizontal velocity of the pelvis sacral marker, and calculated this at S1, K1, K2, S2 and K3 for each trial. We also analyzed the time period of the movement phases (ghost, launch, flight and support phases) in each trial, as well as the average phase acceleration (change in approach speed divided by phase time). The kicking foot speed was estimated using the speed of the kicking foot toe marker (scalar value). In the analysis of group and participant variability for these outcomes, we calculated both the absolute and the relative variability. The relative inter-participant variability was defined as the proportion of the group standard deviation (SD) relative to the group mean (expressed as a percentage). The absolute intra-participant variability (player inconsistency) was calculated using the SD of each participant's ten trials. The relative intra-participant variability was expressed as the percentage of the participant SDs relative to the participant mean values.

Lastly, we investigated the correlations between foot speed, approach speed at K2, support phase deceleration and launch phase approach acceleration using the Pearson coefficient. We assessed the statistical significance of these correlations using p-values and a 95% confidence interval.

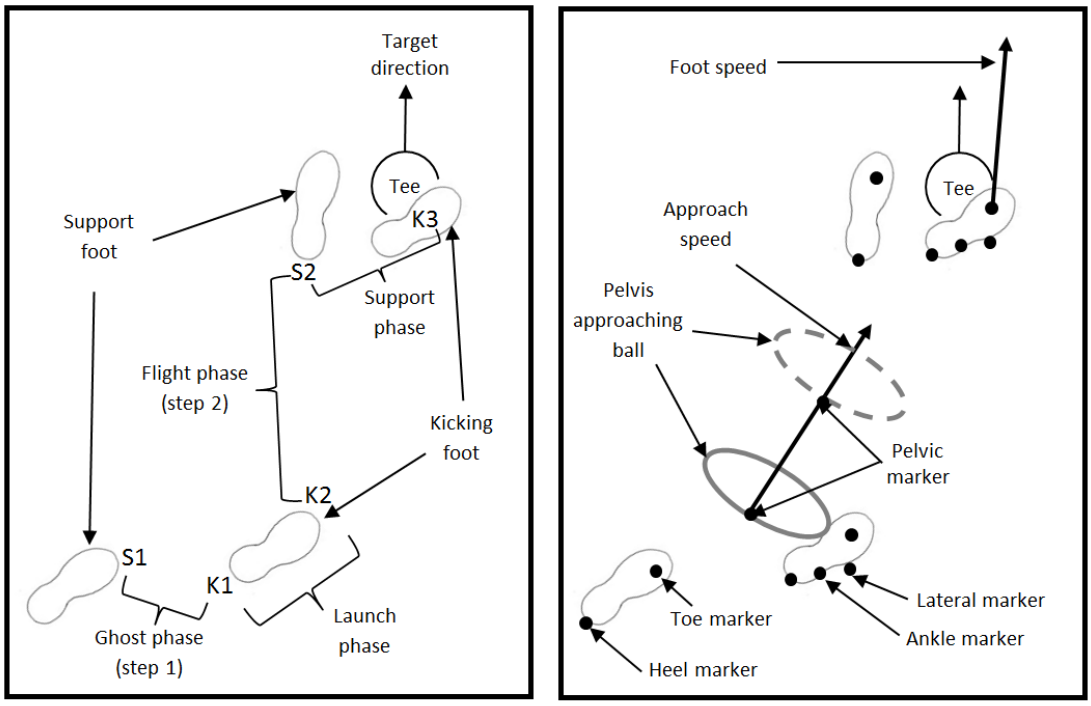

(a) Events used to define kick phases definitions (b) Markers used to calculate outcomes

Figure 33: A top view illustration of different foot positions relative to the tee during a right-footed goal kick that were used to define (a) the events S1 through to K3 that divide the kick into time phases and (b) the foot and pelvic markers used to define foot speed and toe speed. Note that the instantaneous foot speed near impact was calculated using the toe marker. Due to toe marker occlusions caused by the ball, the toe marker was virtually reconstructed from the marker cluster consisting of the heel, ankle and lateral foot markers.

6.3. Results

The cohort demonstrated a distinctive pattern of acceleration and deceleration during the three approach phases analyzed (launch, flight and support) despite appreciable variability in timing and speed (Figure 34). Launch typically began just before the support leg left the ground, resulting in a near-zero ghost phase time for the group, and its duration was almost twice that of flight and support. We observed a notable acceleration during launch, with approach speeds increasing from 2-3 $m.s^{-1}$ to a peak of 3-4 $m.s^{-1}$. During flight, participants decelerated in almost equal magnitude and lost approximately half the speed gained during launch by S2. This was followed by a much larger deceleration during the support phase which reduced approach speeds to 1-2 $m.s^{-1}$ at ball impact.

Despite this typical approach speed profile, there was notable group variability in the measured outcomes (Table 1). In terms of approach speed, absolute inter-participant variability was similar throughout, ranging from 0.33-0.41 $m.s^{-1}$. In contrast, relative standard deviations (RSDs) for inter-participant variability were as high as 27.2% at the moment of ball contact (K3) and as low as 9.2% at the end of flight (S2). Similarly, support phase deceleration was more than twice as variable as flight phase deceleration in absolute terms, whereas flight phase deceleration was considerably more variable in relative terms. In contrast, both the relative and absolute measures of phase time variability decreased with each successive phase. It should be noted that the large variability in ghost times reflects the fact that some participants are walking during this phase (K1 precedes S1) and others are running (S1 precedes K1). This is also reflected in that K1 approach speeds were generally higher when K1 occurred after S1 (Figure 34). Note that this correlation is no longer observed after launch.

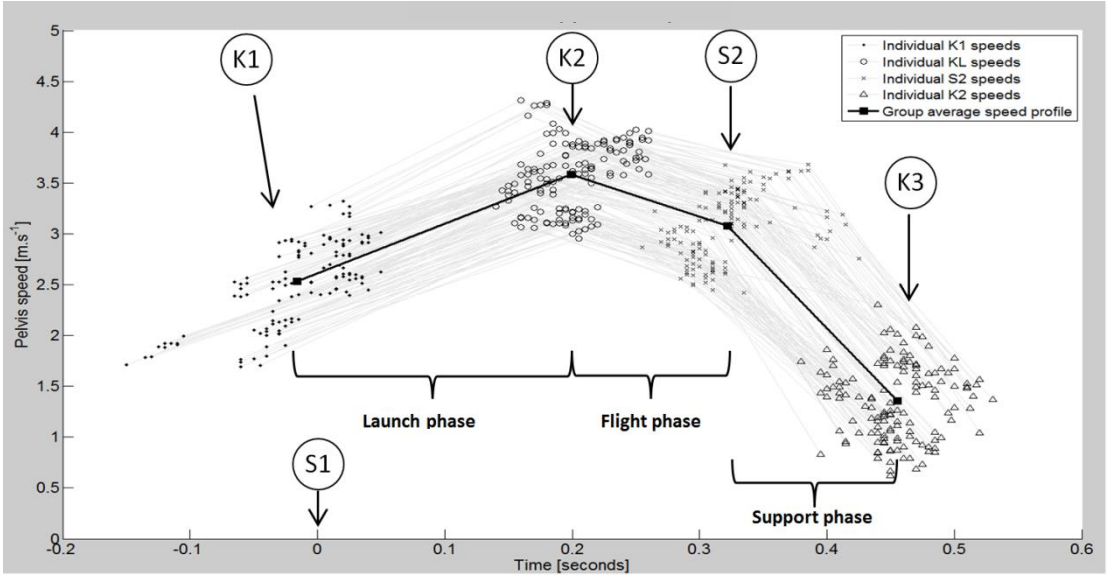

Figure 34: Individual and group approach speed over time at key points in the kick. The support leg foot off event (S1) was chosen as the zero point in time, such that participants having a walking ghost step i.e. an initial kicking leg foot contact (K1) before S1, are reflected as beginning at a negative point in time. The subsequent distributions of individual speeds at K2, S2 and K3 are relative to S1 and thus express the cumulative variability of the preceding phases.

Analysis of the intra-participant variability revealed more consistent speed and timing and less consistent acceleration and deceleration (Table 9). The K1, K2 and S2 approach speeds varied per participants by approximately 2-3% RSD for their ten kicks. However, approach speed RSDs increased during the support phase to around

10 ± 4% for K3. Phase time variability per participant was slightly higher on average (4-6%), however this decreased with each successive phase similarly to the intra-participant variability results. The acceleration and deceleration were the least consistent per participant (8-19%). Also mirroring the inter-participant variability results, intra-participant variability in acceleration and deceleration was largest during flight in relative terms and largest during the support phase in absolute terms.

Table 9**:** Analysis of approach speed, phase time, phase acceleration and foot speed. Intra-participant variability was defined using the standard deviation of each participant's 10 kicks. Relative inter-participant variability refers to the ratio between group SD and group mean, whereas relative intra-participant variability refers to the ratio between participant SD and participant mean (expressed in %). Note that relative variability is not applicable to ghost phase time since the mean is close to zero.

Measurement outcome	Group distribution [mean (SD)]	Relative inter-participant variability [RSD %]	Intra-participant variability [mean (SD)]	Relative intra-participant variability [mean (SD) of RSD %]
Approach speed ($m.s^{-1}$)				
K1	2.53 (0.41)	16.2	0.07 (0.02)	2.8 (0.9)
K2	3.59 (0.33)	9.2	0.08 (0.02)	2.2 (0.5)
S2	3.08 (0.32)	10.4	0.1 (0.03)	3.2 (1.0)
K3	1.36 (0.37)	27.2	0.14 (0.06)	10.2 (4.0)
Approach phase time (s)				
Ghost phase	-0.016 (0.040)	-	0.013 (0.006)	-
Launch phase	0.210 (0.038)	18.1	0.012 (0.005)	5.8 (2.5)
Flight phase	0.118 (0.019)	16.1	0.007 (0.002)	5.9 (1.7)
Support phase	0.128 (0.015)	11.7	0.005 (0.002)	4.0 (1.8)
Approach phase accelerations ($m.s^{-2}$)				
Launch phase	5.16 (0.89)	17.2	0.43 (0.27)	8.1 (4.6)
Flight phase	-4.3 (1.3)	30.2	0.76 (0.3)	18.7 (7.3)
Support phase	-13.53 (2.91)	21.5	1.47 (0.54)	10.3 (2.9)
Foot speed ($m.s^{-1}$)				
Peak	21.32 (1.27)	6.0	0.43 (0.18)	2.0 (0.9)
K3	16.52 (1.56)	9.4	0.94 (0.48)	5.8 (3.2)

A comparison of peak foot speed and foot speed at ball strike revealed a 20% loss of foot speed for the group just before impact (Table 10). Foot speed at impact also

showed a marked increase in inter- and intra-participant variability, whereas peak foot speed contained the lowest group and participant variability in the study.

Table 10: Pearson's correlation (r) between foot speed, approach speed, acceleration and deceleration as an explanation of variance

	Max foot speed	K3 foot speed	K2 approach speed	Support deceleration
K3 foot speed	0.28*	-	-	-
K2 approach speed	0.44*	0.19*	-	-
Support deceleration	0.01	-0.27*	-0.32*	-
Launch acceleration	-0.01	-0.16	0.41*	-0.17

* Significant ($p < 0.05$)

The analysis of variance revealed three significant medium-sized ($r > 0.3$) correlations in the data. Firstly, larger maximum foot speeds were mildly associated with faster approach speeds at the beginning of launch. Launch acceleration was also positively correlated with approach speed. Thirdly, increased support phase deceleration was moderately associated with decreased approach speed. Perhaps most notably, maximum foot speed had practically no correlation with support phase deceleration or launch phase acceleration.

6.4. Discussion

This study presents novel reference data for approach speeds, timing and acceleration amongst professional rugby union goal kickers obtained using optical motion capture. The results show that despite notable inter-participant variability in approach kinematics (RSDs of 10-30%), the group demonstrated a consistent pattern of acceleration and deceleration during the approach to the ball that resulted in relatively consistent maximum foot speeds (6%). Similarly, intra-participant variability was relatively low for maximum foot speed (2%), despite much higher inconsistencies in timing (5%), approach speed at contact (10%) and deceleration (10-18%). It was observed that approach speed was more tightly controlled in the early stages of the run-up, giving way to increasing temporal control closer to ball strike. This is reflected in the relatively large variability shown for the flight and support phase decelerations. Variability in speed loss during the flight phase suggests that the coiling action in preparation for the strike action may be less controlled than the rest of the kick. We also found that support phase deceleration had a negligible

correlation with kicking foot speed. This suggests that loading of the support leg before ball strike may be a source of instability rather than used as strategy for improving momentum transfer during the kinematic sequence. In contrast, we did find a moderate positive correlation between peak approach speed at K2 and foot speed. In summary, the data suggests that both the generation and dynamic control of foot speed is largely insensitive to approach strategy used, although a faster run-up may assist in improving foot speed in some cases. These findings provide a basis for future research in this sporting code and may be useful for the development of evidence-based coaching methods.

Foot speeds at ball contact in this study (16.52 ± 1.56 $m.s^{-1}$) were very similar to those found by Zang *et al.* [8], who tested seven skilled university-level goal kickers using a three-dimensional motion capture system (16.8 ± 1.6 $m.s^{-1}$). However, this is markedly lower than the results reported for elite rugby league kickers by Ball [12] using high-speed video analysis (21.2 ± 1.7 $m.s^{-1}$) and by Ball, Talbert and Taylor [13] using three-dimensional motion capture (21 ± 1 $m.s^{-1}$). Nonetheless, their findings are almost identical to this study's results for peak foot speed before contact (21.32 ± 1.27 $m.s^{-1}$), which occurred approximately 10-20 ms before ball contact. They also report foot speed just before ball contact rather than at foot contact, supposedly to avoid filtration effects near high frequency impacts. However, upon inspection the authors were unable to find any notable effect on foot speed results due to smoothing of the toe marker trajectories. This phenomenon of foot speed deceleration before contact is also noted by Lees *et al.* [14] in a review of soccer kicking studies. Another hypothesis is that the kickers extend their knee into a locked position before impact in order to increase the effective mass of the kicking leg [4]. It may also be that the knee joint and associated musculature is approaching a passive mechanical limit for rotation speed at this point (the kicking leg is almost straight), or that this is an active strategy for avoiding injury [6].

Ball *et al.* [13] is the only study we found that reports on approach speeds. They found that approach speed at kicking foot off (K2) was 3 ± 0.8 $m.s^{-1}$, which is slower and more variable than the cohort in this study (3.59 ± 0.33 $m.s^{-1}$). This may be simply due to the small sample size in their study (N=4). They provide no information about the approach speed at contact of the kicking leg (K1) or non-kicking leg (S2), but they do report that the center of mass was moving at 2.6 ± 0.4 $m.s^{-1}$ at impact (K3). In contrast, we found that the pelvis was moving more slowly at this point (1.36 ± 0.37 $m.s^{-1}$) which is an important finding as it suggests

that a large proportion of the center of mass velocity at impact is due to movement of the kicking leg (rather than the pelvis). Nevertheless, the fact that the pelvis speed is non-zero supports the contention of Ball *et al.* [13] that elite kickers remain moving through the ball at contact rather than employing a stationary 'snap kick' technique. Another notable finding from this study is that group variability in approach speed converged during the launch phase (K1 to K2) but diverged during the support phase (S2 to K3). This suggests that kickers regulate leg drive during the acceleration phase to normalize their approach speed, perhaps in relation to the number of prior steps taken. In contrast, approach speeds diverge during the deceleration phase. This suggests that kickers are not regulating pelvis speed before contact to a normative value, although the reasons for this are not clear.

We could only find one rugby union study reporting on phase timing during goal kicking. Sinclair *et al.* [15] assessed the support phase time (0.13 ± 0.01 s), which is almost identical to the results presented here (0.128 ± 0.015 s). Soccer kicking researchers [16] also report similar times for the support phase (0.12 ± 0.008 s), suggesting that this may be normative across some sporting codes. However, the authors could find no analysis of ghost, launch or flight phase timing in the literature even though this has a significant bearing on approach dynamics and overall kicking technique. The ghost time parameter may be useful in categorizing different run-up styles, as a positive ghost time implies a running penultimate step and a negative time implies that the kicker is still walking at this point (feet are both grounded at K1). Furthermore, launch phase times could be helpful in understanding the acceleration phase and how different kickers generate power for the instep. One important finding of the timing analysis was that the group variability in phase times decreased towards ball strike. This implies that the observed divergence in approach speed during deceleration was due to variability in forces and not time. Furthermore, it suggests that kickers are more similar in terms of rhythm and timing but less so in terms of force control and support leg stability during the support phase.

The analysis in this study of acceleration and deceleration magnitudes and variability during the different phases is a novel contribution to the literature. Notably, intra- and inter-participant variability for flight phase deceleration was the largest of all variables. Since the approach speed vector is largely perpendicular to gravity, this phenomenon is more likely to be due to the counteractive movement of the kicking leg and opposite arm in the coiling action during flight. We also found a large deceleration during the support phase, more than twice the magnitude of the

acceleration in the launch phase. The deceleration is in agreement with the principle of kinematic sequencing wherein distal summation of speed is facilitated by proximal segment decelerations [7]. Potthast *et al.* [10] investigated support phase dynamics in soccer kicking, finding that increased deceleration of the center of mass before ball strike was correlated with increased foot speed. This phenomenon was also observed in rugby punt kicking by Ball [11] using an analysis of ground reaction forces on the support foot. He states: "(ground reaction forces) were related to kick performance. A larger peak vertical and braking force was related to larger foot speeds indicating stronger bracing might exist about which the kick leg can swing, or more momentum gets transferred to the kick leg" (p. 458). This study's findings are in direct opposition to this, as foot speed was negligibly correlated to support phase deceleration. It should be noted that this study provides a clearer analysis of momentum transfer in terms of the kinematic sequence than Potthast *et al.* [10], since the center of mass also reflects distal segment motion (e.g. leg swing) whereas we assessed pelvic marker movement which reflects the motion of the proximal segment in the kinematic sequence. Similarly, the analysis by Ball [11] is also not directly relatable to loss of momentum at the pelvis because the effect of ground reaction forces depends on support leg biomechanics.

No studies could be found assessing the intra-participant variability of the outcomes for this study for any population. Nonetheless, these reference values for the consistency of execution amongst skilled kickers may assist coaches seeking to assess the repeatability of technique. Interestingly, peak foot speed was reproduced more consistently by the participants than all other variables (2 ± 0.9%). The approach speeds of this cohort were next best, varying by 2-4% during each participant's battery of kicks – except for at ball strike where this rose to around 10%. Phase time consistency was slightly lower (4-6%), although in contrast this improved moderately towards ball strike. The least repeatable variables were the acceleration and deceleration results. This suggests that players are able to produce very repeatable foot speeds despite considerable variability in approach dynamics. These findings highlight the fact that inconsistent kicking distances may not be explained by variability in foot speed. However, this data may provide insight into the movement strategies and real-time compensations made by kickers during the approach to maintain control of foot speed.

This study was limited primarily by issues related to ecological validity. The indoor floor and stud-free footwear conditions differed from an on-field environment and

may have affected ground reaction forces. However, participants were given ample opportunity to familiarize themselves with the testing conditions (through practice-kicks) prior to data collection and the effect may be negligible. The consecutive and identical nature of the kicks during testing is also different to a game scenario and may have reduced intra-participant variability. However, it is likely that players execute the same run-up regardless of ball position on the field. We did not simulate physical fatigue during the protocol, and it is unclear how the physiological state of kickers affects kicking performance. It is also not known whether the laboratory conditions affected the psychological preparation of the kickers compared to an in-game scenario. These factors warrant further investigation in field-test studies. Lastly, we chose to instruct players to kick a mid-range distance (40m) rather than a maximal distance kick. This may influence insights into this populations as well as comparisons with studies investigating maximal effort trials. On the other hand, we are of the view that data from maximum effort trials would also not be directly applicable when coaching goal kickers.

6.5. References

[1] K. L. Quarrie and W. G. Hopkins, "Evaluation of goal kicking performance in international rugby union matches," *J. Sci. Med. Sport*, vol. 18, no. 2, pp. 195-198, 2014.

[2] K. Ball, "Biomechanical considerations of distance kicking in Australian Rules football," *Sports Biomech.*, vol. 7, no. 1, pp. 10-23, 2008.

[3] G. Shan and X. Zhang, "From 2D leg kinematics to 3D full-body biomechanics – the past, present and future of scientific analysis of maximal instep kick in soccer," *Sports Med. Arthrosc. Rehabil. Ther. Technol.*, vol. 3, no. 1, pp. 23-32, 2011.

[4] A. Lees and L. Nolan, "Biomechanics of soccer: A review," *J. Sport Sci.*, vol. 16, pp. 211-234, 1998.

[5] L. Stoner and D. Ben-Sira, "Variation in movement patterns of professional soccer players when executing a long range and a medium range in-step soccer kick," in *Biomechanics VII-B: International series on Biomechanics*, A.

Morecki, Ed., Baltimore, University Park Press, 1981, pp. 337-341.

[6] E. Kellis and A. Katis, "Biomechanical characteristics and determinants of instep soccer kick," *J. Sport Sci. Med.*, vol. 6, pp. 154-165, 2007.

[7] C. A. Putnam, "Sequential motions of body segments in striking and throwing skills: Descriptions and explanations," *J. Biomech.*, vol. 26, no. 1, pp. 125-135, 1993.

[8] Y. Zhang, G. Liu and S. Xie, "Movement sequences during instep rugby kick: a 3D biomechanical analysis," *Int. J. Sports Sci. Eng.*, vol. 6, no. 2, pp. 89-95, 2012.

[9] T. B. Andersen and H. C. Dörge, "The influence of speed of approach and accuracy constraint on the maximal speed of the ball in soccer kicking," *Scand. J. Med. Sci. Sports*, vol. 21, no. 1, pp. 79-84, 2011.

[10] W. Potthast, K. Heinrich, J. Schneider and G. Brueggemann, "The success of a soccer kick depends on run up deceleration," in *ISBS-Conference Proceedings Archive*, 2010.

[11] K. Ball, "Loading and performance of the support leg in kicking," *J. Sci. Med. Sport*, vol. 16, no. 5, pp. 455-459, 2013a.

[12] K. Ball, "Kick impact characteristics for different rugby league kicks," in *International Conference on Biomechanics in Sports*, vol. 28, Konstanz, University of Konstanz, Sports Science, 2010.

[13] K. Ball, D. Talbert and S. Taylor, "Biomechanics of goal kicking in rugby league," in *Science and Football VII: The Proceedings of the Seventh World Congress on Science and Football*, Routledge, 2013b.

[14] A. Lees, T. Asai, T. Anderson, H. Nunome and T. Sterzing, "The biomechanics of kicking in soccer: A review," *J. Sports Sci.*, vol. 28, no. 8, pp. 805-817, 2010.

[15] J. Sinclair, P. Taylor, S. Atkins, J. Bullen, A. Smith and S. Hobbs, "The influence of lower extremity kinematics on ball release velocity during in-step place kicking in rugby union," *Int J Perform Anal Sport*, vol. 14, no. 1, pp. 64-72, 2014.

[16] B. D. McLean and D. M. Tumilty, "Left-right asymmetry in two types of soccer kick," *Br. J. Sports Med.*, vol. 27, no. 4, pp. 260-262, 1993.

7. Paper 6: Rotational Alignment to Tee and Target of the Thorax, Pelvis and Feet during Expert Rugby Union Goal Kicking

Abstract: *Goal kicking is the most common means of scoring points in professional rugby union. To understand this complex motor task and improve coaching, researchers have investigated goal kicking biomechanics using gold-standard motion capture systems. However, there are no reports on the rotation profiles of body segments in the horizontal plane which is an important aspect of technique. We tested 15 professional goal kickers using an optical motion capture system and analyzed the angular alignment of the thorax, pelvis and foot segments to the tee and target. We found high inter-individual variability in approach angles and segment orientations (group SDs: 5-15°), although intra-individual variability was low (subject SDs: 1-4°). However, we did observe characteristic patterns of retraction and protraction in the pelvis, thorax and spine angle that support the notion of a 'tension-arc' movement strategy. The angulation of these segments at ball contact was correlated to the approach angle, but ranges of motion were not. The support foot was notably rotated external to the approach line at ball contact, whereas the kicking foot was notably rotated external to the target line. These findings support coaching cues in the literature regarding upper body movement, but contradict those relating to foot alignment.*

Submitted: UK *J. Sports Sci.* (20 August 2015)

7.1. Introduction

In the past two decades, motion capture technologies have begun to play an important role in the quest to understand and optimize athletic performance [1]. Modern motion capture methods such as stereophotogrammetry enable estimation of musculoskeletal biomechanics in three-dimensional and at high temporal and spatial resolutions [2], allowing comprehensive and detailed technique analyses for sports [3]. These measurement capabilities have already facilitated a deeper understanding of the biomechanical determinants of performance in global sports such as golf [4] and soccer [5]. They also provide an objective means of assessing intra- and inter-individual variability in expert technique, which has become a topic of debate within the field of motor learning and motor control during recent years [6-8]. However, technique and performance variability in many sporting codes remain under-

researched using three-dimensional motion capture. In these cases, more quantitative movement studies are needed to develop scientific knowledge that can inform evidence-based coaching practise.

One important and complex motor task that is not well documented in the literature is rugby union goal kicking [9]. Goal kickers usually score the majority of points registered during a professional match and thus often play a pivotal role in the outcome of games and competitions [10]. Due to the difficulty of reliably executing this particular motor task under physical and psychological pressure, elite goal kickers – who have success rates above 80% - often attract lucrative player contracts. However, current knowledge regarding expert goal kicking technique is largely based on insights from qualitative analyses and anecdotal sources [11]. In contrast, there is very little gold-standard motion capture research of highly skilled kickers analysing technique, identifying key performance indicators or examining the effects of targeted interventions. This lack of objective data on expert performance limits the ability of coaches to apply scientific principles in their efforts to accelerate skill acquisition and maintain performance levels.

A limited number of motion capture studies have researched goal kicking in small groups of amateur goal kickers. It has been established that, like other 'ballistic' sports involving throwing, striking or kicking, goal kicking involves a proximal-to-distal kinematic sequence in the kicking leg and the pelvis which requires counteractive rotation of the trunk and opposite-side arm to maintain core stability [12, 13]. One of the key performance indicators of this action is foot speed just before ball contact, which is associated with kick distance [14, 15]. However, there are no reports on the angulation of the kicking foot at ball contact – which is also likely to affect kick direction and momentum transfer to the ball. Similarly, while studies have also found that the distance of the support leg foot from the tee before ball contact may be an important factor affecting performance [16, 17], none have reported on the orientation of the support foot relative to the target line. Moreover, despite descriptions of hip, knee and ankle joint angles during goal kicking [18, 19], no studies have investigated the angular alignment of the individual pelvic and thoracic segments during the approach to the ball and whether this is affected by the overall run-up angle.

It is likely that the rotational alignments of the thorax, pelvis and feet relative to the target line are important interdependent factors affecting goal kicking biomechanics.

The articulated nature of the musculoskeletal system implies that differences in support foot orientation during placement next to the tee would also reflect in changes to the proximal body segment kinematics and kinetics. Similarly, the angulation of the kicking foot at ball contact is dependent upon the movement of proximal segments in the horizontal plane. Therefore, it may be that thoracic and pelvic kinematics play an important role in correctly positioning the kicking foot at ball contact. It should also be noted that rotational alignment of these segments is influenced by the angle of approach to the ball during the run-up. Larger angles of approach might be expected to increase the average rotation of the body segments during the run-up, although this has not been established. All in all, it remains unclear how the motor strategies employed by skilled goal kickers differ in relation to these rotational alignment variables, and how these variables influence each other. Therefore, to fill the aforementioned gap in the literature, the first aim of this study was to describe the rotational alignment of the thorax, pelvis and feet relative to the target line and approach line during professional goal-kicking. The second aim was to investigate the correlations between these body alignment angles in order to answer the following questions: Do elite kickers with a smaller approach angle:

a) position their support foot next to the tee more parallel to the target at contact?

b) position their kicking foot more parallel to the target at contact?

c) undergo a smaller range of pelvic and thoracic rotation?

7.2. Methods

7.2.1. Participants

Fifteen rugby union place-kickers (age: 26.4 years (range: 20-32), height: 1.79 m (1.72 – 1.91) and weight: 87 kg (82.4 – 93.3), were tested for the study. At the time of data collection, all participants were competing at a professional level. The participants gave informed consent before testing and approval for the research was obtained from the institutional committee for human research ethics.

7.2.2. Instrumentation and setup

We recorded the goal kicking technique of the participants in a motion analysis laboratory using an 8-camera optoelectronic motion capture system (Vicon MX T-series, Vicon Ltd, Vicon UK). Marker trajectories were captured at a sampling rate of

200Hz along with kinetic data from a floor-level force-plate (FP9060 model, Bertec Corp.) at 1000 Hz. The Vicon cameras were calibrated in Vicon Nexus software (version 1.8.4) using a standard 5-point wand waving routine, and the force plate output was set to zero before the start of every test.

The kicking tee was placed in the same position for each trial such that the support leg foot landed on the force plate. Four passive-reflective markers (14 mm diameter) were placed on the tee (front, back, left and right) and another three markers were placed on the ball: on the top point and on the left and right such that the midpoint of these two markers approximated the center of the ball. We also placed markers on the participant (on the thorax, pelvis and foot segments) according to the standard Vicon Plug-in Gait (PiG) protocol by a trained clinician with five years of experience working in clinical gait analysis.

The anatomical coordinate system of the thorax was defined using markers placed on four bony landmarks: the spinous process of the 7th cervical vertebra (C7), the xiphoid process of the sternum (STRN), the spinous process of the 10th thoracic vertebra (T10) and the supra-sternal notch (CLAV). The primary axis (Z) defined as the vector running from the midpoint of STRN and T10 to the midpoint of CLAV and C7. The secondary axis (X), points forwards with respect to the body from the midpoint of C7 and T10 to the midpoint of CLAV and STRN. The Y axis is computed using the Z and X axes and points to the left. The origin of the thorax is defined as half a marker diameter back from the CLAV marker along the X axis. The Z axis is perpendicular to the transverse plane.

Four markers were used to define the anatomical coordinate system of the pelvis. These were placed on the crest of the right anterior iliac spine (RASI) , left anterior iliac spine (LASI), right posterior iliac spine (RPSI) and left posterior iliac spine (LPSI). The primary Y axis of the pelvis is defined by the vector running from the LASI marker to the RASI marker. The secondary X axis runs from the midpoint of RPSI and LPSI to the midpoint of RASI and LASI. The Z axis is computed as being perpendicular to the transverse plane containing the X and Y axes.

The anatomical coordinate systems of the feet were defined using a heel marker placed on the shoe at the midpoint of the calcaneus, a toe marker placed on the shoe above the second metatarsal head, an lateral ankle marker placed on the lateral malleolus and a medial ankle marker placed on the medial malleolus. To avoid

occlusions of the toe marker typically experienced near the time of ball contact, we also placed a non-anatomical marker on the kicking foot shoe that could be used as a reference marker (together with the heel marker and mid-point of the ankle markers) to reconstruct the toe marker during the dynamic kicking trials.

7.2.3. Data collection and preprocessing

The participants executed ten consecutive goal kicks using their own kicking tee but used the same standard rugby ball (Gilbert, Grays of Camridge (International) Ltd) provided for all the tests. Participants wore running shoes instead of rugby boots due to the hard flooring of the laboratory. Each participant was instructed to aim their kicks towards a target on the far wall. A steel framed net placed between the kicking tee and the target was used to restrict the flight of the ball after impact (Figure 35).

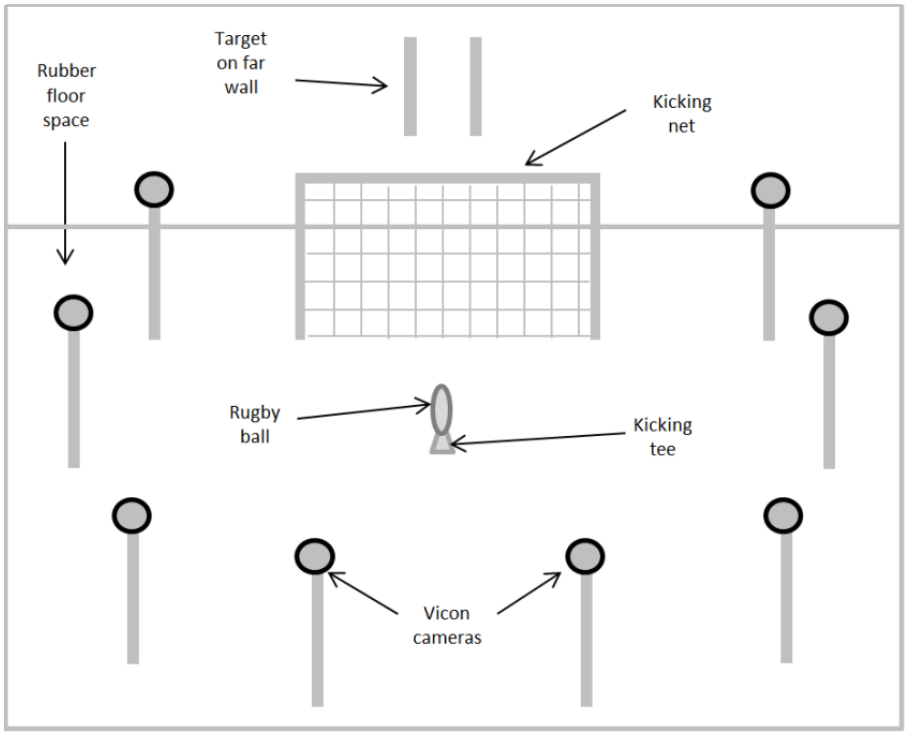

Figure 35: Schematic of test set up showing Vicon cameras positions relative to ball, net and target

The target on the wall was positioned such that the line from the tee to the target was parallel to the one axis of the laboratory coordinate system. Each participant performed their own warm up routines before testing. This was followed by 5-10 practice trials after marker placement to become accustomed to the testing

environment. Ten kicking trials were then recorded – recordings were started 2 s before the beginning of the run-up (after a verbal cue given by the participant) until 2 s after ball strike.

Reconstruction and labeling of the body marker trajectories was carried out in the Vicon Nexus software using the standard functions provided. Gap filling and smoothing was performed using the Nexus Woltring filter algorithm (MSE value of 20 mm). The Vicon PiG model was used to calculate segmental kinematics for the thorax, pelvis and foot segments using marker data. These angles were smoothed using a zero-phase, fourth-order low-pass Butterworth filter with a cut-off frequency of 15 Hz.

7.2.4. Data analysis

The analysis considered the final two steps of the run-up up until kicking foot contact with the ball (Figure 36a). We divided the kick into three phases in time (launch, flight and strike) using four events: kicking foot contact (KFC), kicking foot off (KFO), support foot contact (SFC) and ball contact (BC). The launch phase starts at KFC and ends at KFO – during which the kicking leg in in contact with the ground and the player 'launches' into the powerful in-step motion towards the tee. The launch phase is followed by a flight phase from KFO to SFC in which neither foot has contact with the ground. At SFC the support foot is planted beside the tee, initiating the strike phase in which the player's kicking leg undergoes vigorous hip and knee extension until BC. The trajectories of the markers placed on the ball and feet we exported together with the force plate data to a custom Matlab script (Release 2012b, The Mathworks, Inc.) which estimated the kick events. The BC event was estimated to occur at the time sample before the ball markers velocity exceeded a minimum threshold magnitude. We used a threshold of 30 N on the vertical ground reaction force measured by the force plate to detect SFC. The KFC and KFO events were then detected using the derivatives of foot marker kinematics.

The rotational alignment of the thorax, pelvis and foot segments relative to the target were calculated using horizontal plane angle between the anteroposterior axes of the segments relative to the axis of the laboratory coordinate system which was coincident with the line between the tee and the target (Figure 36b). However, this method of calculating rotational alignment contains two sources of variability for a group: variability due to postural changes and variability in the angle of approach to the ball. Therefore, we also assessed rotational alignment normalized for the angle of

approach in order to isolate variability related to posture (Figure 36b). This was done by subtracting the approach angle from the alignment angle relative to the target. The approach angle was calculated as the angle of the vector from the midpoint of the four pelvis markers (RASI, RPSI, LASI and LPSI) to the marker at the back of the kicking tee at K1. Both sets of segmental alignment data were assessed for the thorax, pelvis and feet at KFC, KFO, SFC and BC for each trial, as well as the range of motion for the thorax and pelvis during the launch, flight and strike phases.

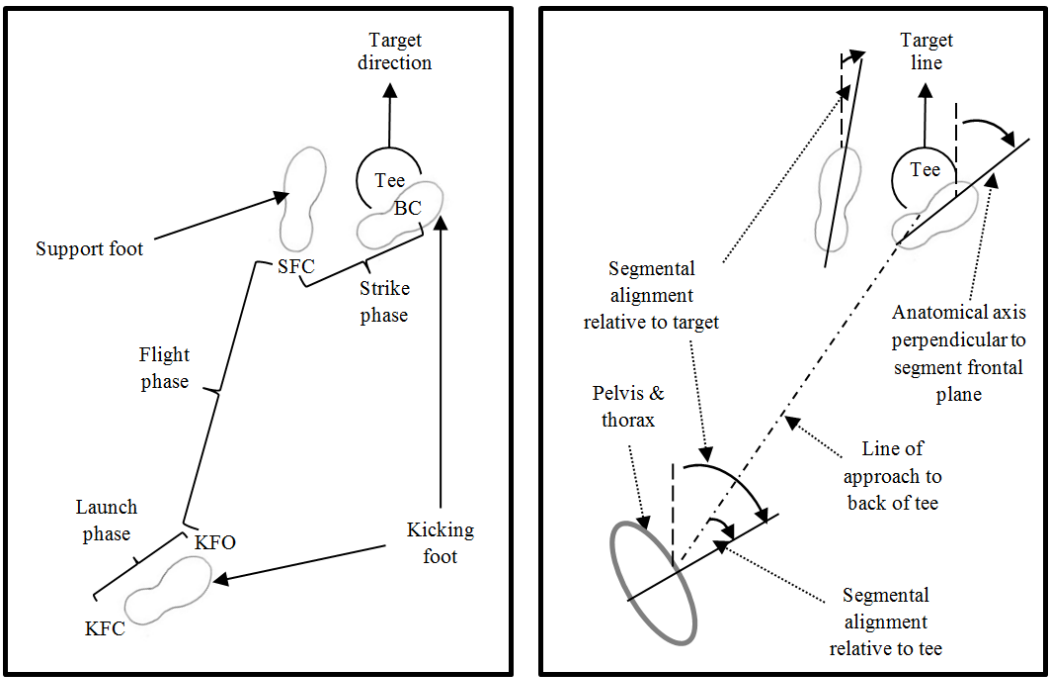

Figure 36: A top view illustration for a right-foot goal kick of (a) the temporal events and phases used to analysis the kick and (b) the alignment of the thorax, pelvis and foot segments relative to the target. Note that in this diagram all segmental angles are clockwise positive angles for a right-footed kicker. For the pelvis and thorax, this is referred to as retraction on the kicking leg relative to tee and target. Negative alignment is termed protraction.

Positive alignment angles (as shown in Figure 36b) indicate retraction of the segment on the kicking leg side relative to the tee or target, whereas negative angles would indicate protraction of that the segment on the kicking leg side relative to the tee or target.

In order to answer some of the questions posed, we assessed the strength of the association between the alignment outcomes using Pearson's correlation coefficient (r). We utilized the commonly accepted values for small, medium and large effect sizes ($r > 0.1$, $r > 0.3$ and $r > 0.5$) suggested by Cohen.

7.3. Results

On average, the participants approached the tee at a relatively large angle of 59° to the target (Table 11). Throughout the goal kick, pelvic alignment remained in overall protraction relative to the tee (Table 11 and Figure 37). Pelvic alignment was also relatively stable before the strike phase, as demonstrated by a very slight 1° protraction during launch followed by a small 5° retraction during flight. However, during the strike phase the pelvic protracted by 24°, culminating in a pelvic protraction of 27° relative to the tee by ball contact. In contrast to the pelvis, the thorax was retracted at the beginning of the launch phase and demonstrated its largest range of motion - 24° of protraction - during this phase (Table 11 and Figure 37). Like the pelvis, thoracic alignment was relatively stable during the flight phase. However, the thorax moved counter to the pelvis and retracted during strike.

Over the duration of the goal kick, the spine angle had a parabolic form beginning and ending in retraction of the thorax relative to the pelvis (Figure 37). The spine moved from 17 ± 9° retraction at KFC to 10 ± 7° protraction of the thorax relative to the pelvis at KFO – a net protraction of 27° caused primarily by thoracic motion. In contrast, the support phase contained a rapid 38° retraction in the spine angle due primarily to pelvic motion. Interestingly, the direction of the spine angle motion changed near the middle of the flight phase, caused by a combination of changes in thorax and pelvis rotation.

At ball contact, both the kicking foot and the support foot were rotated towards the target relative to the line of approach (Table 11 and Figure 38). The support foot was rotated by a notable 39° towards the target relative to the approach, while the kicking foot was almost parallel to it and thus rotated a large 48° from the direction of the target. In contrast, at the beginning of the launch phase (KFC) the kicking foot was rotated slightly away from the target relative to the line of approach by 9°.

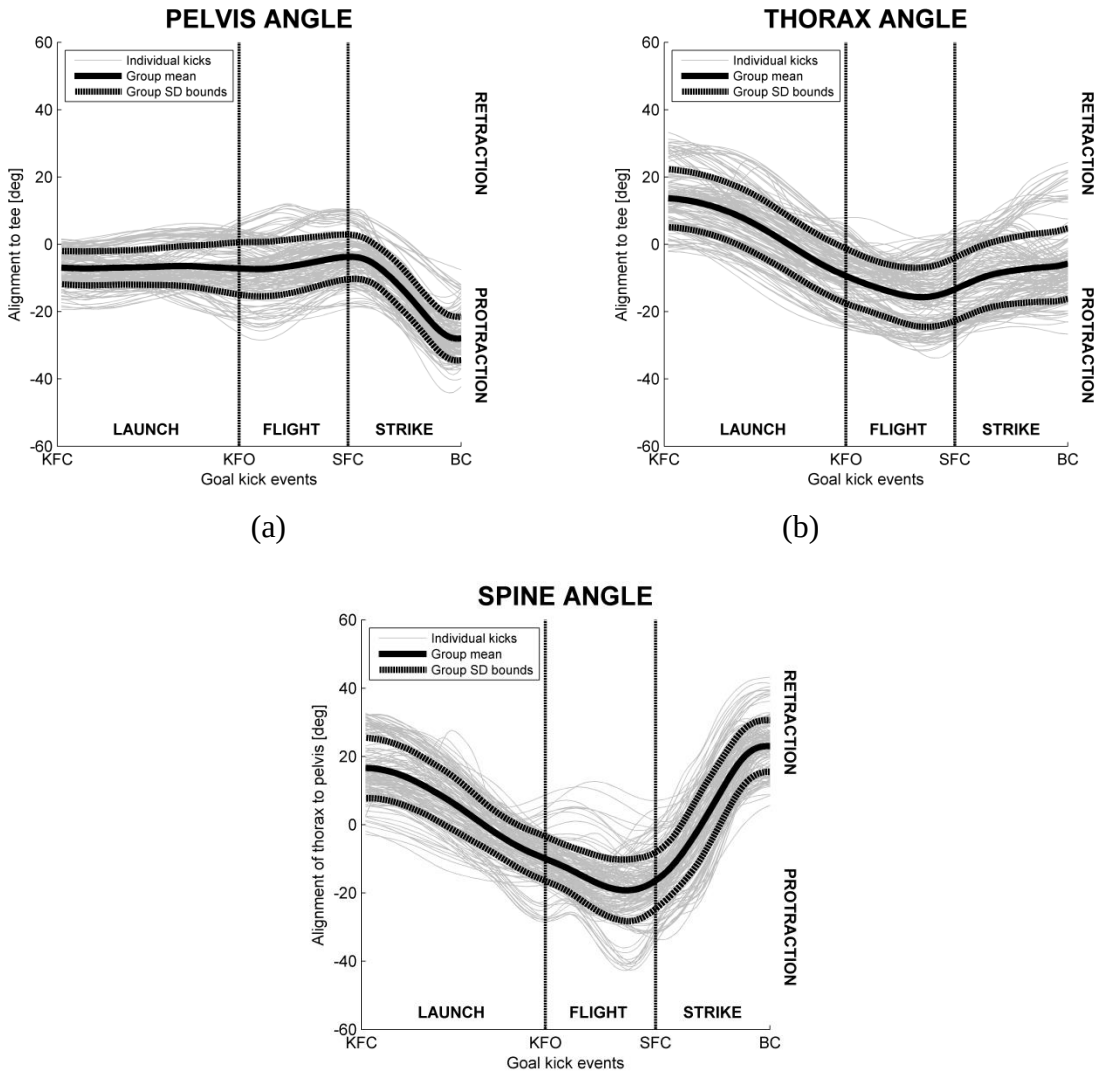

Figure 37: Absolute alignment in the transverse plane for the (a) pelvis and (b) thorax segments during the three phases of the goal kick, as well as relative angular alignment approximating the (c) spine angle. Absolute angles for the pelvis and thorax are relative to the line from tee to target, whereas the spine angle refers to the transverse plane angle of the thorax relative to the pelvis alignment. Positive values for all plots indicate retraction of the segment on the side of the kicking leg.

The rotational alignment of the thorax, pelvis and feet demonstrated marked inter-individual variability (Table 11). Furthermore, it was observed that the group variability of the segment alignments to the tee was notably lower than the segment alignments to the target. It was also found that the group variability for most

segmental alignment outcomes was higher than the group variability in approach angle. Relative to the tee, inter-individual variability was also shown to be lower for the pelvis alignment (group SDs: 4 - 7°) than for the normalized thorax and foot alignments (group SDs: 8 - 10°).

Table 11: Results from point analysis of rotational alignment to tee and target for the thorax, pelvis and foot segments. The angle of approach, defined as the line from the center of the pelvis to the tee, is given as a reference for the 'alignment to tee' results as this was used as part of the calculation. Ranges of motion during the three movement phases are also reported for the thorax and pelvis. For each outcome, intra-individual variability is reported as the group mean and SD of the participant SDs.

Time (phase or event)	Alignment to target [mean (SD) [max, min]]	Alignment to tee [mean (SD) [max, min]]	Intra-individual variability [mean (SD) [max, min]]
Approach angle [deg]			
KFC	53 (5) [63, 43]	-	1 (0) [2, 0]
Pelvic range of motion [deg]			
Launch phase	-1 (7) [20, -21]	-	3 (2) [5, 1]
Flight phase	5 (5) [17, -9]	-	2 (1) [3, 1]
Strike phase	-24 (6) [-4, -36]	-	2 (1) [4, 1]
Pelvic alignment [deg]			
KFC	47 (6) [59, 25]	-6 (4) 1, -18]	2 (1) [4, 1]
KFO	46 (8) [62, 27]	-8 (7) [5,-23]	2 (0) [4, 1]
SFC	50 (8) [69, 33]	-3 (6) [12, -18]	2 (1) [3, 1]
BC	27 (8) [41, 8]	-27 (6) [-9, -39]	2 (1) [4, 1]
Thoracic range of motion [deg]			
Launch phase	-24 (8) [-7, -46]	-	2 (1) [4, 1]
Flight phase	-3 (6) [13, -18]	-	3 (1) [3, 1]
Strike phase	8 (9) [28, -12]	-	4 (3) [9, 1]
Thoracic alignment [deg]			
KFC	67 (10) [87, 43]	14 (9) [33, -1]	2 (1) [4, 1]
KFO	44 (11) [67, 22]	-10 (9) [9, -27]	2 (1) [4, 1]
SFC	41 (12) [64, 19]	-12 (10) [-6, -31]	3 (1) [5, 1]
BC	49 (13) [84, 18]	-4 (10) [26, -24]	4 (3) [9, 1]
Foot alignment [deg]			
Kicking foot at KFC	60 (10) [83, 40]	7 (9) [24, -14]	2 (1) [4, 1]
Support foot at BC	13 (15) [29, -3]	-39 (8) [-25, -65]	2 (1) [4, 1]
Kicking foot at BC	48 (10) [77, 8]	-5 (10) [21, -36]	4 (2) [8, 1]

In contrast to the inter-individual variability, the group demonstrated consistently low intra-individual variability (Table 11). The most consistently executed outcome was the angle of approach which varied per participant by approximately 1°. Most other parameters varied per participant by 2 ± 1°, although intra-individual variability increased slightly during the strike phase. The least consistent execution per participant was found for the alignments of the thorax and kicking foot at ball contact (4 ± 3°).

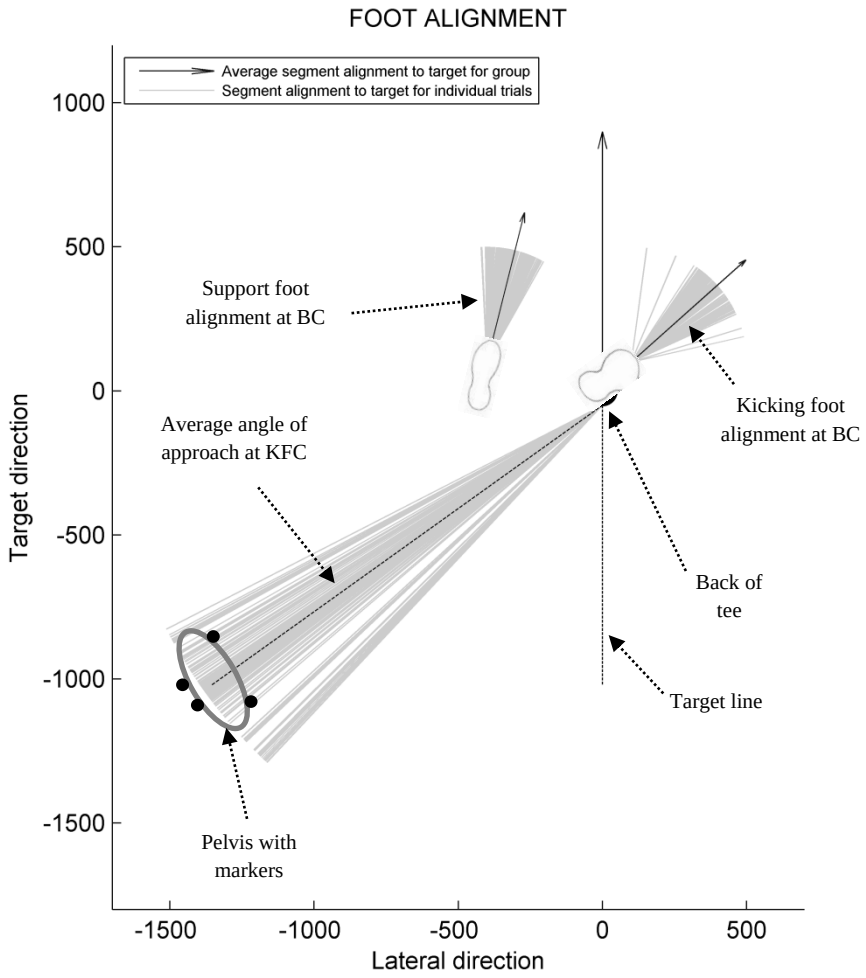

Figure 38: Visualization of foot alignment relative to the target line and angle of approach to the tee.

We investigated the statistical correlation between some of the study outcomes and found three large ($r > 0.5$) and significant ($p > 0.05$) interactions (Table 12). The rotational alignments of the pelvis and thorax at BC in relation to the target line were

strongly correlated with the angle of approach, and thus also with each other. We also found six significant medium sized ($0.3 < r < 0.5$) effects. There were inter-correlations between larger angles of approach, larger ranges of pelvic rotation during strike and larger kicking foot angles at KFC. A larger range of thoracic retraction during launch and larger kicking foot angle at KFC were also associated with reduced support foot alignment to target at ball contact. Notably, kicking foot angulation at BC did not have any notable correlation with the other outcomes. Many of the remaining correlations were found to be significant but small ($r < 0.3$).

Table 12: Effect sizes between rotational alignment outcomes relative to the target line based on Pearson's correlation coefficient (r). Statistically significant correlations ($p > 0.05$) are indicated with an asterisk (*).

	Approach angle	Kicking foot at KFC	Kicking foot at BC	Support foot at BC	Pelvic ROM in strike	Pelvis at BC	Thorax ROM in launch
Approach angle							
Kicking foot at KFC	0.47*						
Kicking foot at BC	0.1	0.2*					
Support foot BC	0.24*	-0.31*	-0.01				
Pelvic ROM in strike	0.39*	0.35*	0.2*	0.24*			
Pelvis at BC	0.58*	0.41*	0.24*	0.05	0.3*		
Thorax ROM in launch	0.27*	0.29*	0.19*	-0.33*	0.26*	0.25*	
Thorax at BC	0.58*	0.05	0.03	0.3*	0.16*	0.64*	0.1

7.4. Discussion

This study presents the first quantitative description of expert body segment alignment to tee and target during rugby union goal kicking using optical motion capture. We conducted a detailed analysis of 150 kicking trials from a group of 15 professional goal kickers and found high levels of inter-individual variability in transverse plane motion of the pelvis, thorax and feet (group SDs of 5-15°). Nevertheless, we did find a clear pattern of thoracic retraction during the launch phase and pelvic protraction during the strike phase which produces a characteristic spine rotation profile during the goal kick. We also found that on average the support foot was oriented 13° inwards from the target line at ball contact despite approach angles ranging from 50° to 68°. The kicking foot was placed approximately parallel to the line of approach during the instep and positioned roughly diagonally in relation

to the target line at ball contact. A correlation analysis revealed that the angle of approach is strongly associated with thorax and pelvis alignment at BC as well as pelvic range of motion during strike, but not so much the thoracic range of motion during strike. Support foot alignment at BC was moderately related to thorax rotation during launch and kicking foot angulation at KFC, while the kicking foot angle at BC showed no correlations to other outcomes. Despite the large differences between participants, we found that each participant executed the kick with very consistent alignment to tee and target. Intra-individual variability was typically in the region of 2 ± 1° for most outcomes, although the thorax and kicking foot alignments were less consistent (participant SDS: 4 ± 3°) during the strike phase. The findings from this study suggest that while there may be no normative reference for optimal body alignment, kickers should strive for a high level of consistency in their alignment to both tee and target.

Recent research based on dynamical systems theory has suggested that intra-individual movement variability may have a functional role in reducing overuse injuries and facilitating adaptability in the motor control system [7, 8]. However, this study found quite consistent segmental alignment for expert goal kickers. This may imply that this aspect of technique is more tightly controlled than others, although it is also likely that the controlled nature of the environmental and task constraints reduced demands on the movement system for adaptations and injury avoidance [6]. On the other hand, the relatively high inter-individual variability in the results strongly supports the emphasis placed on organismal constraints by proponents of dynamical systems theory. Despite considerable differences in technique, expert goal kickers are capable of producing similar levels of performance [16]. This necessitates more in-depth research of kicking combining insights and methodologies from motor control and biomechanics to understand underlying performance mechanisms and find coaching practices that can cater to the unique characteristics of individual athletes [20].

According to a study by Bezodis *et al.* [13], one important performance mechanism in expert goal kicking is control of angular momentum about the longitudinal axis. This is achieved by using the non-kicking side arm to counteract angular momentum generated by motion of the kicking leg - avoiding instability in the transverse plane. These results shed more light into the interaction between the pelvis and thorax as a result of these limb movements. Driven by extension and abduction of the non-kicking side arm during launch and the first half of flight, the thorax protracts

strongly from an initial retraction on the kicking side. Due to the lack of pelvic rotation over this time, the spine angle passes from retraction into protraction – which is suggestive of a build-up of tension in the lumbar spine region. Interestingly, the spine angle rapidly changes direction before SFC as the thorax moves toward retraction – initiating a short ipsilateral rotation phase with the pelvis. After SFC, the pelvis begins rapidly protracting in a contralateral rotation with the thorax. This phenomenon has been identified in skilled soccer kicking as the formation and release of a 'tension arc' [21, 22] wherein the trunk flexors, hip flexors and quadriceps are dynamically pre-lengthened prior to kicking leg protraction in order to increase subsequent muscle forces. This exploitation of the stretch-shortening cycle of muscles has also been observed for the spine angle in expert golf swing biomechanics and is known as 'X-factor stretch', however (unlike we have observed here) the pelvis rotation changes direction first in golf and not the thorax [23]. It appears that where golfers initialize the 'downswing' from the legs, kickers may do so from the upper body during the flight phase. Analysis of X-factor stretch in goal kicking may provide additional insights when considered together with the need to control whole-body angular momentum. However, more research is required to understand the possible effects of this tension arc on kicking distance.

Pelvic stability during launch and flight, despite fast retraction of the kicking leg and extension of the support leg, was a notable feature of the results and may be a helpful indicator of the effectiveness of the non-kicking side arm movement in reducing whole body angular momentum. However, comparable outcomes could not be found in the literature for kicking. This study's findings for range of pelvis rotation during strike (-24 ± 6°) agree very well with the values of -22.2 ± 3.3° reported for a study of professional instep soccer kicking by Lee and Nolan [24]. Higher values of 30° and 36° have been reported for soccer kicking, albeit for maximal distance kicking which was not investigated in this study [25]. Ball *et al.* [26] report pelvic alignment to the target at ball contact of 21 ± 7° for rugby league goal kicking. This is slightly more pelvic protraction than in this study – although this may be related to the larger approach angles for the sample. It is not clear to what extent pelvic retraction and protraction during the flight and strike phase is an active motion as opposed to being a passive result of limb motion. A study by Zang *et al.* [12] suggests that rotation of the pelvis contributes less than 5% to the total foot speed at ball contact. However, this study did not investigate expert goal kicking and did not consider upper body kinematics.

The authors are not aware of any kicking studies investigating foot alignment to tee or target for either the support leg or the kicking leg. However, foot alignment may play an important role in achieving high foot speed and good ball contact. For instance, the finding of a large rotation of the support foot towards the target result in external hip rotation at initial foot contact (SFC). This may be a strategy to facilitate increased pelvic protraction during the strike phase by enabling a larger range of internal hip rotation, and may increase passive tension in the support hip which supports more explosive pelvis rotation. Similarly, angulation of the kicking foot at ball contact may be related to 'body lean' strategies aimed at increasing foot speed by maximizing the lever arm length of the kicking leg at impact. It may also play a role in improving the foot-ball interaction, perhaps by increasing the potential contact surface area, and reducing the risk of the toes touching the ground. However, future research is needed to understand the functional role of foot alignment angles in goal kicking performance.

The approach angle results in this study are considerably higher than values reported in the literature for other kicking sports. Ball *et al.* [26] found that rugby league goal kickers have a relative straight approach angle of 31 ± 12°, although the approach angle definition is omitted. Soccer kicking researchers have reported more diagonal approach angles of 43-45° [25]. A previous study by the authors on rugby union goal kicking found that the angle of the kicking foot toe marker to the tee at KFC was 43.6 ± 6.2° [16]. However, this is about 10° less than the approach angle found in this study when using the line from the center of the pelvis to the back of the tee. This highlights the problem of comparability using different definitions of the approach angle. We found one soccer study that utilized a marker on the left shoulder [27], which would most likely produce different results to the pelvis marker method presented here. When controlling for the approach angle, researchers have also drawn a line on the ground for participants to follow, but it is unclear how this related to the body [28]. Therefore, we would caution against indiscriminate usage of approach angle findings in studies of kicking, as there seems to be no standard definition for this outcome. However, to avoid offsets due to segment rotations, it seems most intuitive to define the approach using a point lying on the central axis of the body rather that a lateral point such as the shoulder. The approach trajectory is also slightly curved during a goal kick, resulting in a slightly different approach angle at different points in time. Therefore, care should be taken to choose an adequate point during the kick to quantify the approach angle – we chose the KFC event as it would be easiest to visualize and adjust during coaching.

The work in this study has a few limitations. Firstly, we did not capture the data on the field of play which may have affected the ecological constraints of the experiment. Participants were required to wear shoes instead of studded boots, although we made every attempt to acclimatize them to the flooring conditions with practice attempts prior to testing. We also controlled the tee and target configuration for all ten kicking trials, which may have reduced the individual variability compared to competitive conditions. However, this allowed us to assess group and individual variability for the same task constraints and thus to isolate variability due to the kicker. Lastly, although the sample size of this study is larger than most of those studies discussed above, it remains a limiting factor for the generalizability of the mean values presented considering the high group variability.

Nevertheless, this study provides a few novel findings that can inform goal kick coaching as well as future research. Bezodis and Winter [11] provide some recommendations for future research based on an interview with a professional coach, and refer specifically to issues of high variability between kickers and the importance of the tension arc being maintained during the flight phase. The results support these two observations. However, the results are not in support of the recommendation by Bezodis and Winter [11] that the support foot be positioned parallel to the target line. The central tendency in the study sample was to orient the foot slightly inward, although this was highly variable. Also, the finding of a large kicking foot angulation relative to the target directly contradict the coaching cue given in the study by Bezodis and Winter [11] that the ball contact should occur with kicking foot “toe down”. Future work should be conducted to obtain detailed analytics of the interaction between boot and ball during the impact phase in order to understand the role of foot angulation.

7.5. References

[1] M. Zhou, “Advances in Sport Science and Computer Science”, Southampton: WIT Press, 2014.

[2] A. Cappozzo, U. Della Croce, A. Leardini and L. Chiari, "Human movement analysis using stereophotogrammetry: Part 1: theoretical background,” *Gait Posture*, vol. 21, no. 2, pp. 186-196, 2005.

[3] A. Lees, "Technique analysis in sports: a critical review,” *J. Sports Sci.*, vol. 20, no. 10, pp. 813-828, 2002.

[4] J. Keogh and D. Reid, "The role of biomechanics in maximising distance and accuracy of golf shots," *Sports Med.*, vol. 35, no. 5, pp. 429-449, 2005.

[5] G. Shan and X. Zhang, "From 2D leg kinematics to 3D full-body biomechanics - the past, present and future of scientific analysis of maximal instep kick in soccer," *Sports Med. Arthrosc. Rehabil. Ther. Technol.*, vol. 3, no. 1, pp. 23-32, 2011.

[6] L. Seifert, C. Button and K. Davids, "Key properties of expert movement systems in sport," *Sports Med.*, vol. 43, no. 3, pp. 167-178, 2013.

[7] M. L. Latash, "The Bliss of Motor Abundance," *Experimental Brain Research. Experimentelle Hirnforschung. Experimentation Cerebrale*, vol. 217, no. 1, pp. 1-5, 2012.

[8] R. Bartlett, J. Wheat and M. Robins, "Is movement variability important for sports biomechanists?," *Sports Biomech.*, vol. 6, no. 2, pp. 224-243, 2007.

[9] S. Mellalieu, G. Trewartha and K. Stokes, "Science and rugby union," *J. Sports Sci.*, vol. 26, no. 8, pp. 791-794, 2008.

[10] K. L. Quarrie and W. G. Hopkins, "Evaluation of goal kicking performance in international rugby union matches," *J. Sci. Med. Sport*, vol. 18, no. 2, pp. 195-198, 2014.

[11] N. E. Bezodis and S. Winter, "Identifying the key technical aspects of rugby place kicking: a qualitative case study of an elite coach," in *Proceedings of XXXII International Symposium on Biomechanics in Sports*, Twickenham, U. K., 2014.

[12] Y. Zhang, G. Liu and S. Xie, "Movement sequences during instep rugby kick: a 3D biomechanical analysis," *Int. J. Sports Sci. Eng.*, vol. 6, no. 2, pp. 89-95, 2012.

[13] N. Bezodis, G. Trewartha, C. Wilson and G. Irwin, "Contributions of the non-kicking-side arm to rugby place-kicking technique," *Sports Biomech.*, vol. 6, no. 2, pp. 171-186, 2007.

[14] K. Ball, D. Talbert and S. Taylor, "Biomechanics of goal-kicking in rugby league," in *Science and Football VII: The Proceedings of the Seventh World Congress on Science and Football*, Routledge, 2013b.

[15] K. Ball, "Kick impact characteristics for different rugby league kicks," in *International Conference on Biomechanics in Sports*, vol. 28, Konstanz, University of Konstanz, Sports Science, 2010.

[16] J. Cockcroft and D. van den Heever, "A descriptive study of step alignment and foot positioning relative to the tee by professional rugby union goal-kickers," *J. Sports Sci.*, pp. "In press", 2015.

[17] S. Baktash, A. Hy, S. Muir, T. Walton and Y. Zhang, "The Effects of Different Instep Foot Positions on Ball Velocity in Place Kicking," *Int. J. Sports Sci. Eng.*, vol. 3, no. 2, pp. 85-92, 2009.

[18] J. Sinclair, P. Taylor, S. Atkins, J. Bullen, A. Smith and S. Hobbs, "The influence of lower extremity kinematics on ball release velocity during in-step place kicking in rugby union," *Int J Perform Anal Sport*, vol. 14, no. 1, pp. 64-72, 2014.

[19] A. Atack, G. Trewartha and N. Bezodis, "A biomechanical analysis of the kicking leg during a rugby place kick," in *ISBS-Conference Proceedings Archive.*, Twickenham, U. K., 2014.

[20] P. S. Glazier and J. S. Wheat, "An integrated approach to the biomechanics and motor control of cricket fast bowling techniques," *Sports Med.*, vol. 44, no. 1, pp. 25-36, 2014.

[21] G. Shan and P. Westerhoff, "Soccer: Full-body kinematic characteristics of the maximal instep soccer kick by male soccer players and parameters related to kick quality," *Sports Biomech.*, vol. 4, no. 1, pp. 59-72, 2005.

[22] A. O. Cerrah, E. O. Gungor, A. R. Soylu, H. Ertan, A. Lees and C. Bayrak, "Muscular activation patterns during the soccer in-step kick," *Isokinet. Exerc. Sci.*, vol. 19, no. 3, pp. 181-190, 2011.

[23] S. J. Brown, W. S. Selbie and E. S. Wallace, "The X-Factor: An evaluation of common methods used to analyse major inter-segment kinematics during the golf swing," *J. Sports Sci.*, vol. 31, no. 11, pp. 1156-1163, 2013.

[24] A. Lees and L. Nolan, "Three dimensional kinematic analysis of the instep kick under speed and accuracy conditions," in *Science and Football IV,* A. Murphy, T. Reilly and W. Spinks, Eds., London, Routledge, 2002, pp. 16-21.

[25] A. Lees, T. Asai, T. Anderson, H. Nunome and T. Sterzing, "The biomechanics of kicking in soccer: A review," *J. Sports Sci.*, vol. 28, no. 8, pp. 805-817, 2010.

[26] K. Ball, D. Talbert and S. Taylor, "Biomechanics of goal-kicking in rugby league," in *Science and Football VII,* New York, Routledge, 2013, pp. 47-52.

[27] C. Egan, M. Verheul and G. Savelsbergh, "Effects of experience on the coordination of internally and externally timed soccer kicks," *J. Mot. Behav.*, vol. 39, no. 5, pp. 423-432, 2007.

[28] J. Scurr and B. Hall, "The effects of approach angle on penalty kicking accuracy and kick kinematics with recreational soccer players," *J. Sport Sci. Med.*, vol. 8, pp. 230-234, 2009.

8. Conclusions

This study presents novel methods for high performance sports analysis using motion capture technologies. Following an introductory chapter on quantitative movement analysis and modern motion capture systems, six stand-alone articles addressing the thesis objectives are presented in chapter format. Papers 1-3 detail the design and validation of new sensor fusion algorithms for measuring hip and crank arm angles during cycling using wireless IMMSs. Papers 4-6 describe the first detailed technique analysis of elite rugby union goal kickers using a gold-standard optical motion capture system.

By comparing the results and findings of these individual studies it can be concluded that the objectives detailed in the problem statement (Chapter 1.3.2) have been successfully achieved. Each article contains details of the limitations of the work, which will not be repeated here. However, it is pertinent to synthesize the overall contribution of the thesis work as a whole and to briefly discuss the future research directions stemming from it.

8.1. A Synthesis of the Project's Primary Contributions

One of the major contributions of the cycling work is that it highlights the efficacy of exploiting domain constraints to overcome three of the most significant sources of error in IMMS tracking: dynamic acceleration, magnetic interference and sensor-to-body frame alignment. We developed innovative dynamic acceleration compensation methods - based on the constraint of pendulum motion - that drastically improved tracking of the gravity vector during pedaling (Papers 1 and 3). We also exploited the mechanical constraints of the bicycle in various ways to enable tracking of the crank arm without need for a magnetometer (Papers 2 and 3). This is significant because we show that IMMS tracking fails without dynamic acceleration compensation or when using a magnetometer (and interferences are present). Lastly, we developed novel sensor-to-body frame alignment methods that are based on state-of-the-art functional calibration approaches and are immune to magnetic interference (Paper 2 and 3). Again, we show that - in contrast - conventional static pose calibration methods fail in the presence of magnetic disturbances (Paper 3).

Another important contribution of the IMMS studies is that it demonstrates the ability of nonlinear complementary filters to track sports motions regardless of initial

estimates and with accuracies comparable to that of the commercial Kalman Filter algorithms. Nonlinear complementary filters are relatively new, and we could not find any cycling studies utilizing these algorithms. However, since complementary filters are much simpler to implement than stochastic algorithms, this work may encourage greater utilization and development of sports specific sensor fusion algorithms in this class. The work presented may also contribute towards this in that it provides a thorough framework for IMMS validations. Paper 1 presents a validation of tracking performance for a proprietary algorithm (Xsens MTw, Xsens Technologies B.V., Netherlands) as well as a custom algorithm using an optical system and marker clusters attached to the pelvis and thigh IMMSs during pedaling at different speeds. In Papers 2 and 3 custom crank angle tracking algorithms were also benchmarked against both the Xsens proprietary algorithm (Xsens MTw, Xsens Technologies B.V., Netherlands) and optical system outputs. We give methodological details for all these validations on body-to-sensor frame alignment as well as alignment between the IMMS and optical system reference frames.

The cycling studies also contribute knowledge relating to the validity of motion capture data. Firstly, in Paper 1 we investigate the difference between outcomes when using a sitting and standing static pose for sensor-to-body frame alignment of the pelvis and thigh segments. We found that skin artifacts occurring between the two postures can have a significant bearing on hip angle results for both IMMS and optical motion capture. This raises important considerations about the body posture at which motion capture markers and IMMSs are placed, as well as at which static calibrations are conducted, relative to the position in which the movement is conducted. Secondly, the cycling studies in Papers 2 and 3 present the first detailed two-segment methodology in the literature for tracking crank angles using an optical motion capture system. We contend that a two-segment approach is necessary to avoid crank angle errors related to non-zero inclinations of the bicycle frame.

The studies of rugby goal kicking produced a large amount of new knowledge on technique and performance variables amongst elite kickers. The analysis focused on three clusters of technique variables: foot positioning during the run-up (Paper 4), approach speed and acceleration during the run-up (Paper 5) and body alignment to the tee and target (Paper 6). We developed a comprehensive framework for analyzing a rugby goal kick, starting with a detailed breakdown of the movement into key phases, which was previously unavailable in the literature. Most of the variables shown in the results for these experiments are also not reported on in the literature

and are thus completely novel, whereas others are only reported for small, amateur groups. We also detail how we overcame some methodological challenges regarding occlusions of the toe marker on the kicking foot (near impact) and the anterior thorax markers using virtual reconstructions from additional segmental markers. This made it possible to track the thorax and foot segment orientations as well as the toe speed during the kick.

Besides providing normative data for elite kicking technique, the rugby studies also provided important insights into movement variability within the group. We found that elite players are able to reproduce their kicking technique very consistently for repeated attempts. This was somewhat expected as the players spend large amounts of time over many years perfecting their kicking routine. Nevertheless, this is an interesting finding as some recent research has suggested that intra-individual variability is to be expected at an expert level and may even have a functional role to play in performance (Section 1.1.3) However, one reason for the low intra-individual variability may be the constraints placed on the task during controlled testing. In addition, we found that there was notable variability between the kicking techniques of different players in the group. It appears that goal kickers are able to obtain high goal kick success rates during matches with different foot positioning, run-up dynamics and body alignment to the target line. We found that, despite these differences, performance variables such as maximum foot speed were relatively consistent within the group despite having rather low correlations with individual technique variables. This demonstrates the non-linear dynamics of movement in general and highlights the need for caution when considering coaching techniques which are based on a putative expert model.

8.2. Future Research Directions

The work in this study will form the basis for continued work in cycling and rugby goal kicking using motion capture technologies. Moreover, the methods presented in this thesis can be expanded or adapted in multiple ways for other projects within the biomedical engineering research group.

The work on cycling analysis using wearable sensor technologies forms part of a wider effort in the research field to develop a full-body biomechanical analysis system that can provide real-time kinetic and kinematic data to cyclists during outdoor riding. This requires the ability to track both lower and upper body segmental

motion for hours in the presence of dynamic accelerations and (in some cases) magnetic interferences both of which are continuous and time-varying. According to the literature, this feat has not yet been accomplished. By incorporating joint constraints, it may be possible to expand the sensor fusion methods in this thesis to include the shank and foot segments, thus enabling a full lower-limb analysis. This may also be accomplished using mathematical optimization methods which exploit the closed kinematic chains during pedaling. However, in order to reliably measure the movement of all of these segments with six degrees of freedom, additional auxiliary sensors such as GPS will probably need to be incorporated into the sensor fusion scheme.

The work on rugby union goal kicking is also on-going, with a number of new studies planned that will expand knowledge of kicking performance. The data collected for this thesis is expected to produce several more publications, and will also form the foundation of future research. The next aim is to investigate how elite technique differs to that in other populations such as youth, amateur level kickers and non-kickers. Technique analysis at different levels of skill may reveal unforeseen key performance indicators, or rule out those which were initially assumed. It will also be very insightful to test these groups with more extensive protocols that involve more environmental factors such as fatigue, stress and variability in kicking distance and target direction. Furthermore, understanding kicking at different age levels may also help us to create talent identification tools and coaching methods which optimize skill acquisition by incorporating training techniques appropriate for different stages of physical and mental development. It will also be important to investigate the role of strength and conditioning in improving kicking performance and reducing injury risk.

As discussed in the Introduction section, full-body biomechanical analysis is on the horizon for outdoor analysis of sports. Therefore, field testing is the ultimate goal for the work in both cycling and rugby union goal kicking. Future directions for cycling include developing innovative ways of validating outdoor measurements. A rotary encoder system could be developed to benchmark crank angle data from wireless IMMSs while out on the road instead of in a laboratory as was done for this project. Although it may be possible for a short stretch of road with state-of-the-art outdoor-enabled optical systems, validating body posture data from IMMSs on the road with a gold-standard technology remain a daunting challenge. Nevertheless, developments in three-dimensional markerless motion capture systems may make it feasible in the near future to perform such a validation with cameras on a moving vehicle. Rugby

goal kicking analysis, on the other hand, is already possible to validate with IMMSs using outdoor enabled stereophotogrammetry and the next phase of the rugby project will include efforts to reproduce the optical motion capture analysis (e.g. approach speed, timing and acceleration) using IMMSs. Outdoor kicking experiments would also provide us with valuable additional information about the outcome of a kick as well as the distance travelled by the ball. This is crucial for determining a link between technique, performance variables and the eventual outcome (goal success or failure).

Lastly, one of the major future directions in quantitative movement analysis capture is advanced analytical tools for extracting nonlinear features from complex datasets. This is crucial for improving the understanding of human movement, particularly in terms of optimizing movement function. Therefore, the aim is to employ state-of-the-art computational modeling techniques such as musculoskeletal modeling and machine learning algorithms to provide deeper insights into the underlying mechanisms of sports performance and injury. By including electromyography and force data to the kinematic measurements covered in this thesis, we may be able to develop sport-specific musculoskeletal models for cycling and goal kicking that reduce soft tissue motion artifacts, identify performance or injury markers on the structural biomechanics level or find optimal movement techniques through simulation experiments. Machine intelligence methods such as artificial neural networks and genetic algorithms also hold the potential for extracting nonlinear features in movement data which are inaccessible using traditional statistical analysis methods. The current analytical tools are just not suitable for investigating the multi-segmental, time-dependent patterns of movement underlying phenomena such as physical coordination and (more broadly) talent. However, artificial intelligence may hold the key unlocking the potential of biomechanics datasets.

This thesis provides the groundwork for realizing these ambitious goals, which ultimately depends on reliable measurements and sufficient knowledge of movement to effectively and efficiently address more important research questions in the future.